University of Alberta

Improving the Stability of Gas-Liquid Sprays by Modifying the Two-Phase Flow Entering the Nozzle

by

Solange Maldonado

A thesis submitted to the Faculty of Graduate Studies and Research in partial fulfillment of the requirements for the degree of Master of Science

Department of Mechanical Engineering

Edmonton, Alberta
Fall 2006

Your file Votre référence
ISBN: 978-0-494-22313-0
Our file Notre référence
ISBN: 978-0-494-22313-0

Abstract

An experimental investigation of the effect of different feeding pipe designs on the stability of gas-liquid sprays is presented. The designs focused on maintaining a more homogeneous mixture of the two-phase flow entering the nozzle, in order to improve the range of stability of the spray. The alternatives evaluated were: different pipe lengths, sudden expansion-contractions of the cross-section, peripheral obstructions and nonintegral roughness. Air and water with flow conditions ranging between 75.7–181.7 kg/min for water and 1–4 m/s for air, were used. The spray stability was assessed through pressure fluctuation signals analysis.

The flow pattern entering the nozzle was confirmed to affect the spray stability. Most of the alternatives, showed a reduction in the strength of the pulsations for unstable conditions. Overall, the best results were obtained with a series of sudden expansion-contractions, broadening the range of stability and presenting a small increment in pressure drop.

Acknowledgements

I would like to thank my supervisor Dr. Brian Fleck for his support and guidance. Thanks for always believing in my work and providing me the great opportunity of participating in this research project.

I would also like to thank Dr. Ted Heidrick for his support during the project.

My sincere thanks to Dr. Alidad Amirfazli for his willingness to help me when I approached him and for his valuable suggestions.

I would like to express my immense gratitude to the personnel at the Syncrude Research Center. Dr. Edward Chan, for his helpful ideas during the discussions we had, and his confidence in my work. Chris Schroeter, for his technical assistance during the experiments. Robert Skwarok, for providing his ideas and expertise to perform the high-speed flow visualization in this thesis. Especially, I want to thank Brian Knapper for his significant support and for the countless discussions and interactions that guided me through the different stages of this project.

Finally, I wish to thank my husband Luis for always being there for me, and for his encouragement and infinite understanding during the difficult times of this project.

To my parents

Table of Contents

1 Introduction **1**

1.1 Two-phase nozzles 1

1.2 Atomization in the fluid coking process 3

1.3 Stability of gas-liquid sprays 4

1.4 Basis for the research 5

1.5 Objectives and outline of the thesis 6

2 Horizontal Gas-Liquid Flow **8**

2.1 Fundamentals of gas-liquid two-phase flow 8

2.1.1 Relevant parameters in two-phase flow 8

2.1.2 Two-phase flow patterns 11

2.1.3 Flow pattern transitions in two-phase flow 12

2.2 Flow patterns and stability of gas-liquid sprays 18

2.3 Altering the two-phase flow pattern 20

2.3.1 Length to diameter ratio (L/D) 20

2.3.2 Sudden expansion-contractions of the pipe cross-section 21

2.3.3 Obstructions 22

2.3.4 Roughness 23

2.3.5 Discussion 23

2.4 Flow pattern and stability detection 24

2.4.1 Differential pressure fluctuations 24

2.4.2 Electrical conductance 25

2.4.3 Pressure fluctuations 25

2.4.4 Discussion 28

3 Equipment and Experimental Procedure **29**

3.1 Equipment description 29

3.1.1 Spray testing facility 29
3.1.2 Mixing device, feeding pipe and nozzle 31
3.1.3 Testing fluids 32
3.1.4 Pressure transducers 33
3.1.5 Modifications to the feeding pipe 35
3.1.6 Video imaging system 39
3.2 Experimental procedure 40
3.2.1 Operating conditions 40
3.2.2 Pressure Measurements 42
3.2.3 Qualitative techniques for stability evaluation 43

4 Pressure Fluctuations Analysis **45**
4.1 Description of the pressure fluctuations 46
4.1.1 Characteristics of the pressure fluctuation signal 46
4.1.2 Pressure fluctuation and spray stability 47
4.2 Pressure fluctuation signal processing 50
4.2.1 Amplitude domain 51
4.2.2 Time domain 54
4.2.3 Frequency domain 64
4.3 Stability evaluation using pressure fluctuations 71
4.3.1 Stability transition 71
4.3.2 Pressure fluctuations along the pipe 73
4.3.3 Discussion 74

5 Effect of the Feeding Pipe on the Spray Stability **75**
5.1 Standard configuration 76
5.1.1 Stability transition and two-phase flow pattern 76
5.1.2 Effect of air to liquid ratio (ALR) and void fraction on stability 78
5.1.3 Frequency of pulsation 78
5.1.4 Repeatability 79
5.2 Different pipe configurations 81
5.2.1 Length to diameter ratio (L/D) 82
5.2.2 Sudden expansion-contractions along the pipe 88
5.2.3 Peripheral obstructions 94
5.2.4 Nonintegral roughness 99

5.3 Overall comparison 102

6 Conclusions and Recommendations **104**

6.1 Conclusions 104

6.2 Recommendations 106

Bibliography **107**

Appendix **112**

A Experimental conditions for different configurations **112**

A.1 Standard 113

A.2 Length to diameter ratio (L/D) 115

A.3 Sudden expansion-contractions along the pipe 117

A.4 Peripheral obstructions 120

A.5 Nonintegral roughness 122

B Videos **123**

List of Tables

3.1 Specifications of the dynamic pressure transducers 34

4.1 Cross-correlation and lag time for an unstable condition 57
4.2 Cross-correlation and lag time for a stable condition 60

A.1 Experimental conditions for the standard feeding pipe 113
A.2 Experimental conditions for the short feeding pipe ($L/D = 16$) 115
A.3 Experimental conditions for the long feeding pipe ($L/D = 74$) 116
A.4 Experimental conditions for configuration with 1x1.25 sudden expansion-contractions along the pipe. 117
A.5 Experimental conditions for configuration with 1x1.5 sudden expansion-contractions along the pipe. 118
A.6 Experimental conditions for configuration with 1x2 sudden expansion-contractions along the pipe. 119
A.7 Experimental conditions for configuration with 4 peripheral obstructions along the feeding pipe. 120
A.8 Experimental conditions for configuration with 2 peripheral obstructions along the feeding pipe. 121
A.9 Experimental conditions for configuration with nonintegral roughness along the feeding pipe. 122

List of Figures

2.1 Dimensionless flow pattern map based on the model by Taitel and Dukler (1976) to predict flow regime transitions in horizontal gas-liquid flow. The dotted line corresponds to the annular-intermittent transition modified by Barnea et al. (1982). 14

2.2 Flow pattern map based on the model by Taitel and Dukler (1976) with gas and liquid superficial velocities as coordinates. Air and water as fluids at 20°C, 2.43 cm ID pipe, and different operating pressures. The transition from intermittent to annular flow is the one modified by Barnea et al. (1982). 17

3.1 Schematic of the commercial-scale spray testing facility at the Syncrude Research Center (Edmonton, Alberta). 30

3.2 Schematic with the arrangement of the nozzle, conduit and mixing device. 31

3.3 Schematic of the standard configuration with pressure transducers along the pipe. Dimensions shown in cm. 33

3.4 Schematic with the set-up for the evaluation of a (a) 38 cm ($L/D \approx 16$), and (b) 180 cm ($L/D \approx 74$) long pipe. Dimensions shown in cm. . . . 36

3.5 Schematic with the set-up for the evaluation of sudden expansion-contractions of the pipe cross-section. Dimensions shown in cm. . . . 36

3.6 Schematic with the set-up for the evaluation of the effect of (a) 2 and (b) 4 peripheral obstructions. Dimensions shown in cm. 38

3.7 Schematic with the set-up for the evaluation of the pipe with nonintegral roughness. Dimensions shown in cm. 39

3.8 Flow map with the experimental conditions for the evaluation of the standard configuration. The dispersed bubble - intermittent transition by Taitel and Dukler (1976), is superimposed as reference. 42

4.1 Pressure fluctuation signal for (a) a stable (2 kg/min of air and 151.4 kg/min of water), and (b) an unstable (2 kg/min of air and 75.7 kg/min of water) condition. The dotted lines correspond to the RMS of the pressure fluctuations. 47
4.2 Spray pattern at certain points of the pressure fluctuation signal for a stable condition (2 kg/min of air and 151.4 kg/min of water). 48
4.3 Images of the spray and flow in the pipe correlated with the pressure fluctuation signal for an unstable condition (2 kg/min of air and 75.7 kg/min of water). Two main sections were identified: (a) important amounts of gas in the pipe and spray with good droplet dispersion, (b) liquid filling the pipe and spray with ligaments and big droplets. 50
4.4 Probability density function of the pressure fluctuation signal for (a) a stable (2 kg/min of air and 151.4 kg/min of water) and (b) an unstable (2 kg/min of air and 75.7 kg/min of water) condition. 52
4.5 Root mean square of the pressure fluctuation signal sampled upstream the nozzle, as function of liquid superficial velocity, for the standard configuration. Each curve corresponds to a constant air flow rate. . . 53
4.6 Mean square value of the pressure fluctuation signal sampled upstream the nozzle, as function of liquid superficial velocity, for the standard configuration. Each curve corresponds to a constant air flow rate. . . 54
4.7 Normalized cross-correlation between the signals recorded at the middle of the conduit and just upstream of the nozzle (R_{21}), for an unstable condition (2 kg/min of air and 75.7 kg/min of water). 56
4.8 Pressure fluctuation signals along the conduit for an unstable condition (2 kg/min of air and 75.7 kg/min of water). 57
4.9 Normalized cross-correlation between signals sampled at the middle of the conduit and just upstream of the nozzle (R_{21}), for a stable condition (2 kg/min of air and 151.4 kg/min of water). 59
4.10 Pressure fluctuation signals along the conduit for a stable condition (2 kg/min of air and 151.4 kg/min of water). 60
4.11 (a) Maximum normalized cross-correlation and (b) mean lag time, between signals sampled at the middle of the conduit and just upstream the nozzle (R_{21}), as function of liquid superficial velocity, for the standard configuration. 62

4.12 Normalized autocorrelation of the pressure fluctuation signal sampled just upstream of the nozzle (R_{11}), for (a) a stable (2 kg/min of air and 151.4 kg/min of water), and (b) an unstable (2 kg/min of air and 75.7 kg/min of water) condition. 63
4.13 PSD of the pressure fluctuation signal sampled just upstream of the nozzle for (a) a stable (2 kg/min of air and 151.4 kg/min of water), and (b) an unstable (2 kg/min of air and 75.7 kg/min of water) condition. Note different scales in (a) and (b). 67
4.14 PSD of the pressure fluctuation signal sampled just upstream of the nozzle for stable (left) and unstable (right) conditions at 3 kg/min (top) and 4 kg/min (bottom) of air. Water flow rates at (a) 166.6 kg/min, (b) 90.8 kg/min, (c) 162.8 kg/min, and (d) 90.8 kg/min. 68
4.15 Area beneath the PSD for frequencies below 40 Hz, of the pressure fluctuation signal sampled just upstream of the nozzle, as function of liquid superficial velocity, for the standard configuration. Each curve corresponds to a constant air flow rate. 70
4.16 Stability transition for the standard configuration, based on the area beneath the PSD for frequencies below 40 Hz ($\widehat{P^2}_{40}$), of the pressure fluctuation signal sampled just upstream of the nozzle. 72
4.17 Area beneath the PSD for frequencies below 40 Hz of the signals sampled (a) at the middle of the conduit (D2), and (b) after the mixing device, for the standard configuration. 73

5.1 Flow map with the operating points and their corresponding stability condition for the standard configuration. The transition dispersed bubble – intermittent flow by Taitel and Dukler (1976) is superimposed as reference. 77
5.2 Frequency of pulsation for unstable conditions as function of the liquid superficial velocity for the standard feeding pipe. 79
5.3 Area beneath PSD for frequencies below 40 Hz ($\widehat{P^2}_{40}$), for different tests performed with the standard configuration, at 2 kg/min of air. . 81
5.4 Area beneath the PSD for frequencies below 40 Hz ($\widehat{P^2}_{40}$), of the pressure fluctuation signal for the (a) *short*, and (b) *long* conduit. 83
5.5 Comparison of short and long conduit with respect to the standard, for (a) 1 kg/min, (b) 2 kg/min, and (c) 3 kg/min of air flow. 84

5.6 Pictures of the flow before the nozzle within a section of the (a) standard, and (b) long conduit, for an unstable condition (2 kg/min of air and 75.7 kg/min of water). 85
5.7 PSD of the pressure fluctuation signal for stable (left) and unstable (right) conditions with the short (top) and long (bottom) conduit. Flow rates at 2 kg/min of air and 151.4 and 75.7 kg/min of water, for the stable and unstable condition, respectively. 86
5.8 Frequency of pulsation as function of the length to diameter ratio (L/D) for an unstable condition (2 kg/min of air and 75.7 kg/min of water). 87
5.9 Area beneath the PSD for frequencies below 40 Hz ($\widehat{P^2}_{40}$), of the pressure fluctuation signal, for the configurations with sudden expansion-contractions: (a) 1x1.25, (b) 1x1.5, and (c) 1x2. 89
5.10 Comparison of the different sudden expansion-contractions with the standard pipe for (a) 1 kg/min, (b) 2 kg/min, and (c) 3 kg/min of air flow. 90
5.11 Flow map of the operating points with their corresponding stability condition for the 1x1.5 configuration. The transition dispersed bubble–intermittent flow by Taitel and Dukler (1976), is superimposed as reference. 91
5.12 Pressure drop along the feeding pipe for the standard and sudden expansion-contractions arrangement. 92
5.13 PSD of the pressure fluctuation signal for stable (left) and unstable (right) conditions, with the 1x1.25 (top), 1x1.5 (middle) and 1x2 (bottom) configurations. Flow rates at 2 kg/min of air and 151.4 and 75.7 kg/min of water, for the stable and unstable condition, respectively 93
5.14 Area beneath the PSD for frequencies below 40 Hz ($\widehat{P^2}_{40}$), of the pressure fluctuation signal, for configurations with (a) 2, and (b) 4 peripheral obstructions along the feeding pipe. 95
5.15 Comparison of 2 and 4 peripheral obstructions with the standard pipe for 2 kg/min of air flow. 96
5.16 Pressure drop along the feeding pipe for the standard conduit and configurations with peripheral obstructions along the pipe. 97

5.17 PSD of the pressure fluctuation signal for stable (left) and unstable (right) conditions with 2 obstructions (top) and 4 obstructions (bottom) configurations. Flow rates at 2 kg/min of air and 151.4 and 75.7 kg/min of water, for the stable and unstable condition, respectively. 98
5.18 Comparison of nonintegral roughness with the standard pipe for 2 kg/min of air flow. 100
5.19 Pressure drop along the feeding pipe for the standard and nonintegral roughness configurations. 100
5.20 PSD of the pressure fluctuation signal for (a) a stable, and (b) an unstable condition, for the configuration with nonintegral roughness. Flow rates at 2 kg/min of air and 151.4 and 75.7 kg/min of water, for the stable and unstable condition, respectively. 101
5.21 Area beneath the PSD for frequencies below 40 Hz ($\widehat{P^2}_{40}$), of the pressure fluctuations, for most of the feeding pipe configurations evaluated at 2 kg/min of air. 102
5.22 Pressure drop along the feeding pipe for configurations improving the gas and liquid mixing along the conduit. 103

List of Symbols

A	pipe cross-sectional area, m^2
A_G	cross-sectional area occupied by the gas phase, m^2
A_L	cross-sectional area occupied by the liquid phase, m^2
c_m	speed of sound in a gas-liquid mixture, m/s
D	pipe diameter, m
$(dP/dx)_{GS}$	superficial pressure drop per unit length of gas, kPa/m
$(dP/dx)_{LS}$	superficial pressure drop per unit length of liquid, kPa/m
F	dimensionless parameter for stratified wavy–intermittent or annular flow transition
f	Fanning friction factor
f_{GS}	Superficial Fanning friction factor of gas
f_{LS}	Superficial Fanning friction factor of liquid
g	gravitational acceleration, m/s^2
G	one-sided power spectral density, kPa^2/Hz
K	dimensionless parameter for stratified smooth–wavy flow transition
n	sample counter
N	experimental sample size
P	pressure, kPa
$\widehat{P^2}_{40}$	area beneath PSD for frequencies below 40 Hz, kPa^2
Q	volumetric flow rate, m^3/s
Q_G	volumetric flow rate of gas, m^3/s
Q_L	volumetric flow rate of liquid, m^3/s
R_{xy}	cross-correlation function between time series x and y
S	power spectral density, kPa^2/Hz
T	dimensionless parameter for dispersed bubble–intermittent flow transition

U	velocity, m/s
U_G	actual velocity of gas, m/s
U_L	actual velocity of liquid, m/s
U_{GS}	superficial velocity of gas, m/s
U_{LS}	superficial velocity of liquid, m/s
X	dimensionless parameter for flow pattern transition

Greek Alphabets

α	void fraction
α_h	homogeneous void fraction
μ	mean of a population
μ_L	dynamic viscosity of liquid, N·s/m^2
ν_G	kinematic viscosity of gas, m^2/s
ν_L	kinematic viscosity of liquid, m^2/s
ρ_G	density of gas, m^3/kg
ρ_L	density of liquid, m^3/kg
σ	standard deviation of a population
τ	lag time between signals
θ	angle of inclination of the pipe

Abbreviations

ALR	air to liquid mass ratio
DFT	discrete Fourier transform
fps	frames per second
GLR	gas to liquid mass ratio
ID	inside diameter
OD	outside diameter
PSD	power spectral density
RMS	root mean square
SMD	Sauter mean diameter

Chapter 1

Introduction

Atomization of liquids is used in several industrial processes. The sought atomization characteristics are not necessarily the same for different applications, thus, numerous nozzles and methods have been developed in order to attain the desired features. For instance, in some applications the liquid is sprayed with the assistance of an atomizing gas, such as the case of the fluid coking process where a mixture of bitumen and steam is sprayed through a nozzle into a fluidized bed. The efficiency of the process for which the spray is generated is highly dependent on the characteristics of the spray. Hence, all efforts towards the enhancement of these features will result in significant improvements for the whole process. In this regard, it is important to clearly understand what components or parameters affect the atomization performance, and work on those that are suitable of positive changes and that will derive in benefits to the characteristics of the spray and, in consequence, the efficiency of the process.

1.1 Two-phase nozzles

Probably the simplest atomization method consists of a nozzle or atomizer with a circular orifice through which the liquid passes achieving a high velocity. This high velocity of the liquid phase with respect to the surrounding gas is what essentially is

necessary to achieve the atomization. A variety of nozzle designs operating with this method is presented in detail in Lefebvre (1989).

A different approach is to use gas to achieve or improve the atomization process. In twin-fluid atomizers, the liquid is exposed to the gas phase, either within the nozzle (internal-mixing) or once the liquid has left the atomizer (external-mixing). Many different designs have been developed for internal-mixing twin-fluid atomizers, using the kinetic energy of a high-velocity gas stream to impinge a jet of liquid and shatter it into droplets.

An alternative method that also uses gas to improve the atomization is flash atomization, where gas bubbles are formed in the liquid, exploding when they leave the nozzle. To generate the bubbles, the temperature of the liquid is raised above the boiling point, or the gas is dissolved into the liquid. One of the limitations of this technique is that it applies to liquids that are volatile or that can hold important amounts of dissolved gas.

To avoid the practical problems associated with flash atomization Lefebvre et al. (1988) introduced the technique of effervescent atomization, where the gas is injected into the liquid phase in order to form a two-phase bubbly flow before the discharge orifice. In the effervescent atomization, as described by Sovani et al. (2001), the kinetic energy of the gas phase is not the means used to improve the atomization. Rather, the atomizing gas has two main functions: (a) reduce the characteristic liquid dimensions from which the drops are formed, by forcing the liquid to occupy only a fraction of the cross sectional area of the discharge orifice, and (b) has a shattering effect on the liquid by the rapid expansion of the gas at the nozzle exit. Roesler and Lefebrve (1989) reported about some of the benefits of this atomization method, and established that when operating in bubbly flow good atomization can be attained at low injection pressure with small amounts of gas.

1.2 Atomization in the fluid coking process

Fluid coking is a continuous process where heavy petroleum residuals are thermally converted into lighter products and coke. In this process, bitumen and steam (atomizing gas) are sprayed through nozzles into a fluidized bed of coke particles with an average diameter of 150 to 200 μm. The reaction occurs when the drops of bitumen deposits as a thin layer on the surface of the hot coke particles. The lighter vapors rise to the top of the reactor, pass through cyclones to remove the entrained coke particles and then are fractionated in a scrubber. The particles from the reactor are stripped with steam and then passed to a burner where they are heated and circulated back to the reactor to continue the process (Matsen, 1996).

The nozzle assembly used in fluid coking differs with respect to the classical effervescent atomizers in that the gas and liquid phase are mixed well upstream and flow through a conduit before entering the nozzle. This conduit, or feeding pipe, is used to insert the nozzle through the refractory lined coker wall. It is worthy to note that there are many nozzles installed in a reactor for the atomization of bitumen; they are located along the height of the coker (which itself is in the shape of an inverted bottle) and configured as rings around the circumference of the reactor. Additionally, besides improving the atomization, the steam used in fluid coking has the function of keeping the nozzle assembly free of blockage when the bitumen feed is shut down.

The performance of the process for which a spray is generated is strongly dependent on the spray characteristics. In the fluid coking process, the best performance (high liquid yield products) can be achieved with wide sprays of fine and uniformly distributed bitumen droplets.

1.3 Stability of gas-liquid sprays

For nozzles that operate with effervescent atomization or similar principles, the stability of the gas-liquid spray generated is related to the uniformity of its distribution. A stable spray is characterized by a good dispersion of the liquid phase. Conversely, an unstable spray is distinguished by certain intermittency in its pattern, with an alternate presence of fine and coarse spray.

Some researchers (Whitlow and Lefebvre, 1993; Roesler and Lefebrve, 1989) have evaluated the atomizer performance and the spray characteristics when using the effervescent atomization method. They have found that as the air to liquid mass ratio (ALR) is increased, for a constant operating pressure, at some point is reached a value at which the spray becomes unstable. The unstable spray was described by Whitlow and Lefebvre (1993) as one formed by voids of air atomizing the accompanying liquid, and interrupted by the emission of liquid ligaments. The transition from the stable to unstable operation was explained by the change of the gas-liquid flow pattern within the nozzle from a homogeneous to an intermittent flow.

In the nozzle assembly used in fluid coking the two-phase flow pattern entering the nozzle, as in effervescent atomizers, has an impact on the characteristics of the gas-liquid spray (Ariyapadi et al., 2005; Tafreshi et al., 2002; Baker et al., 1991). A homogeneous mixture of the gas and liquid entering the nozzle would maximize the effect of the decompression of the gas phase, resulting in a well atomized and properly distributed liquid phase. Contrarily, a non-homogeneous flow entering the nozzle will cause an unstable spray with its characteristic improper axial distribution of the phases. The location of the mixing device well upstream of the nozzle worsens the problem of instability in this kind of assembly, due to the coalescence of bubbles that is favored with the flow of the two-phase mixture through the conduit.

The uneven distribution of the unstable spray pattern has a detrimental effect on the process for which the spray is produced. For instance, in the case of the fluid

coking process where the liquid is sprayed into a fluidized bed, the intermittency of sections with high and low liquid dispersion can favor the formation of liquid-particle agglomerates. The instability of the spray has also shown to have an unfavorable effect on the entrainment rate of solids into the jet in a fluidized bed (Hulet et al., 2003). Effective attempts to widen the range of stability of the spray ejected from these nozzles will undoubtedly lead to better performance of the fluid coking process with higher liquid distillate products as result.

1.4 Basis for the research

The pattern of the two-phase flow within the atomizer importantly affects the stability condition of the gas-liquid spray ejected from the nozzle. It was already discussed that this behavior is more pronounced in the assembly used in fluid coking where the bitumen and steam flows are mixed upstream of the nozzle. Operationally, in the fluid coking process the steam flow is maintained constant, thus, reductions in the bitumen flow rate can cause the appearance of intermittent two-phase flow patterns at the nozzle inlet, and with it, instabilities in the spray. Another possible cause of instabilities is due to the plugging of the nozzle by process deposits.

Additionally, experimental evidence has shown improvements in atomization when using higher amounts of gas relative to the liquid phase. Whitlow and Lefebvre (1993) found that for effervescent atomizers operating in the bubbly flow regime the spray Sauter mean diameter (SMD) decreases for higher ALR or operating pressure. However, the use of higher amounts of gas can cause the appearance of intermittent flow patterns along the feeding pipe, and, consequently, instabilities in the spray.

The idea of being able to address higher amounts of gas relative to the liquid phase without reaching unstable conditions in the spray, is the main motivation of the present research. The broadening of the range of stability could be reached through modifications of the elements in the nozzle assembly used in fluid coking. In 1995

Syncrude Canada Ltd. embarked in a thorough work to improve the designs of the nozzle and mixing device (Chan et al., 2001; Base et al., 1999), and the positive result from this work are the atomizer and mixer that currently operate at the commercial facilities. In this regard, the scope of this thesis is limited to the characterization and improvement to the design of the conduit that connects the mixing device and nozzle.

1.5 Objectives and outline of the thesis

The main objective of this research is to improve the range of stability of a gas-liquid spray by altering the two-phase flow structure entering the nozzle, through modifications in the design of the conduit upstream of the nozzle. Additionally, it is of interest to gain more understanding of the stability phenomenon in this type of nozzle assembly. Several specific objectives have been proposed:

1. Develop a technique to quantitatively diagnose the stability condition of the spray. This technique should be of simple implementation and allow the comparison between the results from the different pipe configurations to evaluate.

2. Characterize the effect of the conduit on the stability of the system. For this, the current configuration must be thoroughly evaluated and characterized. Additionally, different length to diameter ratios are considered with the aim of gain fundamental understanding about the effect of the conduit and the flow-pattern flowing through it on the spray stability.

3. Design and experimentally evaluate different pipe configurations with the objective of widen the current range of stability. The various alternatives should positively alter the distribution of the liquid and gas phase in order to have a more uniform two-phase mixture entering the nozzle.

An introduction to theoretical aspects of gas-liquid two-phase flow, as well as its relation with the stability of gas-liquid sprays is presented in Chapter 2. Detailed de-

scription of the equipment used and the experimental procedure followed is presented in Chapter 3. The analysis of the pressure fluctuations performed for the diagnosis of the spray stability is described in Chapter 4. The evaluation of different feeding pipe configurations, in terms of their effect on the spray stability, is addressed in Chapter 5. Based on experimental results, the conclusions of this study and recommendations for future work are presented in Chapter 6.

Chapter 2

Horizontal Gas-Liquid Flow

2.1 Fundamentals of gas-liquid two-phase flow

Systems that operate with gas-liquid two-phase flow are widely used in industrial applications and are of significant importance in engineering. Consequently, during last decades researchers have directed considerable efforts towards the understanding and characterization of this type of flow. In this section is presented a brief introduction of some parameters widely use in the analysis of two-phase flow, a description of the flow regimes that can be found in horizontal gas-liquid flow, and the approach followed by some researchers to characterize the transition between these regimes.

2.1.1 Relevant parameters in two-phase flow

To account for the presence of a second phase in two-phase flow, certain parameters and expressions have been defined, such as weighting factors, and different designations of velocity. Some of the relevant parameters that later will be referred to are introduced here.

Superficial Velocities

The superficial velocity is the velocity that one of the phases would have if it flowed alone occupying the entire pipe cross-section. The expressions for gas and liquid superficial velocities are given by

$$U_{GS} = \frac{Q_G}{A} \tag{2.1}$$

$$U_{LS} = \frac{Q_L}{A} \tag{2.2}$$

where A is the cross-sectional area of the pipe, and Q_G and Q_L are the volumetric flow rates of the gas and liquid phase, respectively.

Void fraction

The void fraction is the portion of the pipe cross-section occupied by the gas phase, and conceptually is defined as

$$\alpha = \frac{A_G}{A} \tag{2.3}$$

where A_G is the area occupied by the gas phase. When the velocity of the phases is the same (no-slip condition), the flow is called *homogeneous* and the void fraction can be calculated from a knowledge of the volumetric flow rates,

$$\alpha_h = \frac{Q_G}{Q_G + Q_L} = \frac{U_{GS}}{U_{GS} + U_{LS}} \tag{2.4}$$

When the no-slip condition is not valid (nonhomogeneous flow), the void fraction must be estimated through correlations or methods developed for the conditions of interest. Generally, for dispersed bubble flow the homogeneous no-slip model is used (Andreussi et al., 1999; Gomez et al., 1999; Chen et al., 1997). This assumption takes even more validity in horizontal flow, where the slip between the phases can be negligible. Notwithstanding, Daniels (1995) suggests that for the bubble and slug

regimes in horizontal flow (those of interest in this study), the void fraction can be determined using the following expression

$$\frac{\alpha}{1-\alpha} = \left[\frac{1}{0.2 + 1.2\frac{U_{LS}}{U_{GS}}}\right] \tag{2.5}$$

However, a simplification of Equation 2.5 shows that it is equivalent to the homogeneous void fraction divided by 1.2

$$\alpha = \frac{1}{1.2}\left[\frac{U_{GS}}{U_{GS} + U_{LS}}\right] \tag{2.6}$$

Since Equation 2.5 is simply a multiple of the homogeneous void fraction, and there is not valuable information incorporated through its use, the void fraction using the homogeneous model is employed in this study.

Gas to liquid mass ratio

The gas to liquid mass ratio (GLR) is widely used in the analysis of gas-liquid sprays. As indicated by its name, it is simply the ratio of the gas to the liquid mass flow,

$$GLR = \frac{\dot{m}_G}{\dot{m}_L} \tag{2.7}$$

where $\dot{m}_G$ and $\dot{m}_L$ are the mass flow rates of gas and liquid, respectively. When the gas phase is air, this parameter is sometimes expressed as the air to liquid mass ratio (ALR).

Actual velocities

The actual velocities are defined in terms of the actual area of the pipe cross-section occupied by each phase. They also can be expressed in terms of the void fraction and superficial velocities,

$$U_G = \frac{Q_G}{A_G} = \frac{U_{GS}}{\alpha} \tag{2.8}$$

$$U_L = \frac{Q_L}{A_L} = \frac{U_{LS}}{(1-\alpha)} \tag{2.9}$$

2.1.2 Two-phase flow patterns

The two phases in gas-liquid flow can be distributed in a variety of flow patterns or regimes. The importance of the knowledge about the pattern adopted by a gas-liquid mixture, is that the model or approach followed to study its flow behavior depends on the arrangement adopted by the phases. Hosler (1968) suggested that the recognition of the flow pattern in gas-liquid flows is as important as determining whether a single-phase flow is in the laminar or turbulent regime.

In horizontal pipes, the regimes exhibit a non-symmetrical pattern as the result of the gravity effect on fluids with different density. Although a large number of designations have been suggested by different researchers, four basic regimes generally describe the various patterns that can be found in horizontal gas-liquid flows - these are, dispersed bubble, intermittent, annular and stratified flow. Barnea et al. (1980b) present a good description of these regimes:

- *Dispersed bubble.* Is characterized by the distribution of the gas phase as discrete bubbles within the continuous liquid phase. In the transition to this pattern, bubbles are mainly located at the top half of the pipe, and as the liquid rate is increased the bubbles are dispersed more uniformly. This pattern is usually observed at high liquid flow rates.

- *Intermittent.* Is characterized by a non-uniform axial distribution of the liquid and gas phase. Packets of liquid fill the pipe and are separated by zones of gas that contain a liquid layer flowing along the bottom of the pipe. If the packets of liquid are aerated by small bubbles the pattern is known as *slug*, otherwise, the pattern is named *elongated bubble.*

- *Annular.* In this flow pattern the gas phase flows at high velocity as a central core, while the liquid flows as a film around the inside wall of the tube and as drops entrained in the gas core.

- *Stratified.* Is characterized by a complete separation of the phases. The liquid flows along the bottom of the pipe with the gas at the top. When there are no fluctuations at the gas-liquid interface the pattern is called *stratified smooth.* As the gas flow rate is increased, small interfacial waves are formed and the pattern is identified as *stratified wavy.*

The desired distribution of the phases entering the nozzle is that corresponding to dispersed bubble flow; however, the system can operate under intermittent flow when the conditions are not optimum. In consequence, these two flow patterns and the transition between them will receive attention in this thesis.

2.1.3 Flow pattern transitions in two-phase flow

Traditionally the transition between flow patterns in two-phase flow have been determined based on visual observations (Barnea et al., 1980b; Mandhane et al., 1974; Baker, 1954). Experiments are conducted at different operating conditions, pipe geometries and fluid properties. Then, the results are mapped in a two-dimensional plot, usually of superficial velocities, and the transition boundaries are located based on the visual observations. Alternatively, other researchers have directed their efforts towards the development of physical models to analytically predict the flow pattern and the transition limits in gas-liquid flow. Following is a brief description of some of the well known flow pattern maps and models for transition predictions in gas-liquid horizontal flow.

Baker (1954) prepared a generalized plot of the flow pattern regions using the data obtained by other authors. The plot is based on data from 2.54, 5.08 and 10.16 cm pipe. Since most of the data considered was from air-water systems at atmospheric pressure, corrections factors were proposed to adapt the plot to other liquids and gases. Scott (1963) reproduced this chart incorporating modifications to improve the agreement with data of other authors, and found that for pipes having a diameter

smaller than 2.54 cm, the area defined for the different regimes tends to change rapidly as the diameter decreases.

Mandhane et al. (1974) tested the available flow pattern maps with data representing a wide range of flow conditions, and developed a map with physical property corrections. They concluded that there was no observable effect of the pipe diameter for those cases with diameter greater than 2.54 cm, and suggested that any effect was adequately taken into account by using the superficial velocities in the coordinate axes.

Taitel and Dukler (1976) developed a theoretical model describing the transitions through physical mechanisms governing the changes between the flow regimes. They compared the results of the model with the flow pattern map of Mandhane et al. (1974) for a 2.5 cm diameter pipe, and good agreement was found.

Weisman et al. (1979) investigated the effects of fluid properties and pipe diameter on two-phase horizontal flow patterns. They concluded that the relative volumetric flow rates of gas and liquid has the major effect when diagnosing the flow pattern.

Chen et al. (1997) proposed a general model for the transition to gas-liquid dispersed bubble flow, based on the assumption that dispersed bubble flow cannot exist unless the turbulent kinetic energy of the liquid phase is greater than the surface free energy of dispersed spherical bubbles. Nonetheless, they suggested that the model previously presented by Taitel and Dukler (1976) predicts reasonably well the transition to dispersed bubble in horizontal flow.

All of the above mentioned works have resulted in significant improvements towards the understanding and description of the transitions in gas-liquid horizontal flow. However, the model presented by Taitel and Dukler (1976) is selected to be used as reference in this study considering that it has its origin in physical concepts, and has also been validated with experimental results (Barnea et al., 1980b).

Model to predict flow regime transitions by Taitel and Dukler (1976)

Taitel and Dukler (1976) presented the groundbreaking and most durable theoretical model for predicting flow pattern transitions in horizontal and near horizontal gas-liquid flow. Their results were presented in terms of four dimensionless groups X, T, F and K. Figure 2.1 illustrates the generalized flow pattern map based on this model. It must be mentioned that Barnea et al. (1982) revised the criterion for the annular-intermittent flow transition, and modified it in terms of the dimensionless parameter X from a constant value of 1.6 to 0.65 (dotted line).

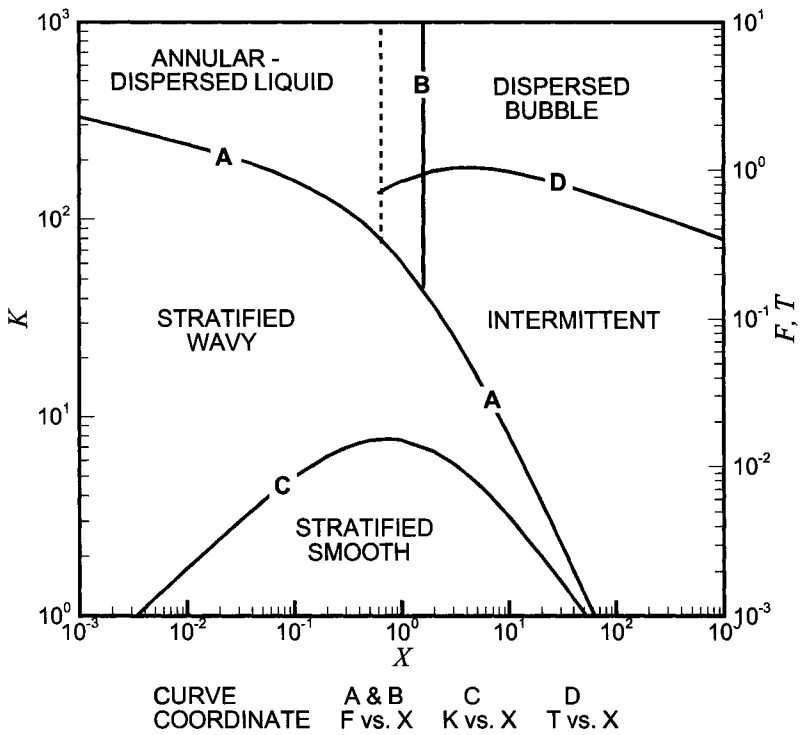

Figure 2.1: Dimensionless flow pattern map based on the model by Taitel and Dukler (1976) to predict flow regime transitions in horizontal gas-liquid flow. The dotted line corresponds to the annular-intermittent transition modified by Barnea et al. (1982).

As can be observed in Figure 2.1, the group X is involved in all the flow pattern transitions. The parameter X was first introduced by Lockhart and Martinelli (1949), and can be calculated knowing the flow rates, fluid properties and pipe diameter. The

expression for X is given by

$$X = \left[\frac{\mathrm{d}P/\mathrm{d}x)_{LS}}{(\mathrm{d}P/\mathrm{d}x)_{GS}}\right]^{1/2} \tag{2.10}$$

where $(\mathrm{d}P/\mathrm{d}x)_{LS}$ and $(\mathrm{d}P/\mathrm{d}x)_{GS}$ correspond to the pressure drop per unit length of liquid and gas flowing alone, and are given by

$$\left(\frac{\mathrm{d}P}{\mathrm{d}x}\right)_{LS} = 4f_{LS}\frac{\rho_L(U_{LS})^2}{2D} \tag{2.11}$$

$$\left(\frac{\mathrm{d}P}{\mathrm{d}x}\right)_{GS} = 4f_{GS}\frac{\rho_G(U_{GS})^2}{2D} \tag{2.12}$$

where ρ_L and ρ_G are the density of the liquid and gas phase, D is the diameter of the pipe, and f_{LS} and f_{GS} are the Fanning friction factor of liquid and gas flowing alone. Considering smooth pipes the Blasius equation can be used to correlate the friction factors,

$$f_{LS} = C_L\left(\frac{U_{LS}D}{\nu_L}\right)^{-n} \tag{2.13}$$

$$f_{GS} = C_G\left(\frac{U_{GS}D}{\nu_G}\right)^{-m} \tag{2.14}$$

where ν_L and ν_G are the kinematic viscosity of the liquid and gas phase. C_L, C_G and n, m are 0.046 and 0.2 for turbulent flow, and 16 and 1 for laminar flow.

In this model it is suggested that the transition to dispersed bubble occurs when the buoyant forces tending to keep the gas at the top of the pipe are overcome by the turbulent fluctuations. This transition is controlled by T, whose expression is defined by

$$T = \left[\frac{(\mathrm{d}P/\mathrm{d}x)_{LS}}{(\rho_L - \rho_G)gcos\theta}\right]^{1/2} \tag{2.15}$$

where g is the acceleration of gravity, and θ is the angle of inclination of the pipe, which is zero for horizontal pipes. According to the authors, the dimensionless group T can be interpreted as the ratio of turbulent to gravity forces acting on the gas. To verify whether certain condition is in the dispersed bubble regime, the calculated value of T is compared with the transition line labeled as "D" in Figure 2.1. Values

of T below this curve correspond to intermittent flow, while those above are in the dispersed bubble regime. It is worthy to note that in reality these transition lines are rather zones where the transition between regimes occurs gradually.

Without further explanation, the expressions of the groups that define the transition from stratified to intermittent or annular flow (F) and from stratified smooth to stratified wavy (K), are given by

$$F = \left(\frac{\rho_G}{\rho_L - \rho_G}\right)^{1/2} \frac{U_{GS}}{(Dg\cos\theta)^{1/2}} \tag{2.16}$$

$$K = F\left(\frac{\rho_L D U_{LS}}{\mu_L}\right)^{1/2} \tag{2.17}$$

where μ_L is the dynamic viscosity of the liquid phase.

The effect of pipe roughness was not considered in this model for the definition of the transitions; however, the authors suggested that the same boundaries continue to apply if $(\mathrm{d}P/\mathrm{d}x)_S$ is calculated considering roughness.

The dimensionless flow pattern map illustrated in Figure 2.1 can also be represented using gas and liquid superficial velocities as coordinates. Although only applicable for a given pipe diameter and fluid properties, this type of representation allows a more direct interpretation of the effect of different variables on the transition boundaries, and facilitates the understanding of the effect of flow rate changes on the expected flow regimes. Figure 2.2 shows the dispersed bubble to intermittent, and intermittent to annular flow transition (modified by Barnea et al. (1982)) in a flow pattern map with liquid and gas superficial velocities for a system with air and water at 20°C, 2.43 cm ID pipe and different operating pressures. The parameters considered to elaborate Figure 2.2 were selected based on the existent conditions in the system to be evaluated, where the pipe ID is 2.43 cm, the temperature is around 20°C and the operating pressure changes as the flow rates are varied. Figure 2.2 shows that the operating pressure has an effect on the flow pattern transition; however, it is observed that this effect becomes smaller when the pressure ratio decreases.

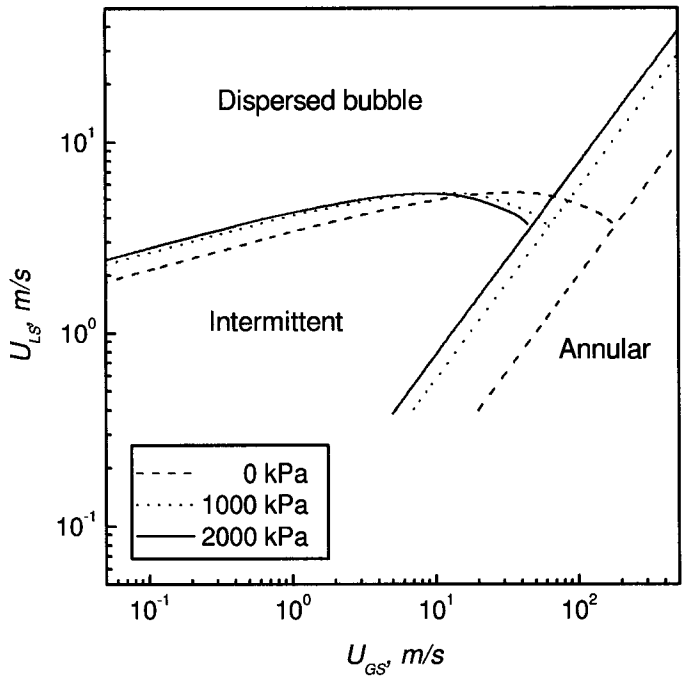

Figure 2.2: Flow pattern map based on the model by Taitel and Dukler (1976) with gas and liquid superficial velocities as coordinates. Air and water as fluids at 20°C, 2.43 cm ID pipe, and different operating pressures. The transition from intermittent to annular flow is the one modified by Barnea et al. (1982).

One of the limitations when using this type of flow pattern map is that the transitions are defined for developed flow or equilibrium conditions; which is not necessarily always the case. Despite this limitation, the use of flow maps offers a good understanding of the effects of different parameters and flow conditions on the performance of the system. In consequence, the concept of plotting operating conditions in a map with superficial velocities as coordinates will be used to select the conditions to evaluate, as well as to present and compare some of the results obtained in the evaluation of different pipe configurations.

2.2 Flow patterns and stability of gas-liquid sprays

Some atomizers have been designed to make the most of the gas decompression to improve the atomization of liquids. That is the case, for example, of the effervescent atomizers and the nozzles used in the fluid coking process. One of the drawbacks found with this type of nozzles is the development of instabilities in the spray caused by the two-phase flow pattern formed inside or upstream the nozzle. In this regard, several studies that have shown this behavior are briefly reviewed in this section.

Roesler and Lefebrve (1989) studied the performance of an aerated-liquid (effervescent) atomizer operating under bubbly flow conditions. They found that when increasing the ALR, for a given operating pressure, the spray eventually becomes unstable. It was suggested that the appearance of these instabilities was marked by the transition from bubbly flow to churn or slug flow (intermittent flow). Additionally, it was found that the transition to unstable operation occurred at higher ALR for higher operating pressures.

Subsequently, Whitlow and Lefebvre (1993) experimentally investigated the performance of a twin-fluid atomizer operating with the effervescent atomization method. They considered conditions over a wide range of ALR, covering the bubbly, transition, and annular flow. They found that as the ALR increases, for a constant operating pressure, at some point a value is reached at which the spray becomes unstable. This undesired condition was correlated to what was called "transition" regime, which consists of an intermittent flow pattern such as slug, plug or churn. For further increase in the ALR, the annular flow regime was reached and the spray became stable again. In summary, they found a strong relation between the gas-liquid flow-pattern within the nozzle and the stability of the spray ejected from the atomizer.

Luong and Sojka (1999) used the interparticle time distribution (Edwards and Marx, 1995) to investigate the dependence of effervescent spray unsteadiness on operating conditions, spatial locations and fluid properties. They mentioned as an example of

unsteady behavior the droplet clustering, which is related to the description given for unstable sprays in Section 1.3. They established that the spray becomes more unsteady when lowering the liquid (glycerine-water mixture) mass flow rate, due to the transition between flow regimes, however; this trend was not exhibited by liquids with higher viscosities, which is probably due to a shift in the transition between the two-phase flow regimes. They also reported that the spray becomes more unsteady at farther downstream distances, as well as towards the edge of the spray.

In the patent of an acoustic method for monitoring and controlling two-phase fluids flowing through feed nozzles, Baker et al. (1991) described that the steam-bitumen mixture sprayed into the fluid cokers can be in a stable regime where the phases are finely mixed and produce the desired atomization, or can have an undesirable pattern where the steam and bitumen pass alternately through the nozzle with adverse consequences for the performance of the spray.

Tafreshi et al. (2002) investigated the effect of variations in the two-phase flow on the atomization performance of a commercial scale injector used in fluid cokers. The conditions evaluated corresponded to dispersed bubble and intermittent flow, and found that changes in the two-phase flow structure significantly alter the atomization. Ariyapadi et al. (2005) reported a technique for characterizing the stability of two-phase sprays and suggested that the flow pattern entering the nozzle strongly influences the stability of the spray.

Conclusively, there is sufficient supporting evidence showing that the two-phase flow pattern within or upstream the atomizer has a major effect on the stability of gas-liquid sprays. In the particular case of the nozzle assembly used in fluid coking, this effect is more distinct due to the presence of a conduit installed between the mixing device and the nozzle. In consequence, approaches intending to reach a more uniform distribution of the gas and liquid phases for a larger extent of flow conditions, will result in a wider range of stability for the spray.

2.3 Altering the two-phase flow pattern

Whilst the design of the mixing device and nozzle also affect the spray stability, the focus of this study is on the characterization of the conduit, and improvement of the current stability range through modifications to this pipe. In order to make a well-informed selection of the alternatives that will be experimentally evaluated, in this section is presented a discussion about some approaches to alter the two-phase flow pattern entering the nozzle through changes in the geometry and configuration of the conduit.

The alternatives are oriented to the enhancement of the mixing process along the pipe to obtain a more uniformly distributed two-phase flow entering the nozzle. Some of the alternatives considered in this regard are: sudden expansion-contractions of the pipe cross-section, obstructions and surface roughness. The study of the effect of the length to diameter ratio is also addressed in order to improve the understanding of the two-phase flow development in horizontal pipes.

2.3.1 Length to diameter ratio (L/D)

For a given diameter, the length of the pipe plays an important role in the flow development and, as consequence, in the flow pattern of the two-phase flow entering the nozzle. For instance, a shorter pipe would limit the coalescence of bubbles for the case of intermittent flow, but might not guarantee a proper homogenization of the mixture leaving the mixing device for conditions that correspond to dispersed bubble flow.

Most studies related to two-phase flow in horizontal pipes have been carried out using length to diameter ratios (L/D) large enough to guarantee fully-developed flow, which is not necessarily the case of the feeding pipe used in fluid coking. Some authors have evaluated what length to diameter ratio is required to obtain results that are independent of the inlet device. Although it was not the objective of their studies,

they assessed this issue in order to assure that the results of their experimental evaluations corresponded to fully-developed conditions. Hoogendoorn (1959) considered different entrance mixers and found that the effect of changes in the inlet device was negligible for $L/D = 60$. Weisman et al. (1979) evaluated experimentally what length to diameter ratio was adequate to consider the observations at the end of a pipe as an equilibrium condition, and they found that when using a simple horizontal "Tee" as the mixing device and in the absence of bends, $L/D = 60$ is enough to ensure equilibrium conditions.

The evaluation of this alternative can offer a better understanding of the pipe length effect on the flow development and its influence on the stability of the gas-liquid spray. Additionally, it is worthy to mention that in the last ring of nozzles in the coker (from top to bottom), the conduits are longer than those installed in the other rings. Consequently, the evaluation of the conduit length effect on the stability, can give insights about the performance of the nozzle assemblies located at the bottom of the reactor.

2.3.2 Sudden expansion-contractions of the pipe cross-section

Kondo et al. (2002) studied the behavior of vertical upward gas-liquid two-phase flow through a round tube with an axisymmetric sudden expansion. Specifically, the bubbly and slug flow were considered, with a sudden expansion using pipes from 2 to 5 cm in diameter. The authors found that the bubble diameter downstream of the sudden expansion is smaller than that upstream. Using high-speed videos the deformation and break-up of bubbles was observed at the sudden expansion. For slug flow, the gas-slugs were divided into small slugs, and then broken-up into smaller bubbles. For bubbly flow, due to the strong shear layer of liquid flow formed above the sudden expansion, the bubbles were deformed and broken up into smaller ones.

The above described behavior was observed in the vicinity of the sudden expansion; however, if the flow is allowed to develop further along the pipe with greater diame-

ter, bubble coalescence would occur, and the effect of the sudden expansion in terms of the redistribution of the phases would disappear. In this regard, it is suggested that a series of short sudden expansion-contractions along the pipe (similar to expansion chambers) could improve the distribution of the two-phase mixture entering the nozzle, by breaking-up the bubbles and improving the mixing along the pipe.

2.3.3 Obstructions

Salcudean et al. (1983) investigated the effect of flow obstructions on void fraction distribution in horizontal air-water flow. Two different forms of obstructions were evaluated, peripheral and central, with a flow blockage of 25%. Experiments were performed for the bubbly, slug and annular regimes. The strongest effect of the obstructions was observed in the bubbly flow, where the phase distributions were affected upstream and downstream. The bubbles decelerated upstream of the obstruction, while significant mixing was noticed downstream. They found that the distribution of the gas phase returned to similar conditions to upstream, after 12 diameters for peripheral obstructions, and 30 diameters for central obstructions. For slug flow, the peripheral obstructions exhibited a greater effect on the phases distribution than the central obstructions, and the flow distribution was observed to recover at around $L/D = 12$. The annular flow was the least affected by the obstructions.

In summary, obstructions can induce mixing in the two-phase flow along a pipe, changing the distribution of the liquid and gas phase. This outcome, undoubtedly, would be beneficial to improve the stability of the gas-liquid spray. However, it is necessary to make a proper selection of the obstruction type, as well as its dimension and location in the pipe.

2.3.4 Roughness

Based on the model for flow pattern transitions in horizontal gas-liquid flow presented by Taitel and Dukler (1976), some modifications were implemented in a later work to include the effect of roughness (Taitel, 1977). It was found that the flow pattern transitions for smooth pipes in terms of the dimensionless parameters (F, T, K and X) are also valid for rough pipes, as long as $(\mathrm{d}P/\mathrm{d}x)_{LS}$ and $(\mathrm{d}P/\mathrm{d}x)_{GS}$ are calculated considering the friction factor for rough pipes.

When plotting the flow map with liquid and gas superficial velocities as coordinates, the only change found because of roughness effect was in the transition between intermittent flow and dispersed bubble. Taitel (1977) suggested that this transition occurs at lower liquid flow rate because of the improvement in turbulence caused by roughness.

The effect shown by increments in the surface roughness would be positive for the feeding pipe leading up to the nozzle, since an enhancement in the turbulence would promote the mixing of the gas and liquid phases along the pipe. However, further considerations must be made since the implementation of roughness in the commercial application should take into account the possible deposition of bitumen on the rough surface.

2.3.5 Discussion

The alternatives discussed from Section 2.3.1 to 2.3.4 will be considered for evaluation, and details about their configuration and dimensions are presented in Section 3.1.5. It is important to note that the alternatives to evaluate, as well as the approach followed for their implementation, are subject to an unavoidable industry design limitation stipulating that 1.3 cm diameter core of the pipe should not have any solid blockage. This free path is required for maintenance purposes, specifically, to insert a "rod" along the assembly to clean the nozzle when it is plugged.

2.4 Flow pattern and stability detection

Traditionally, flow visualization has been a technique used for flow pattern determination in two-phase flow, and it has also been employed to obtain guidance in the interpretation of results when using other techniques. As will be described in Section 3.2.3, the visualization of the spray and flow entering the nozzle will be performed as a qualitative technique in the evaluation of the spray stability. However, it is critical to count on an alternative technique that allows the evaluation of the two-phase flow pattern or, directly, the stability of the spray in a quantitative way. In this regard, following is a description of some of the methods for two-phase flow pattern determination pertinent to this study, as well as some techniques for evaluation of the stability and performance of sprays.

2.4.1 Differential pressure fluctuations

Tutu (1982) found that the statistical analysis of differential pressure fluctuations in vertical pipes could be used for flow pattern recognition. In vertical flow the pressure drop between two adjacent measurements points mainly represents the hydrostatic pressure, and can be indirectly associated to the void fraction in the corresponding section. The pressure drop measurements were normalized using the maximum that could be obtained when the pipe is completely filled with the liquid phase. Then, calculating the probability density function of the normalized differential fluctuations it was found that the peaks were at values of void fraction that characterize the flow regime present in the pipe. For example, for bubbly flow a single peak was found at $1 - \alpha$, for intermittent flow peaks were found at 0 and 1, and for annular the peak was around 0. Analogously, Matsui (1985) suggested that the flow patterns in horizontal gas-liquid two-phase flow could also be identified using statistical analysis of the differential pressure fluctuations. In this case, the measurements were taken at the same cross-section between the bottom and the top of a horizontal pipe, and were considered representative of the fluctuations of the void fraction at the measuring

section.

One of the limitations for the application of the alternative proposed by Matsui (1985), is that in the case being studied the operating pressure is much higher than the maximum differential pressure expected in one diameter of pipe (≈ 0.25 kPa). In consequence, it is not accurate to measure the pressure at the top and bottom of the pipe and subtract them to obtain a differential pressure fluctuation. An alternative is to use differential pressure transducers with fast response; nevertheless, the necessary connections between the pipe and the transducer can slow the response, in addition to the difficulties derived of having a mixture of gas and liquid in the connection lines.

2.4.2 Electrical conductance

The idea with this technique is to have an electrode that is surrounded by the liquid phase, and a probe or tip that will be in contact with liquid or gas. The principle of measurement has its basis in that the alternating presence of gas and liquid can open or close a circuit, obtaining as result zero voltage when the tip is surrounded by gas and maximum voltage when is in contact with liquid; assuming a conducting liquid. Barnea et al. (1980a) proposed an improved technique using a set of probes to detect flow regimes in gas-liquid flow, and the method was based on the analysis of the trace of the voltage between the probes as function of time. The main disadvantages of this technique are the requirement of high conductivity of the liquid phase, and the possible presence of electrochemical effects on the surface of the probes, which could affect the measurements and results. Additionally, the probes used with this technique are intrusive.

2.4.3 Pressure fluctuations

One of the main difficulties found when analyzing pressure fluctuation signals is that their relation with the flow structure is not direct due to their integral character. The

pressure is an energetic parameter that contains information of many processes occurring in the system. Nonetheless, the use of pressure fluctuations is a very attractive option because the measuring technique is simple, the sensor is non-intrusive and is suitable for a wide range of pressure and temperatures. As follows, is presented a brief review of previous work where the analysis of pressure fluctuations was used for detection of two-phase flow patterns and evaluation of sprays performance.

Two-phase flow pattern detection

Hubbard and Dukler (1966) conducted one of the earliest studies to define and predict flow regimes in horizontal two-phase flow using a non-visual parameter. The authors found that the spectral distribution of the wall pressure fluctuations was an acceptable parameter for flow regime identification. They suggested that the variety of flow regimes can be classified in three main categories with different spectral distributions characteristics, these are: (a) *separated flow*, with the maximum around frequency zero and the amplitude decreasing rapidly with increasing frequency, (b) *intermittent flow*, which displays distinct peaks at non-zero frequencies, and (c) *dispersed flow*, with a fairly uniform distribution of power along a certain frequency band. The authors also presented a method to numerically distinguish between the three categories previously described.

Wambsganss et al. (1994) proposed a method for determining the transition from bubble to slug flow in small horizontal channels, based on the root mean square (RMS) of the pressure fluctuations. The flow pattern transition was associated to an abrupt increase in the RMS of the pressure fluctuations that occurs as mass quality (ratio of the mass of gas to the total mass of the mixture) is increased. Later, Cai et al. (1996) analyzed dynamic pressure data presented in previous work (Wambsganss et al., 1994, 1991), using various chaos measuring tools. The correlation dimension was used to quantitatively identify the transition between flow regimes. When plotted as a function of mass quality they found changes in the trends that could be associated

to the flow pattern transition; however, the changes found were not as clear and abrupt as those obtained when using the RMS of the dynamic pressure measurements. The authors indicated that more work was required to improve the technique before it could be applied in the identification of two-phase flow patterns and their transitions.

Kirpalani (1999) presented a signal processing method for characterization of two-phase flow based on wavelet analysis of pressure fluctuations. Specifically, the global wavelet spectrum (averaging in time of the spectral energy plot), and the scale-average wavelet power (fluctuations in power for a specific frequency band), were used to characterize annular, dispersed and slug regimes. It was found that the dispersed flow is characterized by the absence of periodicity with a wider frequency band, which was also illustrated with power spectral analysis. For the slug flow the pulsations were mainly regular and not much additional information could be obtained using wavelets. An intermittency index was suggested to make distinctions between annular and dispersed flow, but the slug flow was not incorporated in this phase of the analysis due to its regular nature.

Gas-liquid sprays performance

Baker et al. (1991) patented a method for monitoring, by means of dynamic pressures, the state of the gas-liquid mixture flowing through feed nozzles. The authors stated that the technique can easily establish whether the mixture exiting the nozzle was originated from appropriate operating conditions. The monitoring process proposed consists of creating a reference power spectrum from a vibrational sensor installed close to the nozzle (accelerometer attached to the nozzle or pressure transducer in contact with the fluid within the nozzle). When a nozzle is to be evaluated, power spectrums are generated and compared with the reference using a pattern recognition algorithm or visually by qualified personnel.

Tafreshi et al. (2002) investigated the effect of two-phase flow variations on the atomization with feed injectors used in fluid coking. A method for two-phase flow

regimes characterization (Kirpalani, 1999) was applied to analyze pulsation patterns in the flow. Wavelet functions were used to generate time-frequency energy plots of pressure fluctuations measured at the pipe wall (near the exit of the nozzle). The authors recognized differences in the plots that coincide with their observations of the flow patterns, and established that the technique could be used to describe the flow quality in terms of the intensity and frequency of the pulses. Nonetheless, this study did not present practical parameters to represent the differences between the different pulsation conditions.

Ariyapadi et al. (2005) presented a technique for characterizing the stability of two-phase sprays, based on the V statistic for cycle detection and analysis. Tests were performed for different nozzles and test fluids in gas-solid fluidized beds and open-air. The authors found that the nozzle geometry and liquid properties had an effect on the spray stability boundary. They also suggested that the stability of the spray is unaffected when injecting in open-air and in a gas-solid fluidized bed.

2.4.4 Discussion

The selection of the technique for stability determination was mainly based on its capability to offer a quantitative measurement of the stability of the spray. In addition, the measuring technique should allow comparison between the different pipe geometries to evaluate, and be of easy implementation for future evaluation in commercial applications.

Considering the weaknesses and strengthes of the techniques previously described, the pressure fluctuations was the alternative chosen for the stability analysis. The details of the transducers and their arrangement are presented in Section 3.1.4, and the methodology employed for the analysis of the pressure fluctuations is introduced in Chapter 4.

Chapter 3

Equipment and Experimental Procedure

3.1 Equipment description

The experiments were conducted in a commercial-scale spray testing facility at the Syncrude Research Centre (Edmonton, Alberta). One of the main advantages of having access to this facility is that it minimizes the scaling-up problems, which allows a more certain extrapolation of the experimental findings to the expected performance at the commercial facilities. The testing facility can manage a broad range of flow rates to test the performance of the different pipe configurations proposed. Additionally, dynamic pressure transducers were employed to record the pipe wall pressure fluctuations, and video imaging was performed to support the results from the analysis of the pressure fluctuations.

3.1.1 Spray testing facility

A general schematic of the commercial-scale spray testing facility is presented in Figure 3.1. The facility currently operates with air and water as testing fluids. The water and air streams are combined in a mixing device and then flow to the nozzle

through the feeding pipe. The spray generated by the nozzle is discharged into a liquid collector tank, from where the liquid is recirculated into the system.

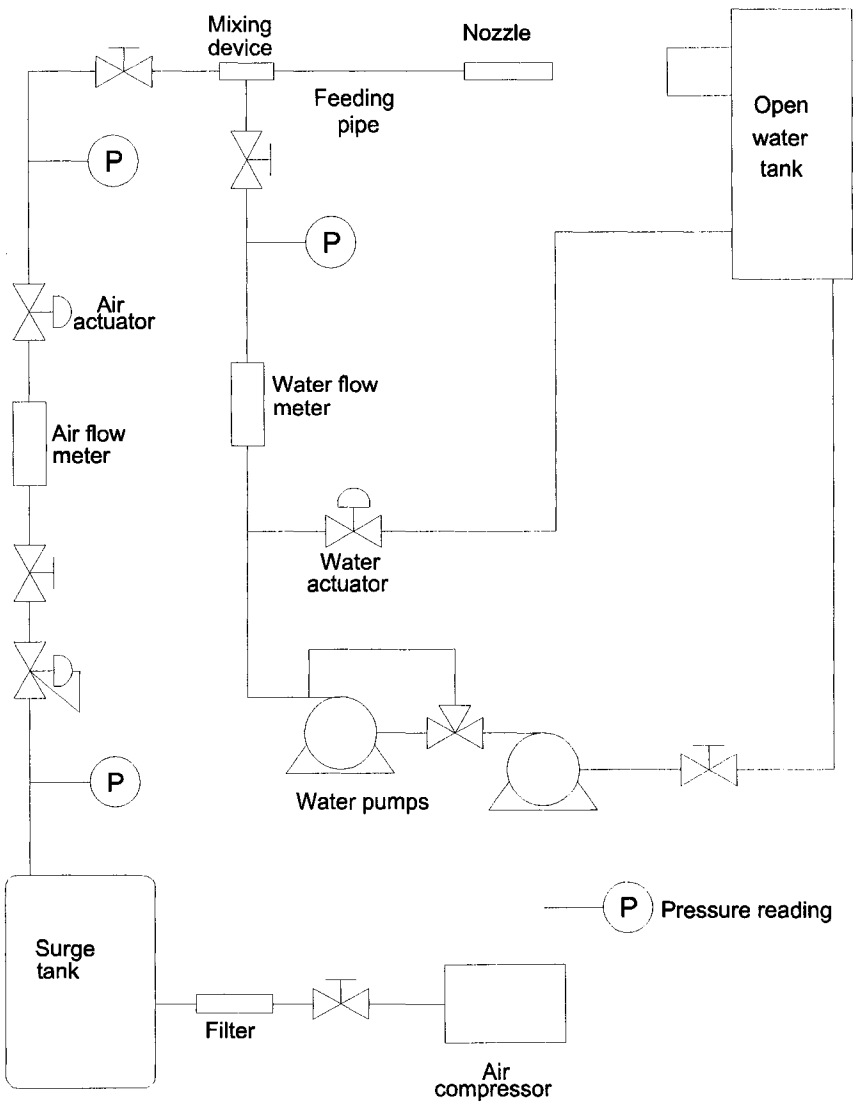

Figure 3.1: Schematic of the commercial-scale spray testing facility at the Syncrude Research Center (Edmonton, Alberta).

The liquid is supplied by either one or two centrifugal pumps, depending on the pressure required for a given flow rate. When one pump is operating, 4 – 25 m^3/hr of liquid can be supplied at 1070 – 1550 kPa, while with two pumps in operation pressures in the range of 2413 – 3882 kPa can be achieved. The gas is delivered by a reciprocating compressor with a capacity of 4.76 m^3/min at 4000 kPa. The air flow is

measured using a Micro Motion coriolis flow meter, while the liquid flow is measured with an electromagnetic flow meter.

A program developed in LabVIEW® permits to either manually or automatically control the flow rates. On the screen interface, the water and air pressure and flow rates are displayed. It also presents a graph with the flows plotted as a function of time. Files in text format can be exported with information of the variables for a given period of interest.

3.1.2 Mixing device, feeding pipe and nozzle

An illustration showing the arrangement of the mixing device, feeding pipe, and nozzle is presented in Figure 3.2. Details of the mixing device and the aspects considered in its design are described in Chan et al. (2001), while the nozzle design and its dimensions are presented in Base et al. (1999).

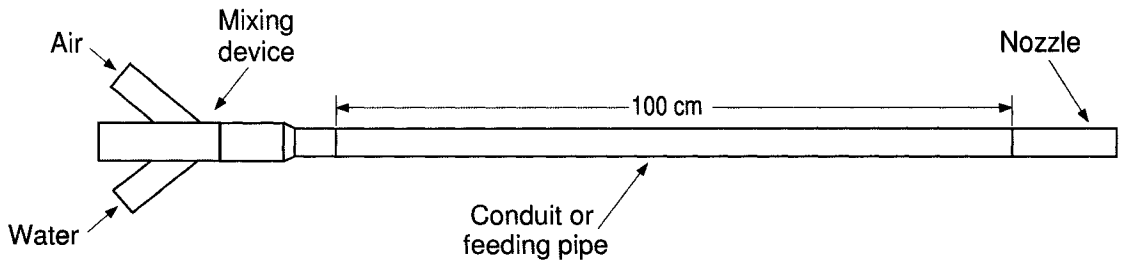

Figure 3.2: Schematic with the arrangement of the nozzle, conduit and mixing device.

The conduit or feeding pipe consists of a 100 cm section of schedule 80 steel pipe with 2.54 cm of nominal diameter (2.43 cm ID and 0.45 cm of wall thickness). These specifications are the same as the pipe used in the commercial operations at Syncrude (Fort McMurray, Alberta). This configuration represents the standard or reference with respect to which the proposed pipe configurations will be compared in terms of their effect on the stability of the spray.

A transparent feeding pipe would ideally facilitate the observation and video recording of the flow structure within the pipe. However, considering the safety standards that must be fulfilled at the Syncrude spray testing facility, the thickness required for a safe transparent pipe would make the visualization difficult and the benefits would probably not compensate the costs involved in obtaining this pipe. Instead, a nozzle constructed with Lexan, including 10 cm of conduit upstream of the nozzle, was used to record high-speed videos.

It must be noted that the design of the mixing device and nozzle were the same for all the experiments, and the focus was on the evaluation of the conduit.

3.1.3 Testing fluids

Air and water were used as testing fluids during the experiments; however, for the operations in the fluid coker the fluids are bitumen and steam. For the range of operating conditions found in commercial operations and those considered in this study, the major difference between the bitumen/steam and water/air systems is found in the surface tension of the liquids, which is around 0.0122 N/m for bitumen and 0.072 N/m for water, respectively. Weisman et al. (1979) investigated the effects of fluid properties on two-phase horizontal flow patterns. The authors varied the surface tension from about 0.068 to 0.038 N/m, and found that the transition of interest in this study, dispersed bubble - intermittent flow, is essentially unaltered. The major change was observed for the transition to stratified wavy, which occurs at significantly higher gas flow rates.

Despite the existing differences between the two-phase mixtures bitumen/steam and water/air, the results from this study can give insights about the performance of the system in the commercial operations.

3.1.4 Pressure transducers

The supporting reasons to select the wall pressure fluctuations for the analysis of the spray stability were presented in Section 2.4.3. Pressure transducers of the piezoelectric type were used to sense the pressure fluctuations due to their capability of measuring rapidly changing pressures. When pressure is applied to the piezoelectric crystal (e.g., quartz), a charge is generated, which is proportional to the pressure applied. The charge generally decays quickly, making this type of sensors suitable for dynamic measurements.

Three piezoelectric pressure transducers, labeled as D1, D2 and D3, were installed at 10, 50, and 90 cm upstream of the nozzle for the standard configuration (See Figure 3.3). This distribution was used for all pipe configurations, with the exception of those with different pipe length. Details of the transducer location for the distinct arrangements are presented in the schematic of their corresponding experimental set-up.

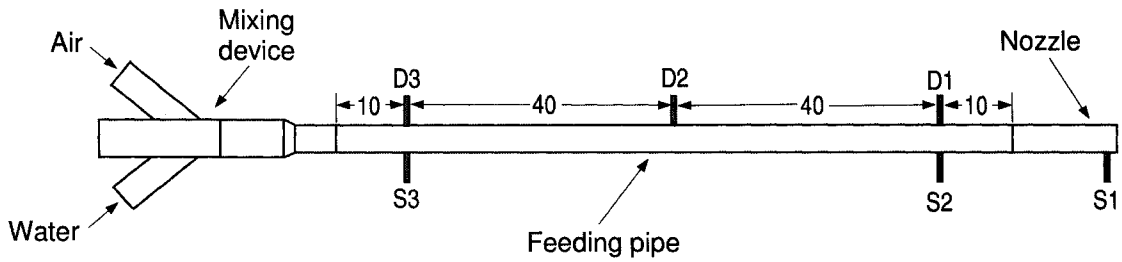

Figure 3.3: Schematic of the standard configuration with pressure transducers along the pipe. Dimensions shown in cm.

Table 3.1 presents the most relevant specifications of the transducers used in the experiments. They were mounted flush with the inside pipe wall to avoid a decrease in the response speed due to the cavity effect. Pressure transducers D1 and D2 correspond to the PCB model 113A21. It consists of an acceleration compensated piezoelectric (quartz) pressure sensor with a microelectronic amplifier incorporated. The transducer D3, PCB model 112A04, also has a piezoelectric sensor, and in

this case the high-impedance output is routed using a special low-noise cable to the impedance-converting amplifier PCB model 422E11, with a sensitivity of 100 mV/pC. An additional transducer D4, which was used in the configuration with a longer pipe, corresponds to the Kistler model 211B5. It has a pair of compression-preloaded quartz assemblies with acceleration compensation. An internal microelectronic circuit converts the charge generated by the piezoelectric material into a high voltage signal. These transducers were powered by the sensor signal conditioner PCB model 442A05, which contains a regulated +24 VDC power supply and 8 adjustable sources of 2 to 20 mA constant current. It also has an increment gain of x1, x10, and x100 per channel.

Table 3.1: Specifications of the dynamic pressure transducers

Performance	**PCB 113A21**	**PCB 112A04**	**Kistler 211B5**
Measurement range (kPa)	1379	690	690
Sensitivity (mV/kPa)	3.6	16.0	8.2
Maximum pressure (kPa)	6895	34475	3447
Resolution (kPa)	0.0207	0.0276	0.0069
Resonant frequency (kHz)	≥ 500	≥ 250	300
Rise time (μs)	≤ 1	≤ 2	2
Low frequency response (Hz)	0.5	-	0.025
Non-linearity (% full scale)	≤ 1	≤ 1	± 1
Label in Figure 3.3	D1, D2	D3	D4

In order to determine the pressure drop through the feeding pipe and nozzle, three pressure transducers, labeled as S1, S2 and S3, were installed at the tip of the nozzle, and 10 and 90 cm upstream of the nozzle, for the standard configuration (See Figure 3.3). This distribution was used for all the pipe configurations, with the exception of those with a different pipe length. The static transducers correspond to the Omega model PX605-300GI, with a range of 0 to 2068 kPa, an accuracy of 0.4 % full scale, and a response time of 5 ms.

The signals from the dynamic and static pressure transducers were recorded using a

supplementary acquisition system with capacity to read 6 signals simultaneously. A program previously developed in LabVIEW® was used. It allows the user to set the scan rate, number of points by data set, number of data sets, file name and file path.

3.1.5 Modifications to the feeding pipe

As presented in Section 2.3.5, the alternatives selected for the characterization of the conduit and the evaluation of its effect on the spray stability are: length to diameter ratio (L/D), sudden expansion-contractions of the pipe cross-section, obstructions, and roughness. The same arrangement presented in Figure 3.3 was considered, and only the feeding pipe was replaced in each case.

Length to diameter ratio (L/D)

The length to diameter ratios (L/D) were selected based on results from previous studies of two-phase flow in horizontal pipes. Hoogendoorn (1959) and Weisman et al. (1979) found that an L/D of 60 allows equilibrium conditions in air-liquid flow. Hence, in addition to the standard pipe (100 cm, $L/D \approx 41$) two other conduit lengths with the same diameter were considered; one above and one below $L/D = 60$. The selected lengths were 38 cm ($L/D \approx 16$) and 180 cm ($L/D \approx 74$). Figures 3.4.a and 3.4.b illustrate their corresponding set-up.

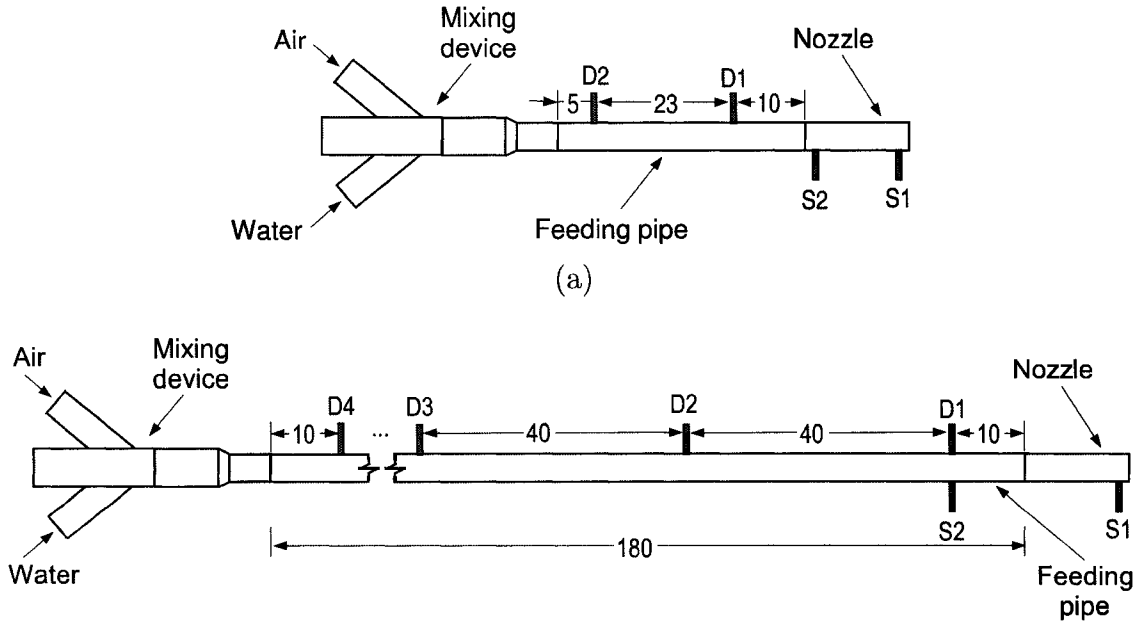

Figure 3.4: Schematic with the set-up for the evaluation of a (a) 38 cm ($L/D \approx 16$), and (b) 180 cm ($L/D \approx 74$) long pipe. Dimensions shown in cm.

Sudden expansion-contractions of the pipe cross-section

This alternative consisted of two sudden expansion-contractions of the pipe cross-section. To implement it, commercially available reducing couplings were used to alternately connect pipe sections of 2.43 cm ID with sections of larger diameter and 7 cm long. The length of the small diameter sections was such that the total length of the arrangement was 100 cm.

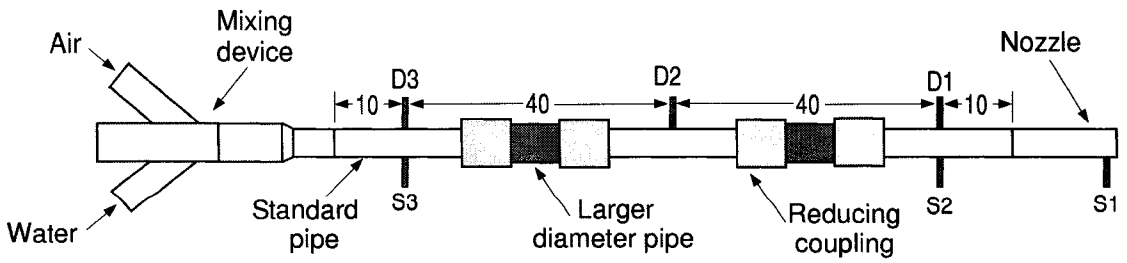

Figure 3.5: Schematic with the set-up for the evaluation of sudden expansion-contractions of the pipe cross-section. Dimensions shown in cm.

The alternatives to evaluate have increments in flow area of 78, 150, and 310 % when using pipes of 3.25, 3.81, and 4.93 cm ID, respectively, for the larger diameter sections. Besides studying the effect of the cross-section expansion-contractions, these three configurations permit to asses the effect of the magnitude of the change in the flow area. Figure 3.5 depicts a general schematic of the set-up for this alternative.

Obstructions

It is specified that for maintenance purposes the central 1.3 cm diameter of the pipe should not have any blockage. In this regard, the obstructions to install along the pipe are of the peripheral type. The inner diameter of the obstructions was defined considering the constraint given above and that a maximum effect on the distribution of the phases was desired. The inside diameter selected was 1.63 cm, which represents a flow area reduction of 55%.

The spacing between the obstructions was defined based on the results from the work of Salcudean et al. (1983), where was suggested that the phase distribution recovers after 12 diameters, for peripheral obstructions. Stipulating that the obstructions would be equally spaced along the pipe, the two following arrangements were considered: (a) 2 obstructions with 33 cm ($L/D = 13.6$) between them, and (b) 4 obstructions with 20 cm ($L/D = 8$) of separation. Figures 3.6.a and 3.6.b depict the experimental set-up for the evaluation of the feeding pipe with 2 and 4 peripheral obstructions, respectively.

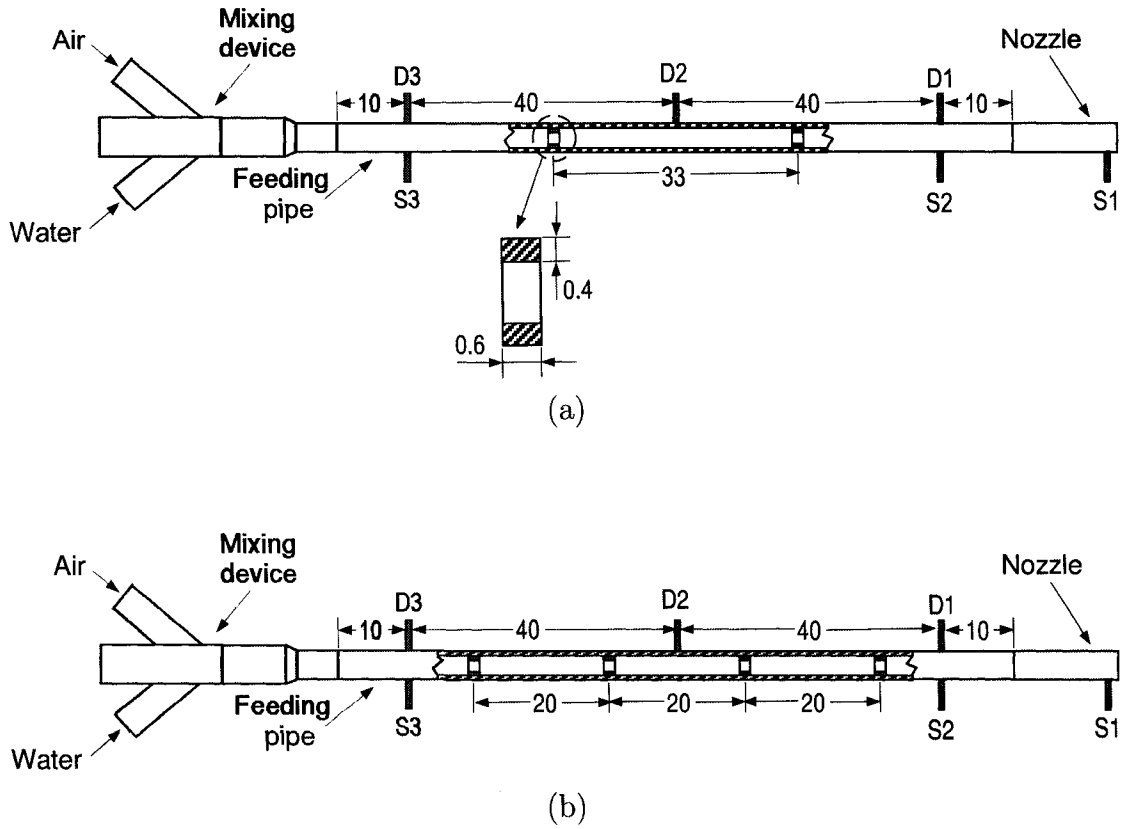

Figure 3.6: Schematic with the set-up for the evaluation of the effect of (a) 2 and (b) 4 peripheral obstructions. Dimensions shown in cm.

Roughness

To define the approach to increase the roughness of the pipe inner surface, the premise was that the change in roughness should be enough to cause a significant positive effect on the structure of the two-phase mixture flowing through the pipe. The alternatives considered were based on a classification or surface roughness in *integral*, which is implemented by restructuring the surface, and *nonintegral*, which is related to the placement of elements (e.g. wire coils) contiguous to the surface (Webb, 1994).

The first alternative considered was to machine the inner surface of the pipe (integral roughness). However, the machining of the surface can reduce the strength of the

pipe and concentration of stresses could appear, compromising in this way the safety of the assembly. The second option considered, and chosen, was based on the concept of nonintegral roughness through the insertion of wire coils along the pipe. For simplicity, a commercially available spring was used with the following specifications: 2.4257 cm OD, 2.0193 cm ID, 0.2032 cm of wire diameter, 2.3 coils per inch, and 25.4 cm in total length. Around 4 springs of this type were installed along the conduit. Figure 3.7 depicts the experimental set-up for the evaluation of the pipe performance with nonintegral roughness.

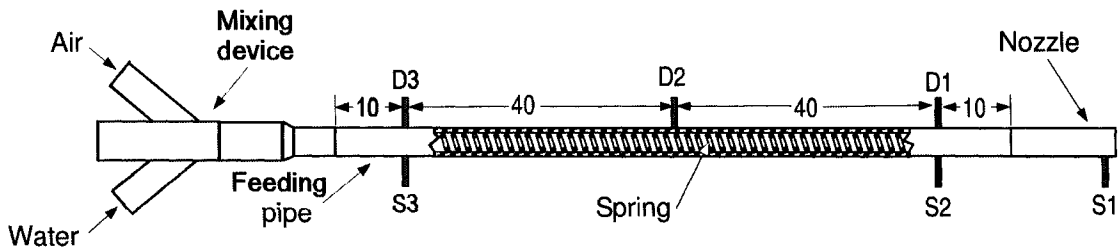

Figure 3.7: Schematic with the set-up for the evaluation of the pipe with nonintegral roughness. Dimensions shown in cm.

3.1.6 Video imaging system

Two different types of videos were used, high-speed and regular-speed, in order to facilitate the understanding of the instability formation process in the spray, as well as to help in the subsequent evaluation of experimental results and validation of the outcomes from pressure fluctuations analyses.

Regular-speed videos of the spray were taken using a Canon PowerShot S410 digital camera. This camera is able to record videos at a maximum of 15 frames per second (fps) with a resolution of 320 x 240 pixels. The videos were taken from a distance that allowed the observation of approximately 24 cm of the spray from the nozzle exit. The objective was to have a record of the spray behavior close to the nozzle tip, which gives a good indication of the spray stability.

The high-speed videos were taken at the spray (close to the tip of the nozzle), and at the short section of pipe and nozzle constructed with Lexan. A Fastcam-X 1280PCI high-speed, digital, monochrome camera was used. It is able to record 1280 x 1024 pixels images at 500 fps, and at reduced resolutions up to 16000 fps. An Auri Sun 1200 W HMI light source was positioned directly opposite to the camera for the videos of the sprays, while front lighting was preferred to observe the dynamics of the system within the transparent nozzle. The high-speed videos were synchronized with data from the dynamic pressure transducer installed just upstream of the nozzle. The videos were analyzed using Photron Motion Tools^{TM}.

3.2 Experimental procedure

An important number of operating conditions were considered for the different configurations. Dynamic and static pressure signals were recorded along the pipe, and were later analyzed using the signal processing techniques presented in Chapter 4. Additionally, for most of the conditions a qualitative evaluation of the stability was performed by direct observation of the spray during the experiments. Video imaging was also considered for some specific conditions corresponding to stable and unstable conditions.

The experimental procedure to be described in this section was preliminarily conducted using the standard configuration. Once the technique for stability determination was validated, the same process was followed with the other arrangements.

3.2.1 Operating conditions

The water and air flow rates were selected in order to have operating conditions in the dispersed bubble, intermittent, and transition zone, with ALR covering the range outlined in the nozzle patent (Base et al., 1999). The model for predicting flow regimes in horizontal gas-liquid flow by Taitel and Dukler (1976) was used as

reference to make the selection of the conditions. It is important to mention that the operating conditions in the commercial case (steam-bitumen system) span the range of dispersed bubble-intermittent flow, according to the model by Taitel and Dukler (1976).

The flow conditions for the standard configuration covered a range of air flow from 1 to 4 kg/min and water flow from 75.7 to 181.7 kg/min, with the pressure in the range of 343.6 to 1573.5 kPa. These conditions correspond to superficial velocities of 2.91 – 11.57 m/s for air and 2.72 – 6.53 m/s for water. The ALR was between 0.55 and 4.41 %, while the homogeneous void fraction was in the range of 0.31 to 0.78.

Figure 3.8 depicts the operating conditions in a flow map with gas and liquid superficial velocities as coordinates. These velocities were calculated with the pressure measured 10 cm upstream of the nozzle, which indicates that the flow conditions represented correspond to those entering the nozzle. The dispersed bubble - intermittent flow transition based on the model by Taitel and Dukler (1976), is superimposed on this flow map. As previously indicated, this transition depends on the operating pressure, thus, a combination of the transitions calculated for 500, 1000 and 1500 kPa was chosen as reference.

Experimentally, these conditions were reached varying the water flow rate from the maximum to the minimum, for each constant air flow. This approach permitted the observation of the progressive change in the stability of the spray, covering a wide range from very stable conditions at higher water flows to unstable at lower water flows.

The operating conditions for the different pipe geometries are within the range of those considered for the standard configuration. However, the selection of the conditions in each case depended on some of the qualitative results that were obtained during the experiments. For those geometries that did not offer an important improvement to the stability of the nozzle, only a limited amount of air flow rates were evaluated.

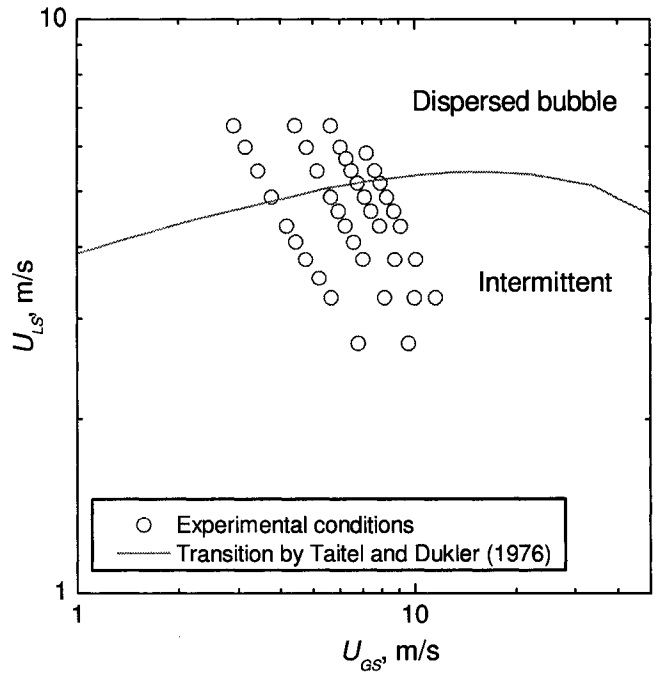

Figure 3.8: Flow map with the experimental conditions for the evaluation of the standard configuration. The dispersed bubble - intermittent transition by Taitel and Dukler (1976), is superimposed as reference.

3.2.2 Pressure Measurements

A preliminary spectral analysis of the pressure fluctuation signal showed that its dominant frequency range is below 100Hz. To satisfy the Nyquist criterion, the sampling frequency should be at least twice the highest frequency component in the signal. However, as will be described later, it was of special interest to establish comparisons between the signals recorded along the pipe. The time lag between these signals was found to be between values of -10 and 10 ms, therefore, the sampling frequency had to be high enough to register these small lag times. In order to optimize the storage capacity and the time required for the analysis, a resolution of 0.5 ms was chosen, which corresponds to a sampling frequency of 2000 Hz. This sampling frequency is one of the reasons supporting the use of dynamic pressure transducers for the pressure fluctuation measurements.

The signals from the three dynamic pressure transducers were simultaneously recorded at 2000 Hz with a sampling time of 50 s. Analogously, the pressure signals from the three static pressure transducers were simultaneously acquired at 200 Hz for 10 s.

3.2.3 Qualitative techniques for stability evaluation

The qualitative techniques relied on visualization of the spray through videos and by direct observations during the experiments. The outcome of the pressure fluctuations analysis was verified using qualitative observations to ensure that the the diagnosis was appropriate. Additionally, high-speed videos were used to facilitate the fundamental understanding of the processes involved in the formation of an unstable spray, and the relation between the pressure fluctuation signal and the stability of the spray.

Direct observation of the spray

Very important information about the stability of the spray was obtained through the direct observation of the spray during the experiments. This technique was regularly used by personnel at Syncrude, and is based on seeing and hearing the spray as it is emitted from the nozzle. Although it is difficult to determine an exact transition from stable to unstable (since the transition is gradual, rather than distinct), it is simple to distinguish between the characteristics of a stable and an unstable spray when observing it.

The stability classification based on the observation of the spray is mainly based on the fluctuations of the spray edges and the sound that it produces. The following descriptions were used to categorize the spray stability:

1. *Stable or smooth.* Borders of spray not fluctuating, and smooth sounding.
2. *Transition or fluctuating.* Borders of jet fluctuating, and smooth sounding. This is within the transition between stable and unstable, but it is not conclusively

one or the other

3. *Unstable or pulsing.* Spray boundaries bouncing, and low frequency audible sound.

The subjective categorizing names presented above (stable, transition, and unstable) are also used when defining the stability condition with other qualitative and quantitative techniques.

Video Imaging

Regular-speed videos of the spray with a duration of 40 s were taken for most of the conduit arrangements at three different operating conditions: 75.7, 113.6, and 151.4 kg/min of water and 2 kg/min of air. Typically, the low liquid flow rate (75.7 kg/min) was pulsing and the high liquid flow rate (151.4 kg/min) was stable. These videos were very useful in giving the opportunity to review them after carrying out the experiments, allowing the validation of previous qualitative evaluations and/or supporting the stability diagnostics obtained from the pressure fluctuations analysis.

High-speed videos were recorded at 2000 and 4000 fps for approximately 6 s, and were synchronized with the signal from the dynamic pressure transducer installed just upstream of the nozzle. Approximately 10% (0.6 s) of each complete video was saved for further analysis. These videos permitted to observe the flow structure just before the nozzle, in the nozzle, and in the spray, for unstable and stable conditions, as well as helped understand the relationship between the pressure fluctuation signal and the stability of the spray. High-speed videos were recorded for some conditions and arrangements that were of more interest.

Chapter 4

Pressure Fluctuations Analysis

The analysis of the pipe wall pressure fluctuations was chosen for evaluation of the spray stability. The implementation of this alternative presents many advantages in terms of the easiness of measuring the pressure fluctuations through sensors that are non-intrusive, and that can be used for different fluids in a wide range of pressure and temperatures. These assets make it an attractive option for implementation in commercial applications. However, the main drawback is the integral nature of this type of signals, which generally contain information of many processes occurring in the system. It is important to be conscious of this feature when analyzing pressure fluctuation signals and drawing conclusions from the results.

This chapter presents a description of the approach followed to analyze the pressure signals. To illustrate the procedure, results obtained from the standard configuration are considered. This permits to have a thorough characterization of this arrangement, which will represent the baseline or reference with respect to which the other configurations will be compared in Chapter 5.

4.1 Description of the pressure fluctuations

As previously discussed, the pressure fluctuations in gas-liquid flow are generally affected not only by the characteristics of the flow, but by many other processes occurring within the system. For instance, Samways et al. (1997) suggested that the pressure at any point in a two-phase flow is provoked by the hydrodynamics of the flow, or by undesired pressure fluctuations from restrictions, pumps, or vibrations from external sources. In this regard, it is of interest to preliminarily understand the characteristics of the pipe wall pressure fluctuations obtained in the nozzle assembly, as well as their relation with the stability of the gas-liquid spray.

4.1.1 Characteristics of the pressure fluctuation signal

Figure 4.1 depicts one second of the pressure fluctuation signal for a stable (2 kg/min of air and 151.4 kg/min of water) and an unstable (2 kg/min of air and 75.7 kg/min of water) condition. The signals were sampled with the pressure transducer (D1) installed just upstream of the nozzle in the standard configuration.

According to the model by Taitel and Dukler (1976), these stable and unstable conditions correspond to dispersed bubble and intermittent flow, respectively. By direct observation, the signal for the stable case does not show a clear pattern. In contrast, the signal corresponding to the unstable condition has a definite shape with a fairly constant frequency that could be anticipated to be between 7 and 8 Hz.

The magnitude of the pressure fluctuations is evidently greater for the unstable case. It is important to mention that the mean pressure for the stable and unstable case is 1070.6 kPa and 528 kPa, respectively, while the corresponding pressure fluctuations are in the range of -20 to 20 kPa, and -150 to 75 kPa, for the period of time displayed. This confirms that the pressure fluctuations are not necessarily proportional to the mean pressure of the system.

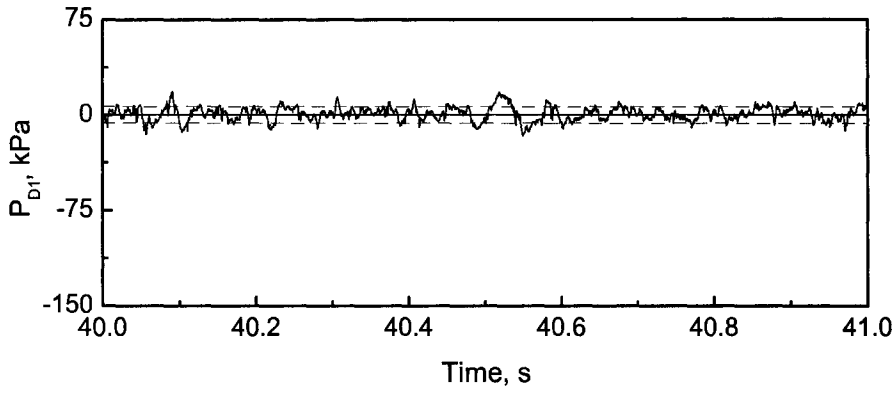

(a)

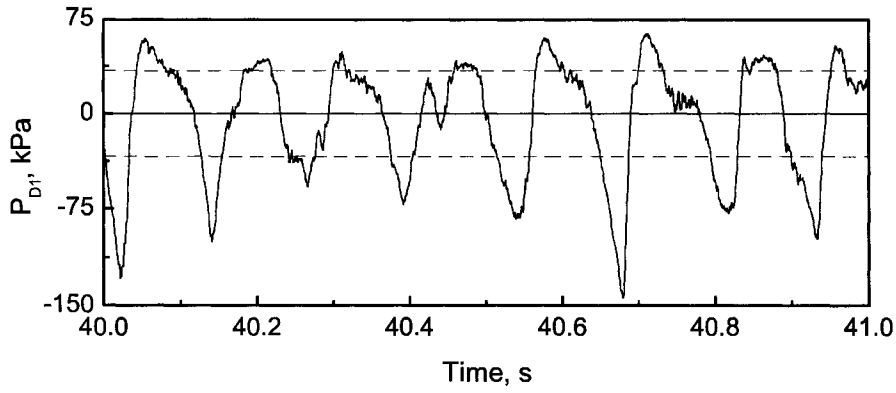

(b)

Figure 4.1: Pressure fluctuation signal for (a) a stable (2 kg/min of air and 151.4 kg/min of water), and (b) an unstable (2 kg/min of air and 75.7 kg/min of water) condition. The dotted lines correspond to the RMS of the pressure fluctuations.

4.1.2 Pressure fluctuation and spray stability

High speed videos were synchronized with the pressure fluctuation signal sampled upstream of the nozzle, as described in Section 3.2.3, to determine whether there was a relationship between the spray stability and the pressure fluctuations. A nozzle constructed with Lexan, including 10 cm of conduit upstream of the nozzle, was connected to the standard pipe and high-speed videos were taken in the pipe section, nozzle and spray.

For the stable case, the spray was relatively uniform without important changes in time or space (See Figure 4.2). Given the stable performance of the spray for this condition, there was not any distinct feature in the spray that could be correlated to the pressure fluctuation signal.

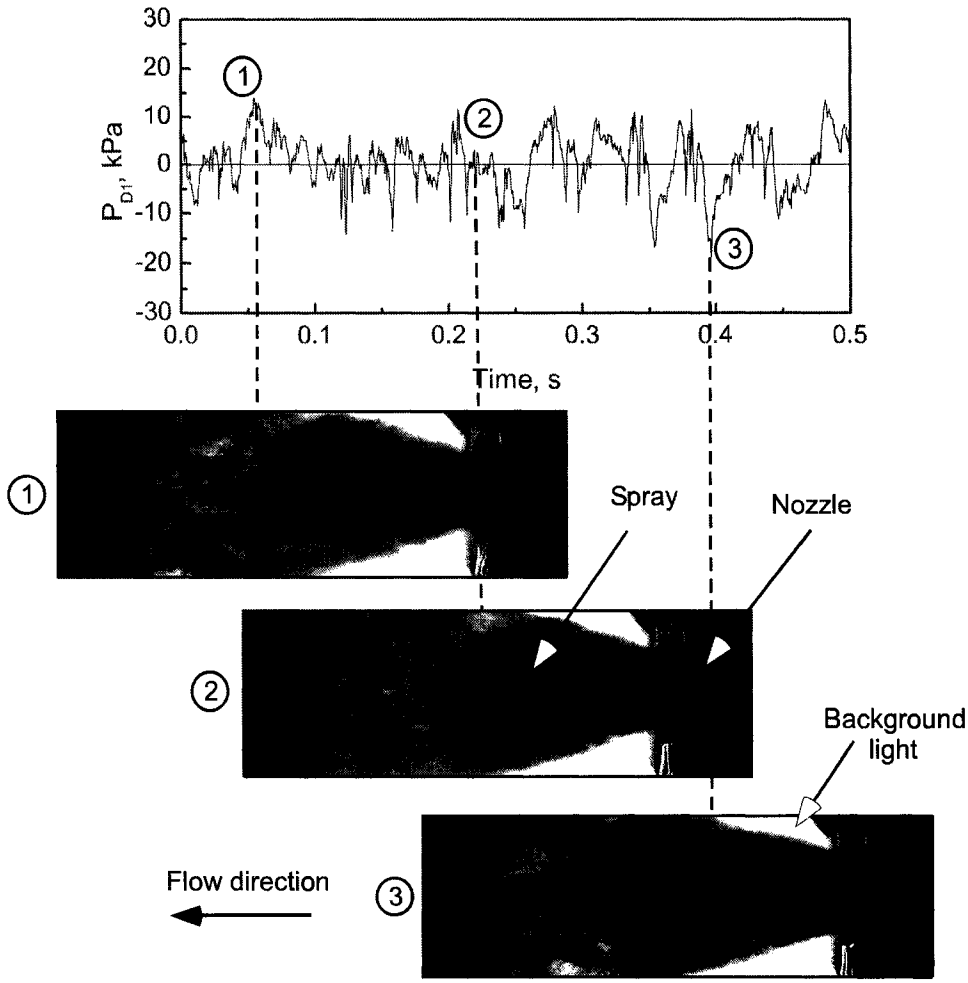

Figure 4.2: Spray pattern at certain points of the pressure fluctuation signal for a stable condition (2 kg/min of air and 151.4 kg/min of water).

Figure 4.3 presents pictures obtained from high-speed videos synchronized with the pressure fluctuation, for an unstable condition. It is important to recall that these videos were recorded using front light for the transparent pipe and nozzle section, whereas back light was preferred for the spray area. Thus, when using front light the water is represented by clear zones due to the light reflection, and the air is associated to the darker areas. The following is a description of some patterns related to the spray instability observed using high-speed videos:

- *Short pipe section*: zones of mainly liquid were followed by zones with important amounts of gas mainly at the top of the pipe. This description is characteristic of an intermittent gas-liquid flow pattern in horizontal pipes.
- *Nozzle*: reverse flow, indicative of recirculation, was observed to occur just before the second contraction, towards the periphery of the nozzle.
- *Spray*, zones of good droplet dispersion were followed by zones with the presence of ligaments and big droplets. This corresponds to the descriptive characteristics previously given for unstable sprays.

Correlating the pressure fluctuations with the above described spray characteristics, it is found that in a cycle of the signal the spray presents a section of good dispersion followed by a section with big droplets and ligaments. This pattern is repeated for all cycles of the signal, permitting to establish a direct relation between the instability of the spray and the pressure fluctuations.

The previous description of the pressure fluctuation signal and its relation with the stability of the spray, does not permit to infer about the phenomena causing the fluctuations in the pressure. A further and detailed analysis based in the cross-correlation between the signals sampled along the pipe is presented in Section 4.2.2, which offers insights about the possible sources originating the pressure fluctuations in the system.

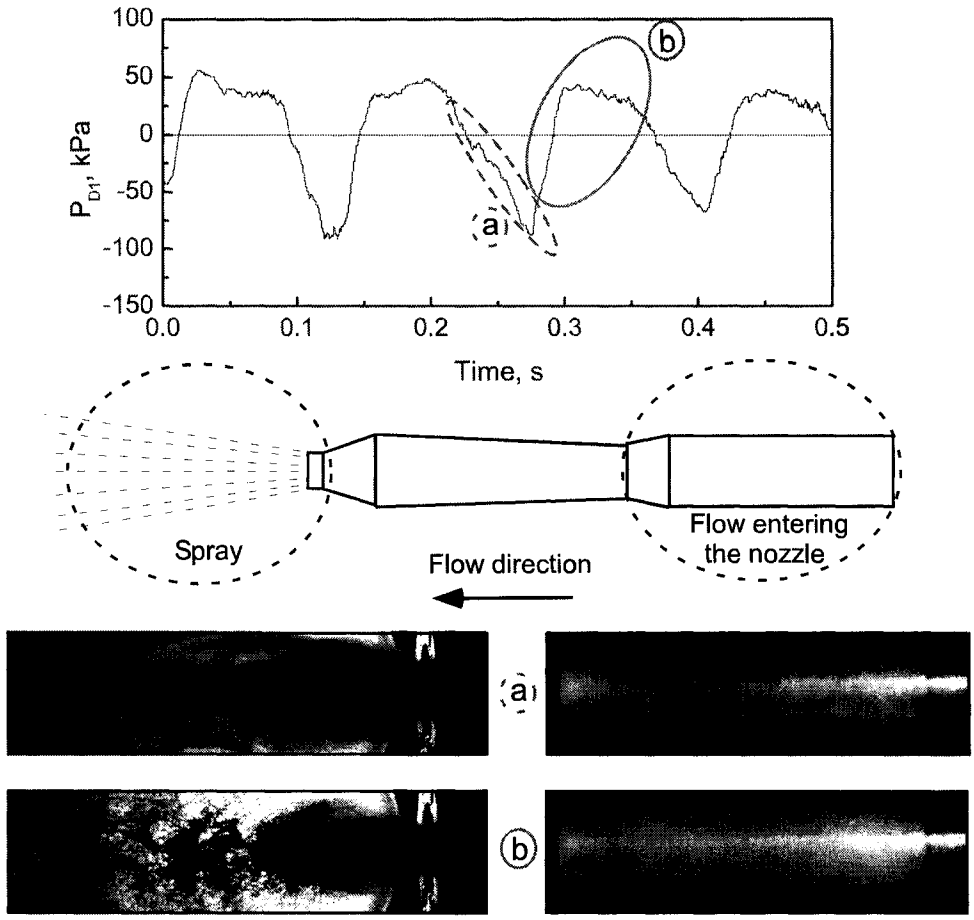

Figure 4.3: Images of the spray and flow in the pipe correlated with the pressure fluctuation signal for an unstable condition (2 kg/min of air and 75.7 kg/min of water). Two main sections were identified: (a) important amounts of gas in the pipe and spray with good droplet dispersion, (b) liquid filling the pipe and spray with ligaments and big droplets.

4.2 Pressure fluctuation signal processing

The aim when defining the technique to analyze the pressure fluctuations was to propose a simple and effective method to determine the stability of the spray and, thus, make a proper comparison between the different feeding pipe geometries in terms of their effect on the spray stability.

The analysis of the pressure fluctuations to be presented is based on statistical tech-

niques that allow the determination of particular characteristics of the signals. Similar to the approach suggested by Drahoš and Ĉermák (1989), the analysis was focused on the amplitude, time and frequency domain of the signal. The pressure fluctuation signals and qualitative results obtained when evaluating the standard configuration are used to illustrate the information that can be obtained from each domain, as well as the performance of the representative parameters that were chosen for the stability analysis. A more detailed description of the statistical functions presented below can be found in Bendat and Piersol (1986), Press et al. (1986), and Otnes and Enochson (1978). See Appendix A.1 for experimental conditions and qualitative evaluation of the standard configuration.

4.2.1 Amplitude domain

The probability density function (PDF) of the pipe wall pressure fluctuations provides some insights about the characteristics of the signal. The PDF can be estimated computing a histogram of the signal, and normalizing it by the total number of data considered. Figure 4.4 depicts the PDF of the pressure fluctuations obtained with the transducer installed just before the nozzle, for a stable and an unstable condition. For the stable case, the PDF is symmetric with respect to the mean zero, whereas for the unstable case certain asymmetry appears, although the mean continues being zero.

Whilst there is a definite difference in the PDF for the stable and unstable case, it is necessary to quantify the information that it presents. To do so, the moments of the data being analyzed can be computed. The first moment is the *mean* which is an indication of the central tendency of the data, and, by definition, is zero in the case of the pressure fluctuations. The second central moment is the *variance*, and can be estimated for a set of data $x_n, n = 1, 2, \cdots, N$, by

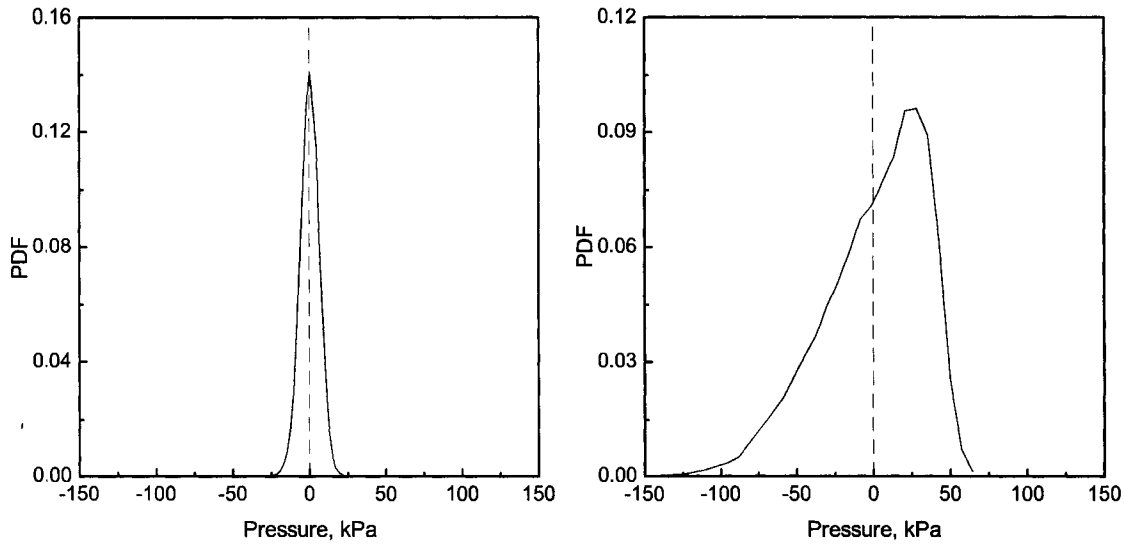

Figure 4.4: Probability density function of the pressure fluctuation signal for (a) a stable (2 kg/min of air and 151.4 kg/min of water) and (b) an unstable (2 kg/min of air and 75.7 kg/min of water) condition.

$$\sigma^2 = \frac{1}{N-1}\sum_{i=1}^{N}(x_i - \bar{x})^2 \tag{4.1}$$

where $\bar{x}$ is the estimation of the mean value of x_n. The positive root mean square of the variance is the well known *standard deviation* (σ). When the mean is not included in Equation 4.1, the statistic is known as *mean square* value of the set of data, and its positive square root is called *root mean square* (RMS) value. Thus, for signals with mean zero, such as the pressure fluctuations, the variance and standard deviation are equivalent to the mean square and root mean square value, respectively.

Figure 4.5 presents the RMS of the pressure fluctuations as function of the liquid superficial velocity (U_{LS}) for different constant air flow rates. Lower values of the RMS correspond to stable conditions, and as the spray becomes unstable the RMS is observed to increase. However, the stability transitions cannot be clearly defined from these trends.

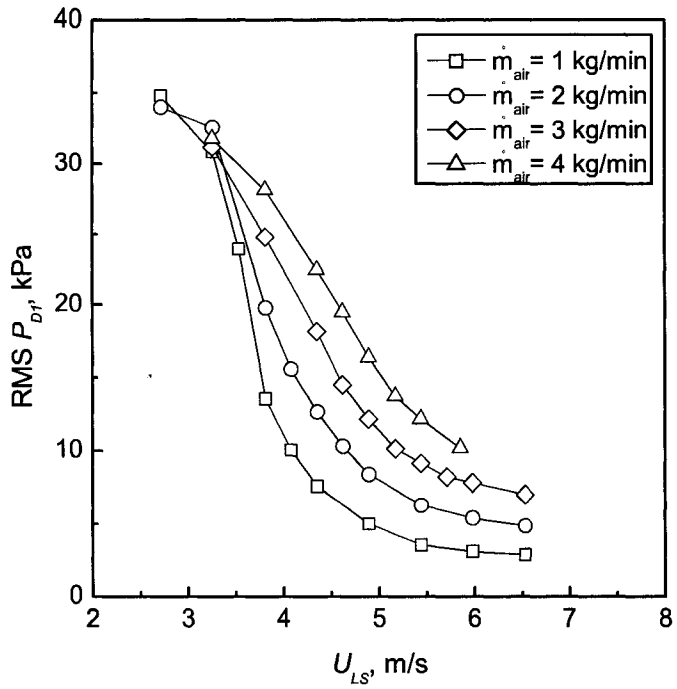

Figure 4.5: Root mean square of the pressure fluctuation signal sampled upstream the nozzle, as function of liquid superficial velocity, for the standard configuration. Each curve corresponds to a constant air flow rate.

Figure 4.6 illustrates how the mean square value of the pressure fluctuation signal changes with liquid superficial velocity (U_{LS}) for different constant air flow rates. The low values correspond to stable conditions and are associated with higher liquid flow rates. As the liquid flow is reduced, for a given air flow, the spray becomes unstable and the mean square value increases. The conditions at which the slope in the trends substantially changes, correlate well with the transition between stable and unstable conditions observed during the experiments. This suggests that a transition zone can be defined around these conditions, as presented in Figure 4.6.

From the analysis of the pressure fluctuations in the amplitude domain, it is clear that the mean square value allows the distinction between the stable and unstable conditions, and presents trends that give indication of where the transition zone is.

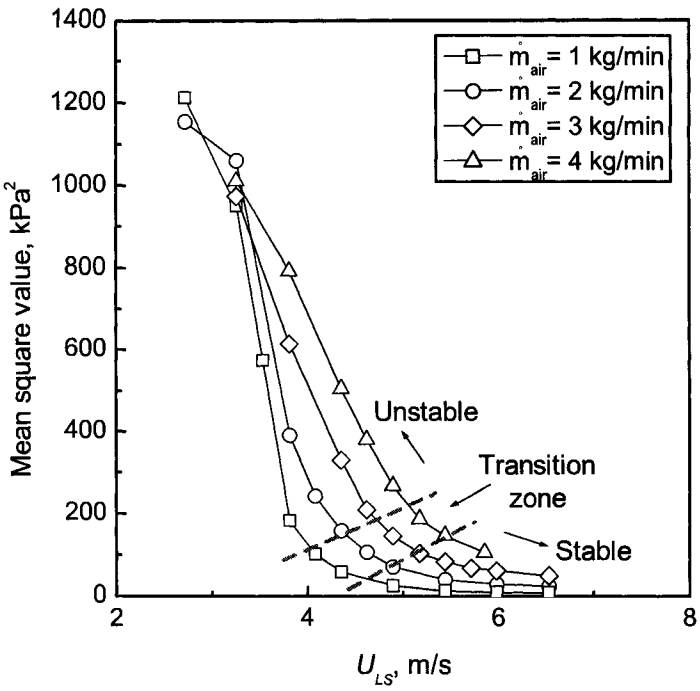

Figure 4.6: Mean square value of the pressure fluctuation signal sampled upstream the nozzle, as function of liquid superficial velocity, for the standard configuration. Each curve corresponds to a constant air flow rate.

4.2.2 Time domain

The analysis in the time domain is related to the evaluation of the cross-correlation function (CCF) and autocorrelation function (ACF).

Cross-correlation function (CCF)

The cross-correlation facilitates the determination of mean time delays between signals, as well as the path followed by them during their propagation. For instance, Lin and Hanratty (1987) calculated the cross-correlation between two pressure signals, and used the time delay at the maximum cross-correlation value to determine the velocity of slugs in two-phase intermittent horizontal flow. Alternatively, Huang et al. (2005) determined the average propagation velocity of pressure waves in air-water bubbly and slug flow using the time shift for the maximum cross-correlation between

two pressure fluctuation signals. Knapper and House (2005) employed this technique to analyze the stability of the spray issued from a nozzle assembly as the one used in this study.

The cross-correlation is used here to analyze the relationship between the signals recorded at different locations along the pipe, and, if possible, identify the sources that generate the pressure fluctuations. This type of analysis is mostly applicable in configurations with no disturbing elements between the measuring points; such as the standard pipe and the conduits with different lengths.

The cross-correlation function for two continuous time series $x(t)$ and $y(t)$, is given by

$$R_{xy}(\tau) = \lim_{T\to\infty} \frac{1}{T} \int_0^T x(t)y(t+\tau)\mathrm{d}t \tag{4.2}$$

For negative values of τ, the relation $R_{xy}(-\tau) = R_{yx}(\tau)$ is considered to compute the CCF. The unbiased estimation of the cross-correlation function between two discrete time series, x_n and y_n, with $n = 1, 2, ..., N$, is given by

$$\hat{R}_{xy}(\tau) = \begin{cases} \frac{1}{N-\tau} \sum_{n=1}^{N-\tau} x_n y_{n+\tau} & \text{for } \tau = 0, 1, \cdots, (N-1) \\ \\ \frac{1}{N-|\tau|} \sum_{n=1-\tau}^{N} x_n y_{n+\tau} & \text{for } \tau = -(N-1), \cdots, -2, -1 \end{cases} \tag{4.3}$$

Expressions in equation 4.3 can be normalized using the maximum value of the cross-correlation, which is $\sqrt{\hat{R}_{xx}(0)\hat{R}_{yy}(0)}$, where $\hat{R}_{xx}(0)$ and $\hat{R}_{yy}(0)$ are the mean square value (variance plus mean) of x_n and y_n, respectively. In the normalized cross-correlation, the maximum value of unity is reached when x_n and y_n are completely identical functions separated by a time lag τ.

As τ increases, less data contribute to the calculation of the cross-correlation, resulting in a more uncertain estimation due to the finite sample size. In this regard, some authors suggest that this estimation is valid for $\tau \leq (5 - 10\%)$ of the total length of the signals (Hubbard and Dukler, 1966; Otnes and Enochson, 1978). Consequently,

the cross-correlation between the pressure fluctuation signals (sampled for 50 s) was estimated up to 2.5 s.

Figure 3.3, in Section 3.1.4, illustrates the position of the dynamic pressure transducers D1, D2 and D3, for the standard configuration. Recalling, transducer D1 is installed 10 cm upstream the nozzle, D2 is at the middle of the conduit and D3 is after the mixing device. R_{31}, R_{32} and R_{21} represent the cross-correlation between the transducers D3-D1, D3-D2, and D2-D1, respectively.

Cross-correlation for an unstable condition

Figure 4.7 presents the normalized cross-correlation between the signals sampled with the transducers installed at the middle of the conduit and just upstream the nozzle (R_{21}), for an unstable condition. The same shape is observed when evaluating R_{31} and R_{32}. Note that when zooming in on the zone of the maximum cross-correlation it is found that the mean time delay between the signals is negative and on the order of milliseconds.

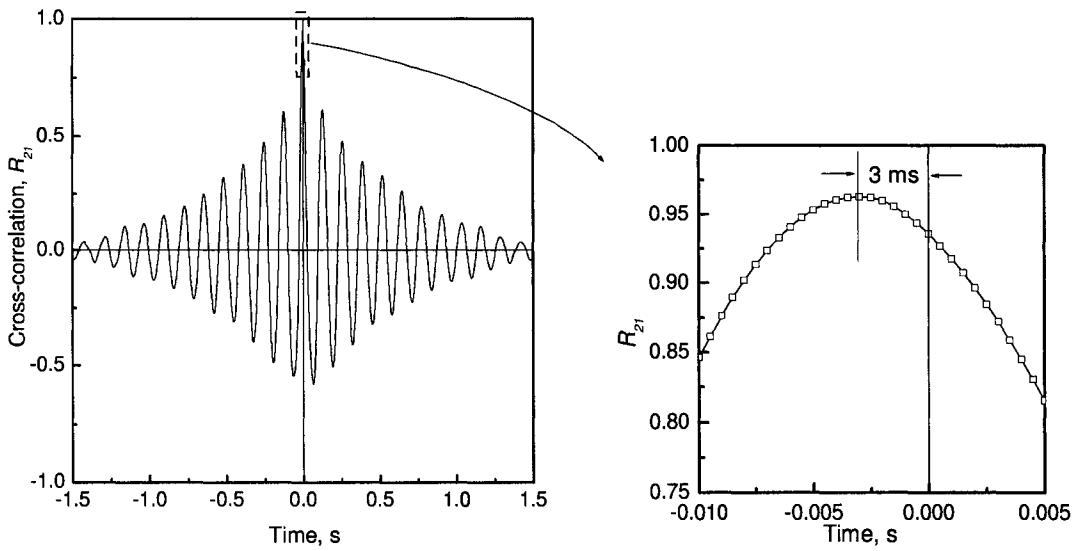

Figure 4.7: Normalized cross-correlation between the signals recorded at the middle of the conduit and just upstream of the nozzle (R_{21}), for an unstable condition (2 kg/min of air and 75.7 kg/min of water).

Table 4.1 presents the maximum value of the normalized cross-correlations R_{31}, R_{32} and R_{21}, and their corresponding lag time. In general, the value of the maximum cross-correlation is close to its upper limit (one), and is also higher when the signals are sampled at closer measuring points. The mean lag time for R_{32} and R_{21} is around half of that found in R_{31}, which is expected considering that the distance between the measuring points in the former cases is half of the distance in R_{31}.

Table 4.1: Cross-correlation and lag time for an unstable condition

Case	Max Norm. R_{xy}	Lag Time, τ (ms)
R_{31}	0.905	-5.5
R_{32}	0.940	-2.0
R_{21}	0.963	-3.0

The negative lag time indicates that the signal propagates in the upstream direction. This is clearly illustrated in Figure 4.8 where the pressure fluctuation signals from the three transducers are plotted for a common time. It is also evident that the strength of the signal decreases with distance in the upstream direction, which suggests attenuation in that direction.

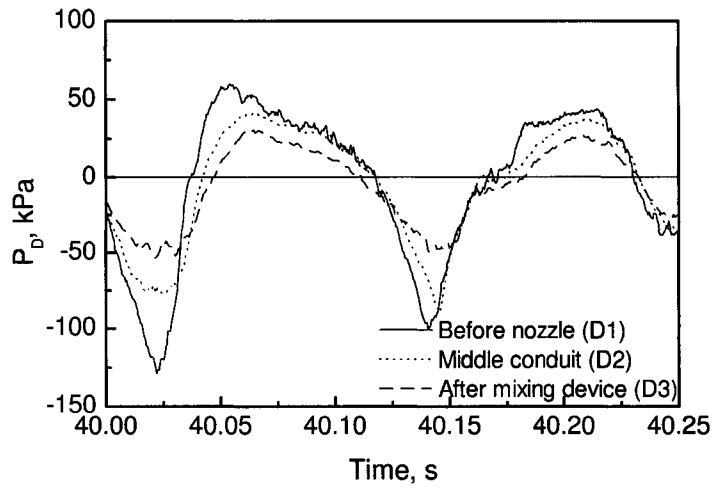

Figure 4.8: Pressure fluctuation signals along the conduit for an unstable condition (2 kg/min of air and 75.7 kg/min of water).

Since the signal propagates in the upstream direction, it can be inferred that the fluctuations in the pressure for unstable conditions are not mainly caused by the local fluctuations of the two-phase mixture flowing in the downstream direction. The question arising would be: *What is the source of these pressure fluctuations traveling in the upstream direction?*, and *What is the explanation for the travel time?*

An estimation of the signal propagation velocity can be performed dividing the distance between the transducers by the mean lag time. For instance, when considering R_{21}, a propagation velocity of 133 m/s is obtained. The uncertainty of this calculation is high ($\approx$ 17 %) because the lag time has a resolution of ± 0.5 ms due to the sampling frequency used (2000 Hz). Despite this fact, it is evident that the propagation velocity is high and, in advance, can be associated to the sound velocity. It is well known that the speed of sound in a two-phase gas-liquid mixture is lower than in either the gas or liquid phase. Nguyen et al. (1981) presented expressions to determine the sonic velocity for different two-phase flow regimes. According to Nguyen et al. (1981), the sonic velocity for homogeneous flow can be estimated by

$$c_m = \frac{1}{(1-\alpha)\sqrt{\left(\frac{1-\alpha}{c_L^2} + \frac{\alpha\rho_L}{\rho_G c_G^2}\right)} + \alpha\sqrt{\left(\frac{\alpha}{c_G^2} + \frac{(1-\alpha)\rho_G}{\rho_L c_L^2}\right)}} \tag{4.4}$$

where c_G and c_L are the sonic velocity in the gas and liquid phase, respectively. Using Equation 4.4, the estimated speed of sound for the same unstable condition (0.779 of homogeneous void fraction and 528 kPa of operating pressure) is approximately 116 m/s. This velocity is smaller than the calculated value using the mean time delay from the cross-correlation function. However, the agreement is good considering the uncertainty in the estimation of the velocity using the mean time delay, and the fact that Equation 4.4 assumes that the phases are well dispersed, which is not the case for the unstable conditions.

Despite the differences between the calculated and measured velocities, the idea of waves traveling at the sound speed in the upstream direction is still valid. Accordingly, it is suggested that the pressure fluctuation signals in the unstable case are

fast-propagating pressure waves generated by some of the processes occurring in the nozzle (coalescence and/or eruption of bubbles). In addition, given the high cross-correlation, it is assumed that the pressure fluctuations traveling in the upstream direction are capable of overcoming the local fluctuations at the measuring points.

Cross-correlation for a stable condition

Figure 4.9 presents the normalized cross-correlation between signals sampled at the middle of the conduit and just upstream of the nozzle (R_{21}), for a comparatively stable condition. The cross-correlation functions R_{31} and R_{32}, depict the same shape. When zooming in on the zone of the maximum cross-correlation it is found that the mean time delay between the signals is positive and on the order of milliseconds. Additionally, it is observed that the cross-correlation rapidly decreases, which is unlike the behavior found for the unstable condition.

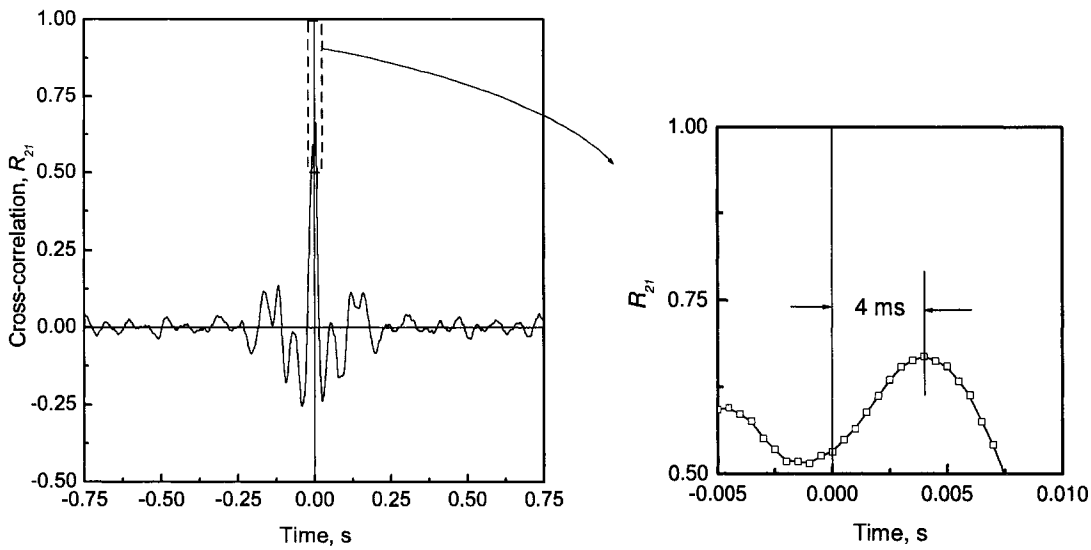

Figure 4.9: Normalized cross-correlation between signals sampled at the middle of the conduit and just upstream of the nozzle (R_{21}), for a stable condition (2 kg/min of air and 151.4 kg/min of water).

The maximum of the normalized cross-correlations R_{31}, R_{32} and R_{21}, and their corresponding shift time are presented in Table 4.2. The maximum cross-correlation is

smaller than in the unstable case. The mean lag time for R_{32} and R_{21} is around half of that for R_{31}. Figure 4.10 depicts the pressure fluctuation signals from the three transducers for a common time, showing less correlation between the signals than in the unstable case.

Table 4.2: Cross-correlation and lag time for a stable condition

Case	Max Norm. R_{xy}	Lag time, τ (ms)
R_{31}	0.373	8.5
R_{32}	0.691	3.5
R_{21}	0.669	4.0

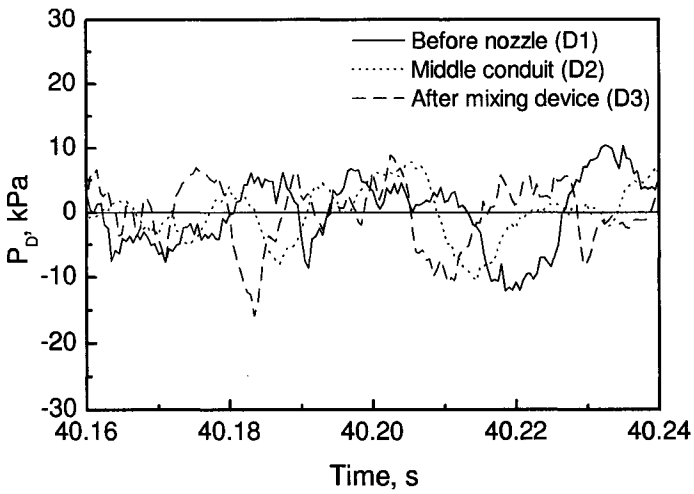

Figure 4.10: Pressure fluctuation signals along the conduit for a stable condition (2 kg/min of air and 151.4 kg/min of water).

The positive lag time for the stable case suggests that the signal is propagated downstream. The calculated propagation velocity considering the lag time at the maximum cross-correlation between the signals at the measuring points 1 and 2, is 100 m/s. Using Equation 4.4 the speed of sound for the same stable condition (homogeneous void fraction of 0.486 and operating pressure of 1070.6 kPa) is 102 m/s. Given that at the stable conditions the flow is more homogeneous, a good agreement is expected between the speed of sound calculated using the expression given by Nguyen et al. (1981), and

that estimated from the lag time at the maximum cross-correlation. Discrepancies in this case, can be due to the uncertainty in the estimation of the propagation velocity.

The velocity and direction of propagation suggest that the pressure fluctuation at each measuring point is a combination of the phenomena occurring in the mixing device (which gives the maximum cross-correlation and positive lag time), and the local fluctuations and sources from other sections of the system. The lower value of the maximum cross-correlation found for the stable case, is probably indicating that signal to noise ratio is lower for the forward propagating perturbations originating at the flow mixer, than for the backward propagating perturbations generated at the nozzle for the unstable case.

Cross correlation for all conditions

Figure 4.11 depicts the maximum normalized cross-correlation and lag time between the pressure fluctuation signals sampled at the middle of the conduit (D2) and just upstream of the nozzle (D1), as function of liquid superficial velocity (U_{LS}), for different constant air flow rates. In general, for stable conditions the cross-correlation between the signals is small with positive lag time, whereas for unstable conditions the cross-correlation is higher with negative lag time. This confirms the findings of Knapper and House (2005).

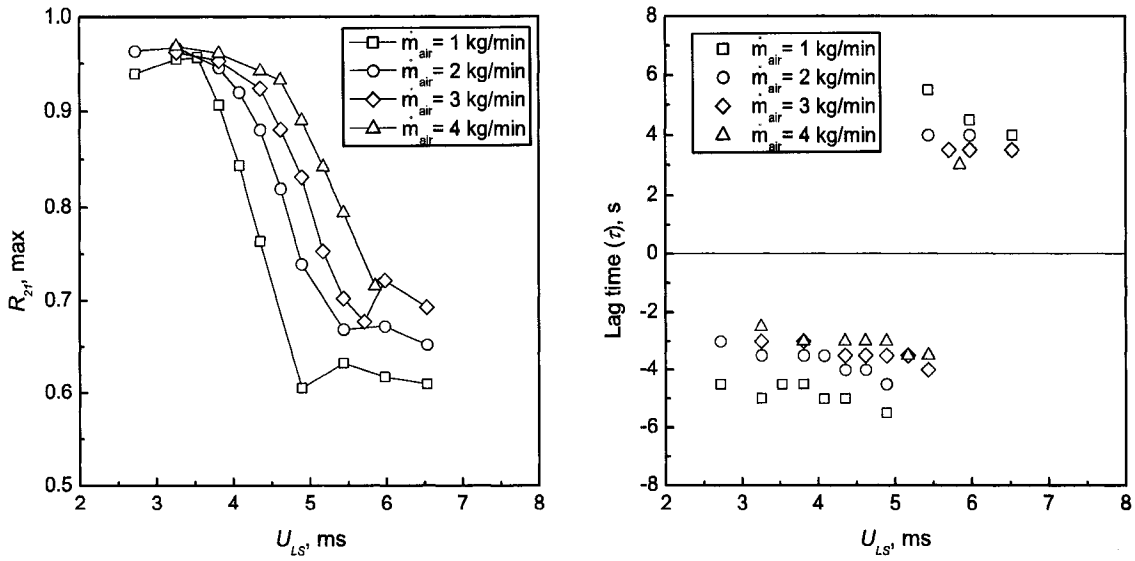

Figure 4.11: (a) Maximum normalized cross-correlation and (b) mean lag time, between signals sampled at the middle of the conduit and just upstream the nozzle (R_{21}), as function of liquid superficial velocity, for the standard configuration.

The CCF cannot be considered a reliable way to make comparisons between different configurations, given that it is mostly applicable for configurations with no additional elements between the measuring points. However, this type of analysis is very effective to identify important characteristics of the signals and their direction of propagation for different stability conditions. For unstable conditions very large disturbances are originated from the nozzle, whereas for stable conditions the disturbances from the mixer dominate.

Autocorrelation function (ACF)

The autocorrelation function (ACF) is a special case of the cross-correlation where the time series $y(t)$ equals $x(t)$. It measures the correlation between observations of the same signal at different times, and is defined by

$$R_{xx}(\tau) = \lim_{T\to\infty} \frac{1}{T} \int_0^T x(t)x(t+\tau)\mathrm{d}t \tag{4.5}$$

The autocorrelation is an even function of τ, thus, it is not necessary to evaluate it

for negative values of τ. The unbiased estimation of the autocorrelation function for a sample time series, x_n, with $n = 1, 2, ..., N$, is given by

$$\hat{R}_{xx}(\tau) = \frac{1}{N-\tau} \sum_{n=1}^{N-\tau} x_n x_{n+\tau} \qquad \text{for } \tau = 0, 1, \cdots, (N-1) \tag{4.6}$$

The maximum of the ACF occurs at $\tau = 0$ and equals the mean square value of the signal. Using the maximum value, the autocorrelation can also be normalized to obtain values between 1 and -1. As in the case of the cross-correlation, the ACF must be estimated satisfying the condition: $\tau \leq (5-10)\%$ of the total length of the signal. Figure 4.12 shows the normalized autocorrelation for the pressure fluctuation signal recorded just upstream of the nozzle for a stable and an unstable condition.

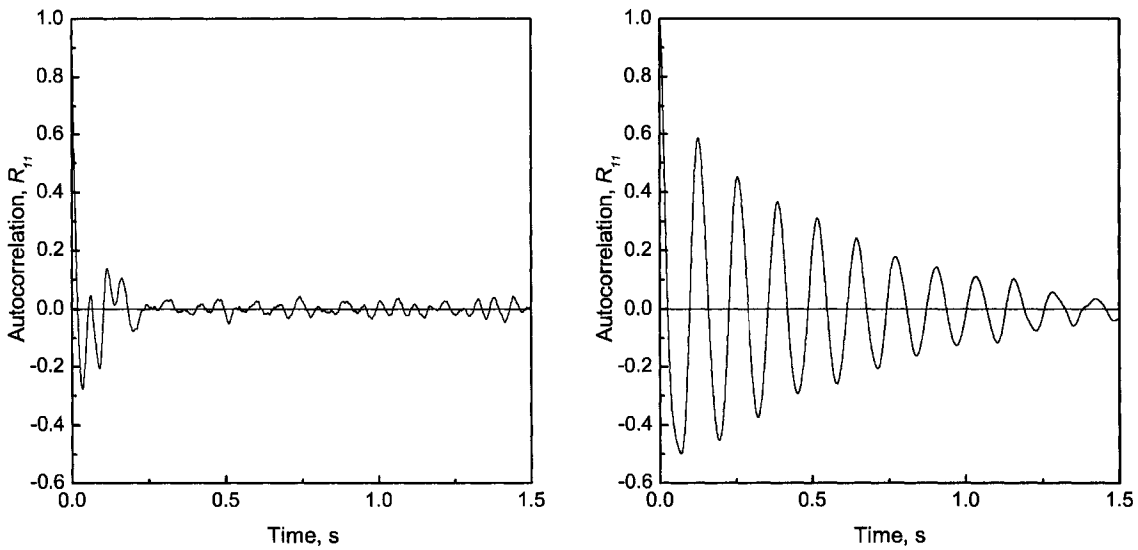

Figure 4.12: Normalized autocorrelation of the pressure fluctuation signal sampled just upstream of the nozzle (R_{11}), for (a) a stable (2 kg/min of air and 151.4 kg/min of water), and (b) an unstable (2 kg/min of air and 75.7 kg/min of water) condition.

The form of the ACF for the stable case shows that the correlation between observations decreases rapidly, while for the unstable case the ACF has an oscillating damped form with a frequency between 7 and 8 Hz. The oscillating form is an indication of the periodicity of the signal; however, the decrease of the strength in time is because the signal is not perfectly periodic. This kind of behavior was observed by Vial et al.

(2001) when identifying regimes in bubble columns and air lift reactors. The authors found that for heterogenous conditions the ACF was characterized by an oscillating component superimposed on random processes, while for the homogeneous regime the shape of the ACF reflected typical random processes. In the present study, the auto-correlation analysis reinforced the observation of the differences between the signals for stable and unstable conditions.

4.2.3 Frequency domain

Some applications require the representation of the data in the frequency domain. The Fourier transform permits one to go from the time to the frequency domain representation, and vice versa. The expressions for the Fourier transform are given by,

$$X(f) = \int_{-\infty}^{\infty} x(\tau) e^{-i2\pi f\tau} \mathrm{d}\tau \tag{4.7a}$$

$$x(\tau) = \int_{-\infty}^{\infty} X(f) e^{i2\pi f\tau} \mathrm{d}f \tag{4.7b}$$

where $x(\tau)$ and $X(f)$ correspond to the representations of the process in the time and frequency domain, respectively.

The power spectral density (PSD) is a representation of the mean square value distribution of the data over the frequency domain. *Parseval's theorem* establishes that the total power of a signal is the same when calculated in the time or frequency domain:

$$Total\ Power \equiv \int_{-\infty}^{\infty} |x(\tau)|^2 \mathrm{d}t = \int_{-\infty}^{\infty} |X(f)|^2 \mathrm{d}f \tag{4.8}$$

$|X(f)|^2$ is the power spectral density of $x(\tau)$, and considering the *Wiener-Khinchin Theorem* it is equivalent to the Fourier transform of the autocorrelation function. The units of the PSD are $[(units\ of\ parameter)^2/Hz]$. The PSD is given by

$$S_x(f) = |X(f)|^2 = \int_{-\infty}^{\infty} R_{xx}(\tau) e^{-i2\pi f\tau} \mathrm{d}\tau \tag{4.9}$$

and by the inverse transformation, the autocorrelation can be expressed as

$$R_{xx}(\tau) = \int_{-\infty}^{\infty} S_x(f) e^{i2\pi f\tau} \mathrm{d}f \tag{4.10}$$

For $\tau = 0$, Equation 4.10 becomes the area underneath the PSD and represents the mean square value of the time series, i.e., the variance plus the square of the mean,

$$R_{xx}(0) = \int_{-\infty}^{\infty} S_x(f) \mathrm{d}f = \sigma^2 + \mu^2 \tag{4.11}$$

and the area underneath the PSD within a frequency range will give an indication of the data mean square value for the specified range. Additionally, at $f = 0$ the PSD equals the square of the mean (μ^2).

The power spectral density function is an even function defined for positive and negative frequencies. A one-sided power spectral density $G_x(f)$ can be defined to consider only the range of positive frequencies. The one-sided function $G_x(f)$ is zero for $f < 0$, while for $f \geq 0$ is given by

$$G_x(f) = 2S_x(f) = 2\int_{-\infty}^{\infty} R_{xx}(\tau) e^{-i2\pi f\tau} \mathrm{d}\tau \tag{4.12}$$

Power spectral density estimation

If a continuous function is adequately sampled, i.e., $X(f) = 0$ for all $f > fc$ (fc is the Nyquist critical frequency, which is half of the sampling frequency), the Fourier transform of the function can be estimated from the finite number of points sampled. Now, the expression given in Equation 4.7a can be approximated by a sum given by

$$X(f_k) = \Delta\tau X_k = \Delta\tau \sum_{n=0}^{N-1} x_n e^{-i2\pi kn/N} \qquad \text{with } k = -N/2, \cdots, N/2 \tag{4.13}$$

where X_k (final sum in Equation 4.13) is known as the *discrete Fourier transform* (DFT). The DFT has taken great importance in the estimation of the PSD because of the availability of the *fast Fourier transform* (FFT), which is a highly efficient algorithm for the calculation of the DFT.

A simple way of estimating the power spectrum is by computing the DFT of the time series, squaring the result, and dividing by the number of data. This estimate is known as the *periodogram*, and should be normalized by the sampling frequency if the power spectral density is sought, instead of the power spectrum. The following is an estimation of the power spectrum for a time series x_n, with $n = 1, 2, \cdots, N$

$$\hat{S}_x(f_k) = \frac{1}{N}|X_k|^2 \qquad k = -N/2, \cdots, N/2 \tag{4.14}$$

and the one-sided power spectrum estimation is given by

$$\hat{G}_x(f_k) = \frac{2}{N}|X_k|^2 \qquad k = 0, 1, 2, \cdots, N/2 \tag{4.15}$$

An inherent problem of this estimate is that the variance is high, and it does not decrease when increasing the amount of data considered. To reduce this variance, the signal can be broken into sections and the discrete Fourier transform of these sections can be averaged at each frequency. This decreases the frequency resolution, but also lessen the variance of the estimation.

The DFT presented in Equation 4.13 can be viewed as that of an infinite time series multiplied by a rectangular window that is always zero except during the sampling time. The Fourier transform of this window has components at higher frequencies, which allows *leakage* of power at frequencies separated from that where the estimation is being done. One way of reducing this effect is to introduce a time window with a central peak as narrow as possible and with the tails falling off as quick as possible, such as the Hamming and Hanning windows. One of the drawbacks of the data windowing is that relevant information is discarded around the beginning and end of each record. To counteract this effect the time series can be divided into *overlapped* segments; 50% of overlapping between the segments is commonly used. The method of averaged and modified periodograms through the use of data windowing and overlapping is known as *Welch's method.*

PSD of pressure fluctuations

To estimate the PSD of the pressure fluctuations, the data were divided into 8 sections, a Hanning windowing was applied with an overlapping of 50%. Given that the FFT algorithms require a block size that is a power of 2, 65536 points of the time series total length were used to estimate the PSD of the pressure fluctuations. Figure 4.13 presents the PSD of signals for the same stable and unstable conditions considered in previous analyses.

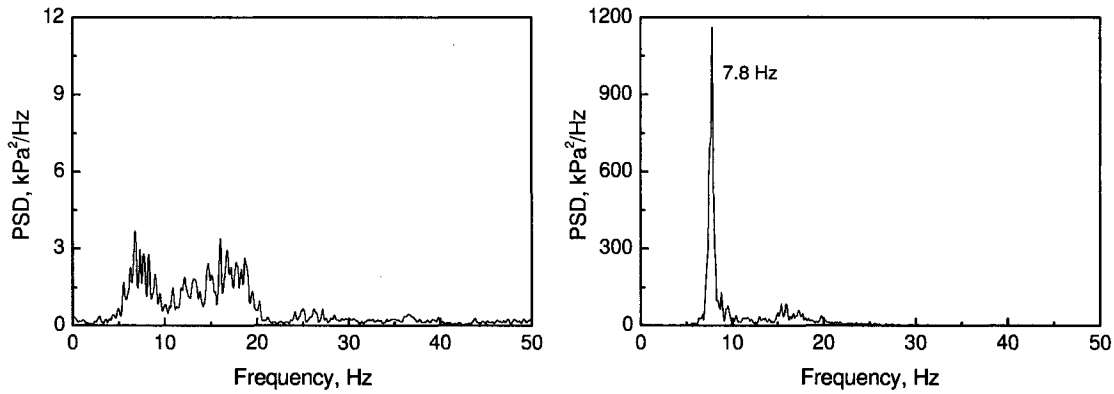

Figure 4.13: PSD of the pressure fluctuation signal sampled just upstream of the nozzle for (a) a stable (2 kg/min of air and 151.4 kg/min of water), and (b) an unstable (2 kg/min of air and 75.7 kg/min of water) condition. Note different scales in (a) and (b).

Figure 4.13 illustrates that the PSD for the unstable case presents a dominant peak at 7.8 Hz. The presence of this peak is an indication of the periodicity of the signal for this condition. Contrarily, for the stable case, no dominant peak is present and the energy is observed to be distributed over a range of frequencies (5–20 Hz). This suggests that the signal for the stable case is non-periodic and contains no dominant frequency. However, when comparing the two PSD it is evident that the magnitude is much higher for the unstable case.

Prior to evaluating alternatives to quantify the information presented by the PSD, some additional conditions are considered to gain more understanding of the PSD

characteristics. Figure 4.14 depicts the PSD of signals corresponding to stable and unstable conditions for 3 and 4 kg/min of air. For unstable conditions a dominant frequency is still found, although some energy is distributed in other frequencies. Despite these slight differences for different air flows, the PSD of the pressure fluctuation signal still presents distinctive differences for stable and unstable conditions.

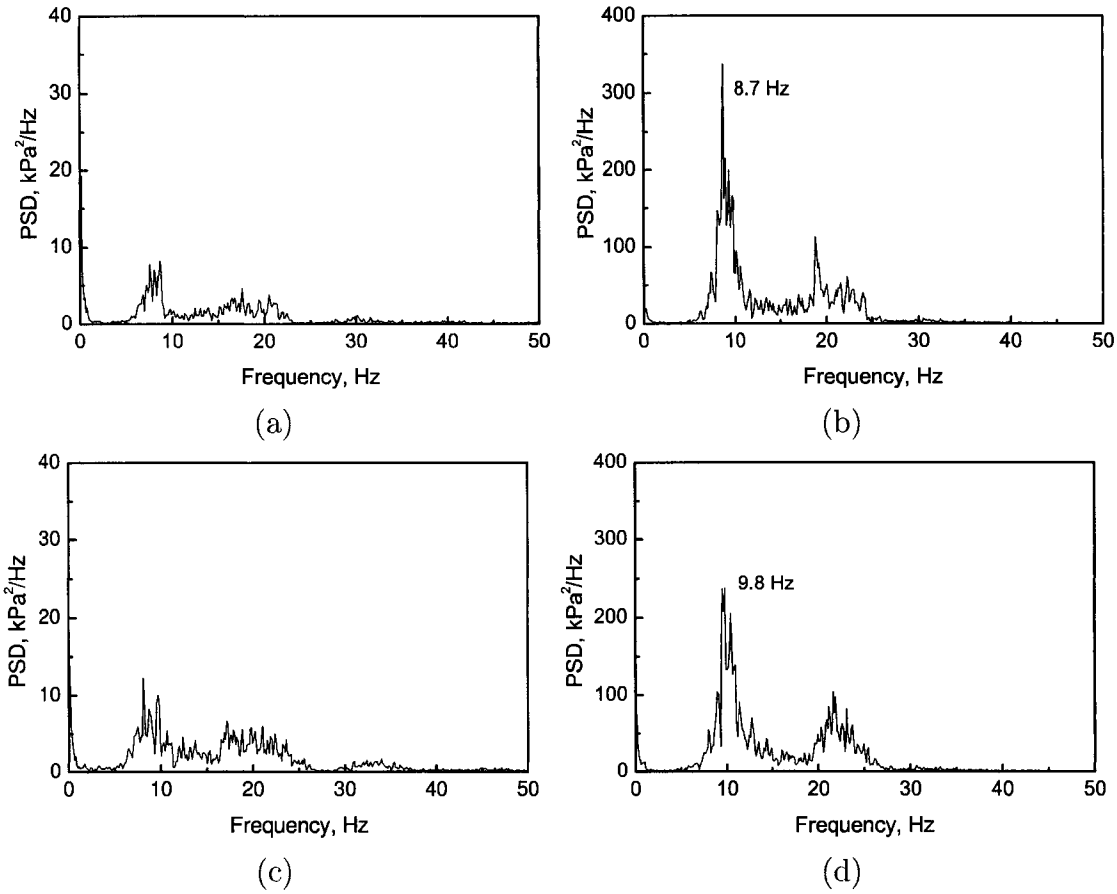

Figure 4.14: PSD of the pressure fluctuation signal sampled just upstream of the nozzle for stable (left) and unstable (right) conditions at 3 kg/min (top) and 4 kg/min (bottom) of air. Water flow rates at (a) 166.6 kg/min, (b) 90.8 kg/min, (c) 162.8 kg/min, and (d) 90.8 kg/min.

In order to use the information given by the PSD of the pressure fluctuations to establish comparison between different stability conditions and different feeding pipe configurations, a practical parameter must be defined. This parameter could be associated with:

1. *The dominant frequency,* which corresponds to the highest peak of the PSD.
2. *The magnitude of the highest peak.*
3. *The energy contained within a certain frequency bandwidth,* which is equivalent to the area beneath the PSD for a certain frequency range.

It has already been discussed that for stable conditions the signals being evaluated are not periodic, which is evidenced by the absence of dominant peaks and the distribution of the power along a frequency range. In other words, what the PSD is representing is an average or superposition of the dominant frequencies found during the sampling time. In this regard, given the absence of a dominant peak in the PSD for certain conditions, a parameter based on options 1 and 2 would not permit to effectively compare different conditions and configurations.

A parameter based on the energy contained within a certain frequency bandwidth, remains as a possible alternative to be used for stability evaluation and comparison. This option represents the mean square value of the data within a certain frequency range. In this study, 0 to 40 Hz is the frequency range where the main components of the signals are. Figure 4.15 shows the trends of the area beneath the PSD up to a frequency of 40 Hz ($\widehat{P^2}_{40}$), as function of liquid superficial velocity, for different air flow rates.

The area beneath the PSD for the range of frequencies up to 40 Hz allows the distinction between different stability conditions. The low values are associated to stable sprays and correspond to the conditions with higher liquid flow. As the liquid flow is reduced, for a constant air flow, the spray becomes unstable and this parameter significantly increases. Additionally, it is found that the conditions for which the parameter substantially increases, correlate very well with the conditions associated to the stability transition when performing the experiments. Consequently, a transition zone can be qualitatively defined in the vicinity of the conditions where the parameter begins to increase, as depicted in Figure 4.15.

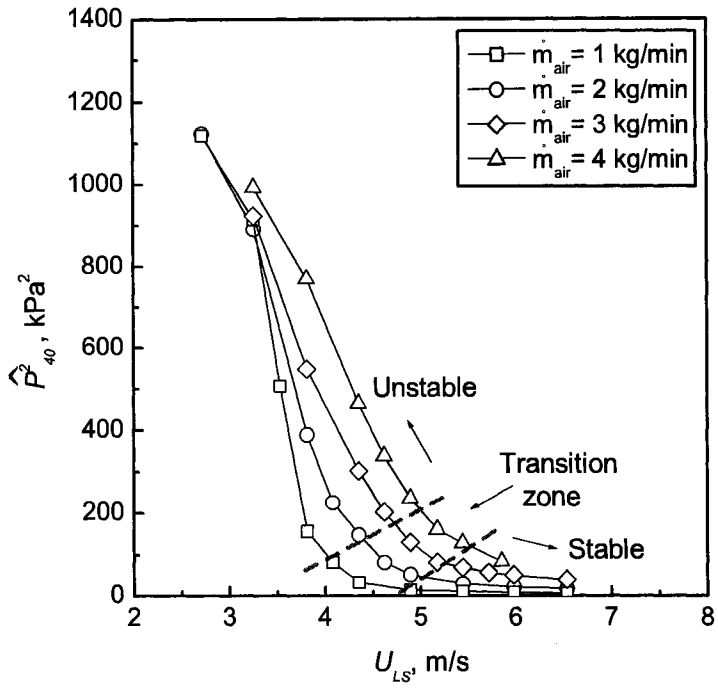

Figure 4.15: Area beneath the PSD for frequencies below 40 Hz, of the pressure fluctuation signal sampled just upstream of the nozzle, as function of liquid superficial velocity, for the standard configuration. Each curve corresponds to a constant air flow rate.

The trends obtained using the area beneath the PSD for frequencies below 40 Hz present a more pronounced break than the trends found with the RMS of the pressure fluctuations, when the conditions pass from stable to unstable. However, when compared to the trends of the mean square value the results are very similar. To quantify the information presented by the pressure fluctuations, it was preferred to consider the area beneath the PSD for frequencies below 40 Hz, which is equivalent to the mean square value of only the main components of the signal ($f < 40\ Hz$). This allows to use the same criterion to determine the stability transition for the different feeding pipe configurations.

4.3 Stability evaluation using pressure fluctuations

The signal analysis presented in the previous section offers significant information regarding the nature and characteristics of the pressure fluctuations. Additionally, through the detailed analysis performed it has been possible to establish relations between the stability of the spray and parameters calculated from the pressure fluctuations. The area beneath the PSD for the frequency range where the main components are present, has shown excellent correlation with the stability observed with qualitative techniques. Thus, a parameter based on the area beneath the PSD for frequencies below 40 Hz ($\widehat{P^2}_{40}$) was chosen to characterize the spray stability for the different feeding pipe configurations.

4.3.1 Stability transition

It has been previously discussed that small values of the parameter, $\widehat{P^2}_{40}$, used to evaluate the stability correspond to stable sprays, while high values correspond to unstable conditions. The stability transition observed during the experiments has been associated to the conditions for which the parameter substantially increases with respect to the generally smaller values of the stable conditions. Based on this, a qualitative transition zone was presented in Figure 4.15. However, it is of interest to define a transition line rather than a wide zone, in order to later make appropriate comparisons of the range of stability for the different configurations.

To define the stability transition based on the trends presented in Figure 4.15, the question to answer would be: *What is a "substantial" increment in the parameter* $\widehat{P^2}_{40}$*?*. For stable conditions, it was found that when the liquid flow rate is decreased by 7.5 kg/min (0.27 m/s in terms of U_{LS}) for a constant air flow, the increment in the parameter $\widehat{P^2}_{40}$ is always smaller than 40%. This maximum value was defined as characteristic of the stability transition, thus, the spray is said to pass from stable to unstable when an increment in the parameter is found to be higher than 40%,

for a 7.5 kg/min reduction in the liquid flow (for a constant air flow). Note that the experimental conditions were not necessarily taken every 7.5 kg/min, thus, in some cases an interpolation between operating points was performed to determine the stability transition.

Figure 4.16 presents the same trends illustrated in Figure 4.15, depicting a stability transition line. The conditions to the right and on the line are identified as stable, while conditions to the left are diagnosed as unstable. It must be noted that an estimation of this transition could be performed by direct observation of the trends; however, it is important to have a consistent criterion to define the transition in all configurations, to allow an appropriate comparison of the range of stability for the different arrangements.

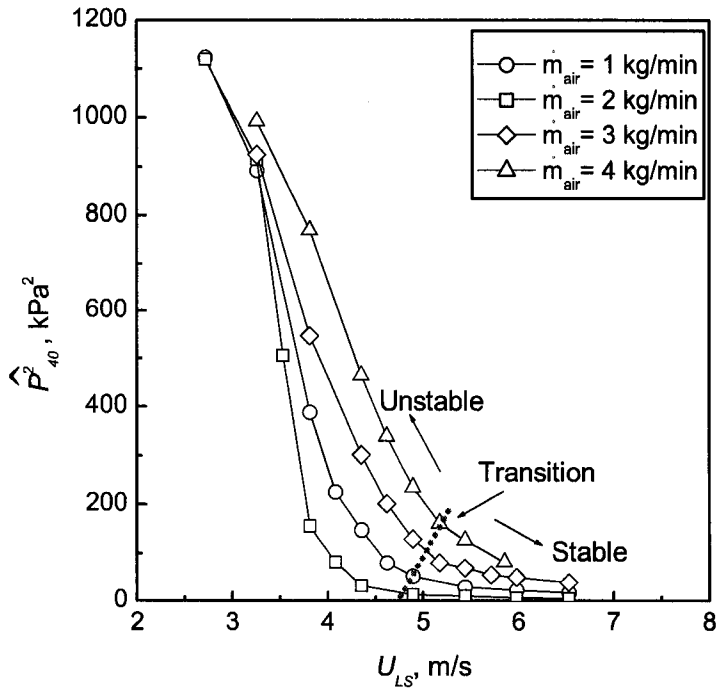

Figure 4.16: Stability transition for the standard configuration, based on the area beneath the PSD for frequencies below 40 Hz ($\widehat{P^2}_{40}$), of the pressure fluctuation signal sampled just upstream of the nozzle.

4.3.2 Pressure fluctuations along the pipe

The results previously presented correspond to the pressure fluctuations sampled 10 cm upstream of the nozzle (D1). However, given that the cross-correlation between the signals along the pipe for the standard configuration is high at unstable conditions, it is expected that the signals at the middle of the conduit (D2) and after the mixing device (D3) would present similar trends to those obtained with the signal sample just before the nozzle. Figure 4.17 presents the trends of $\widehat{P^2}_{40}$ for the signals sampled with the transducers D2 and D3.

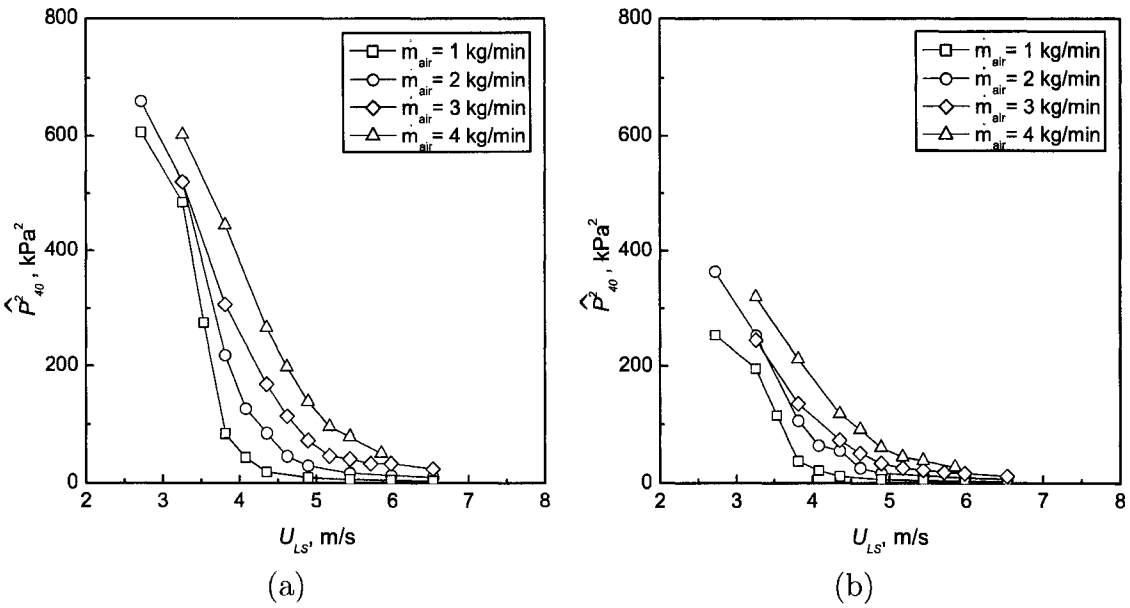

Figure 4.17: Area beneath the PSD for frequencies below 40 Hz of the signals sampled (a) at the middle of the conduit (D2), and (b) after the mixing device, for the standard configuration.

As expected, similar trends are obtained when using signals sampled at different positions along the pipe. This suggests that the analysis could be carried out using any of these signals. However, the similitude between the results at different positions is valid for configurations where the pressure fluctuations can be freely propagated in the conduit. This is not generally the case, as some of the configurations to be evaluated present disturbing elements along the feeding pipe. Additionally, an

appropriate comparison between the different alternatives requires the same local static pressure, which happens at the measuring point just upstream of the nozzle. Consequently, the signal sampled closer to the nozzle (D1) represents the best option to allow comparisons between the different pipe configurations.

Considering that the origin of the pressure fluctuations for the unstable conditions is at the nozzle, the best location to install the transducer is in the nozzle section. This would allow to have signals with a greater strength, and with a similar nature for the different configurations. However, it was not possible to install the transducer in the nozzle section because the wall thickness of the nozzle used in the experiments did not permit to install the pressure transducer flush with the inner surface of the nozzle.

4.3.3 Discussion

In summary, a parameter based on the area beneath the PSD for frequencies below 40 Hz ($\widehat{P^2}_{40}$), which is equivalent to the mean square value of the main frequency components of the signal, will be used to evaluate the stability for the different configurations. Given that some arrangements present disturbing elements between the measuring points, the signal used to estimate the PSD in all cases is the one recorded just upstream of the nozzle. This permits to have the same arrangement downstream of the transducer for the different alternatives, with the exception of the configuration with nonintegral roughness, where the spring was installed along the whole length of the pipe. Additionally, the analysis of the PSD plots, the pressure drop along the different feeding pipes and qualitative techniques, will be employed to better characterize the different configurations.

Chapter 5

Effect of the Feeding Pipe on the Spray Stability

As previously discussed, the distribution of the phases in the gas-liquid mixture entering the nozzle has an important effect on the stability of the spray generated. The structure of the two-phase flow is generally defined by the operating conditions, fluid properties, pipe characteristics, and if the flow is not developed, by the mixing device. In this regard, this chapter presents the evaluation of different feeding pipe configurations to determine what the effect of the conduit on the stability is, and suggests suitable configurations to increase the range of stability of the gas-liquid spray exiting the nozzle assembly.

Besides the standard configuration, the alternatives evaluated are: length to diameter ratio, sudden expansion-contractions along the pipe, peripheral obstructions, and nonintegral roughness. To evaluate the stability of the system for each pipe configuration and make comparisons between them, the parameter used was the area beneath the power spectral density function for frequencies below 40 Hz ($\widehat{P^2}_{40}$), of the pressure fluctuations sampled 10 cm upstream of the nozzle. Qualitative techniques and further analysis of the pressure fluctuations are also carried out to confirm the results obtained when using the area beneath the power spectral density function and discuss particular characteristics of some configurations. The standard configuration is the

reference or baseline with respect to which the different arrangements are compared.

5.1 Standard configuration

The standard configuration was thoroughly evaluated in Chapter 4. It was found that the parameter $\widehat{P^2}_{40}$ allows the distinction between different stability conditions; low values are associated to stable sprays, whereas high values correspond to unstable conditions. The stability transition was established where a substantial increment in the parameter was found. Additionally, analyzing the signals in the time domain, it was observed that for unstable conditions the maximum cross-correlation is high and the pressure fluctuations propagate in the upstream direction, while for the stable condition the maximum cross-correlation is smaller and the signals propagate downstream.

5.1.1 Stability transition and two-phase flow pattern

Figure 4.16, from previous chapter, displays the stability transition for the standard configuration based on the area beneath the PSD for frequencies below 40 Hz ($\widehat{P^2}_{40}$). In terms of operating conditions, the spray is stable at higher liquid flow and looses stability as the liquid flow decreases for a constant air mass flow. Figure 5.1 presents a flow map with liquid and gas superficial velocities as coordinates, showing the operating points evaluated and their corresponding stability condition. The superficial velocities of the conditions plotted in this map were calculated using the mean pressure measured just upstream of the nozzle, consequently, the conditions correspond to the flow entering the nozzle. The transition between dispersed bubble and intermittent flow, based on the model by Taitel and Dukler (1976) for fully developed flow, and described in Section 2.1.3, is superimposed on this flow map. As previously discussed, this flow regime transition depends on the operating pressure, which changes in the nozzle assembly for different flow rates. Thus, the transition shown in

Figure 5.1 is a combination of that calculated for 500, 1000 and 1500 kPa.

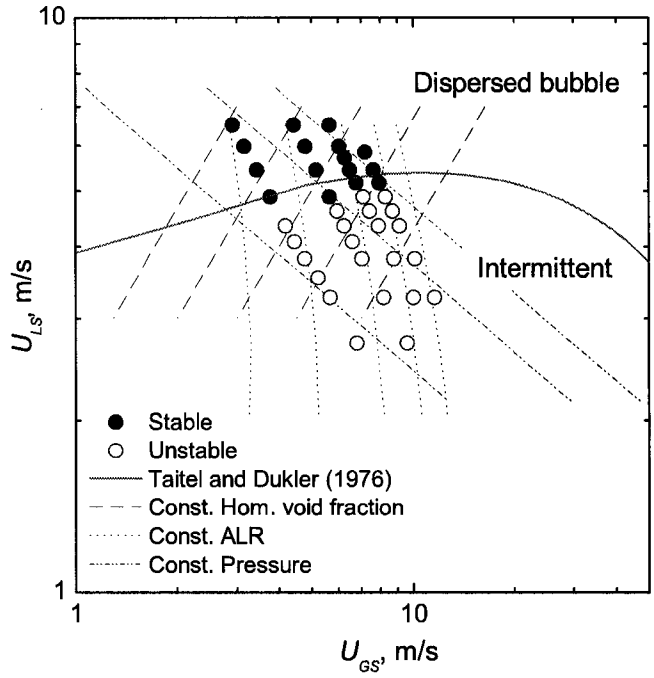

Figure 5.1: Flow map with the operating points and their corresponding stability condition for the standard configuration. The transition dispersed bubble – intermittent flow by Taitel and Dukler (1976) is superimposed as reference.

Excellent correlation is observed between the stability conditions and the flow pattern entering the nozzle, i.e., a stable spray is obtained for dispersed bubble flow, whereas unstable sprays correspond to intermittent flow entering the nozzle. This confirms the effect of the two-phase flow pattern on the stability of the spray, as suggested by other authors (Ariyapadi et al., 2005; Tafreshi et al., 2002; Whitlow and Lefebvre, 1993). The use of flow pattern maps, including the dispersed bubble–intermittent flow transition, was initially considered as a good alternative for indirect evaluation of the stability; however, despite of the good results found for the standard case, this flow regime boundary would not allow the prediction of the stability transition for alternatives where the flow is not developed, such as the cases when the two-phase flow is altered along the pipe.

5.1.2 Effect of air to liquid ratio (ALR) and void fraction on stability

Figure 5.1 depicts lines for constant pressure, ALR and homogeneous void fraction in a flow map with the experimental conditions. It is clear that the ALR does not define the spray stability transition, nor the boundary between dispersed bubble and intermittent flow. It is important to emphasize this idea because it is usually thought that at higher ALR the spray becomes unstable; however, in the system being evaluated for a constant ALR it is possible to have stable or unstable sprays depending on the flow conditions. If a constant operating pressure is considered, the stability of the spray decreases at higher ALR. The same analysis can be applied to the homogeneous void fraction.

5.1.3 Frequency of pulsation

Using the maximum peak of the PSD of the pressure fluctuations, the frequency of the pulses can be determined for the unstable conditions. Figure 5.2 depicts the frequency of the pulsation for the conditions identified as unstable using the transition defined by the area beneath the PSD. The frequency of pulsation is greater at higher air flow rates, but is relatively insensitive to liquid flow.

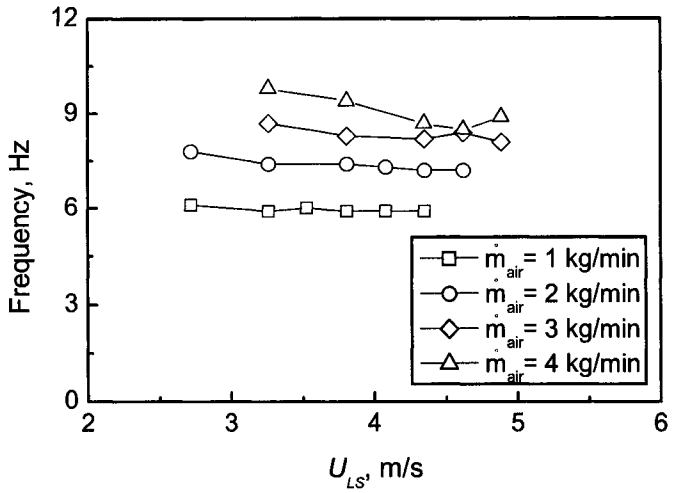

Figure 5.2: Frequency of pulsation for unstable conditions as function of the liquid superficial velocity for the standard feeding pipe.

5.1.4 Repeatability

During the initial stages of this study, the results of the experiments showed similar trends to those already presented; however, important scattering in the data was found. Several alternatives were attempted to find a suitable way to perform the tests, in order to avoid the scattering in the data and attain a satisfactory reproducibility of the results. The main changes in the approach initially followed for the experiments were as follows:

1. Longer sampling time for each set of data. Initially, the pressure fluctuation signal was recorded for 5 s, and was later changed to 50 s.

2. Enough time to allow the control system to reach the sought flow rates. It was found that when the control system was set to the *automatic* mode to maintain the air flow rate constant, time had to be given to allow the control system to keep the same air flow for each new water flow. Thus, before recording the pressure fluctuation signals, it was necessary to wait enough time to obtain the desired flow rates. An alternative approach is to have the control of both, water and air, flow rates in *manual* mode.

3. High backpressure to prevent fluctuations in the flow supplied by the pump. Fluctuations in the supplied water flow were found at lower flow rates, with an associated low pressure. This made it difficult to record the data for 50 s while maintaining a constant flow rate. To avoid this, a valve installed upstream of the liquid line in the mixing device, was closed a certain percentage for lower flows in order to keep the discharge pressure of the pump high, and prevent fluctuations in the water flow.

No thorough testing was performed to evaluate the reproducibility of the results after implementing the above described changes in the experimental techniques. However, to attain an idea about the reproducibility of the conclusions drawn from the analysis of the pressure fluctuations, some tests carried out for the standard pipe at different stages of this study are compared here. The following is a brief description of the tests to compare:

- *Test 1* (July 11, 2005). For this test, no considerations were taken to avoid the fluctuations in the water flow rate, and the condition at 75.7 kg/min was not recorded.
- *Test 2* (September 13, 2005). This test was carried out to compare the results when recording the pressure fluctuations with static and dynamic pressure transducers. The sampling frequency was 200 Hz; however, it is assumed that these results can be compared with those of signals sampled at 2000 Hz because the main components of the signals are below 100 Hz, and the parameter used for comparison considers the components below 40 Hz.
- *Test 3* (January 27, 2006). The results from this test are those finally presented for the standard configuration, and all considerations given above were taken to obtain appropriate data.
- *Test 4* (January 27, 2006). In this case, three operating conditions were recorded again at the end of the test performed on January 27, 2006.

Figure 5.3 presents the results of the area beneath the PSD for frequencies below 40 Hz, for the tests previously described. The trends displayed by the different tests are very similar, conducting to the same result in terms of the stability transition, and the stability condition associated to each operating point. Some discrepancies are found, but they do not change the stability condition from one test to the other. Note that the maximum discrepancy is found at the condition with $U_{LS} = 3.26$ m/s, for the *Test 1*; however, as previously indicated, for this test no considerations were taken to avoid fluctuations in the water flow.

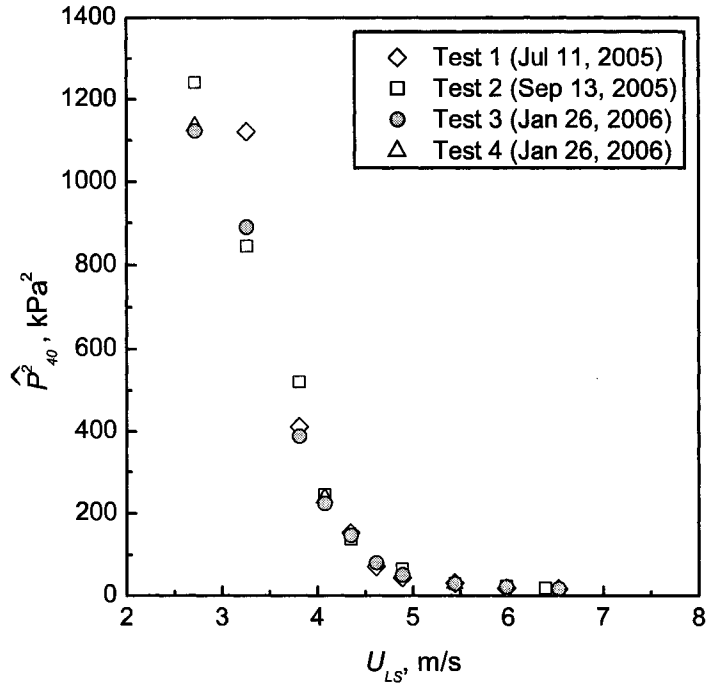

Figure 5.3: Area beneath PSD for frequencies below 40 Hz ($\widehat{P^2}_{40}$), for different tests performed with the standard configuration, at 2 kg/min of air.

5.2 Different pipe configurations

As previously indicated, the different feeding pipe configurations are evaluated using the area beneath the PSD of the pressure fluctuations for frequencies below 40 Hz, and other analyses that allow good characterization. The alternatives with modifications

of the conduit are compared with the standard pipe in terms of their effect on the spray stability. It is important to mention that for all the configurations the mean pressure at the entrance of the nozzle is mainly the same (for the same flow rates), regardless of the pipe configuration. This permits direct comparisons between conditions at the same mass air and water flow, otherwise, the operating points would always have to be represented in terms of superficial velocities, or other alternative that takes into account the effect of the variation in the operating pressure.

5.2.1 Length to diameter ratio (L/D)

The length to diameter ratio has influence in the flow development and, consequently, in the flow pattern of the two-phase flow entering the nozzle. In order to evaluate this effect, the two alternatives considered were pipes with lengths of 38 cm ($L/D \approx 16$) and 180 cm ($L/D \approx 74$), which hereafter will be referred as *short* and *long* conduit, respectively. The length of the standard pipe (100 cm, $L/D \approx 41$) is in between the length of the short and long pipe. The flow conditions considered in both cases covered a range of air flows from 1 to 3 kg/min and water flow from 75.7 to 181.7 kg/min, which correspond to superficial velocities in the range of 2.82–11.52 m/s for air and 2.72–6.53 m/s for water. See Appendix A.2 for experimental conditions corresponding to the short and long pipe.

Figure 5.4 presents the trends of the parameter $\widehat{P^2}_{40}$, for the short and long conduit. As in the standard case, the trends for constant air flows present breaks that have been associated to the transition. The same criteria of an increment of $\widehat{P^2}_{40}$ greater than 40%, was used to estimate the stability transition. It must be mentioned that when defining the transition for the trend corresponding to 1 kg/min of air for the long pipe, the increment between the first two values was of 45%. By observation of the trends and according to what was observed during the experiment this condition cannot be associated to the transition, consequently, the following increment in the parameter higher than 40% was the one taken to define the transition.

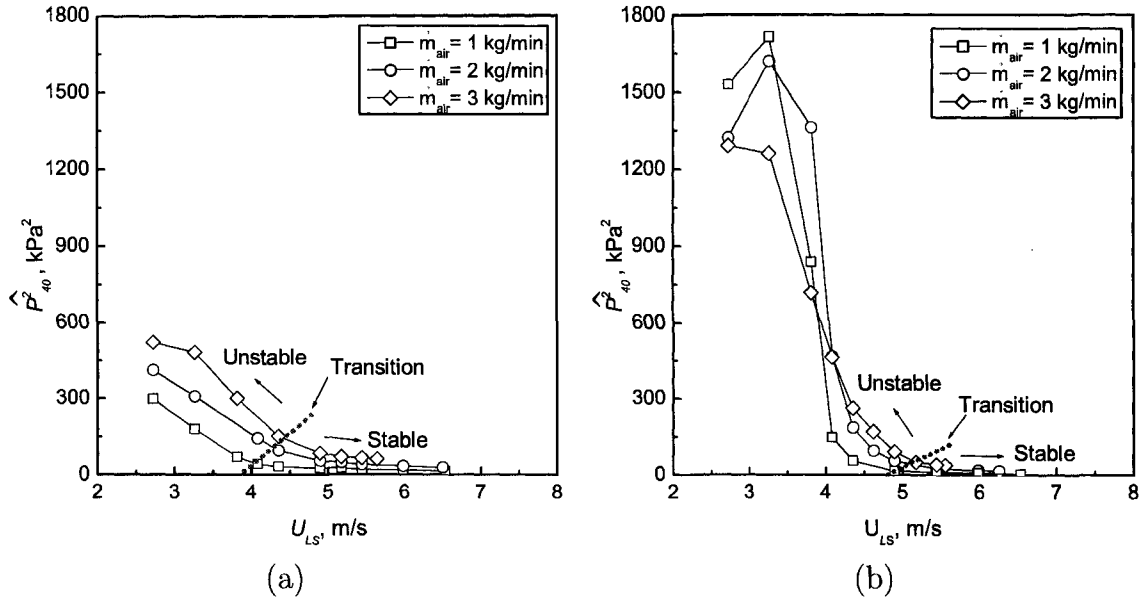

Figure 5.4: Area beneath the PSD for frequencies below 40 Hz ($\widehat{P^2}_{40}$), of the pressure fluctuation signal for the (a) *short*, and (b) *long* conduit.

No important changes are observed in the stability transition of the long conduit with respect to the standard case, whereas for the short pipe the transition is observed to occur at approximately 23 kg/min lower liquid flow rate for the different air flows considered. The transition at a lower liquid flow rate for the short pipe certainly indicates that the flow is not developed for this pipe length.

Figure 5.5 depicts a comparison between the results of the short, long and standard conduit for 1, 2 and 3 kg/min of air.

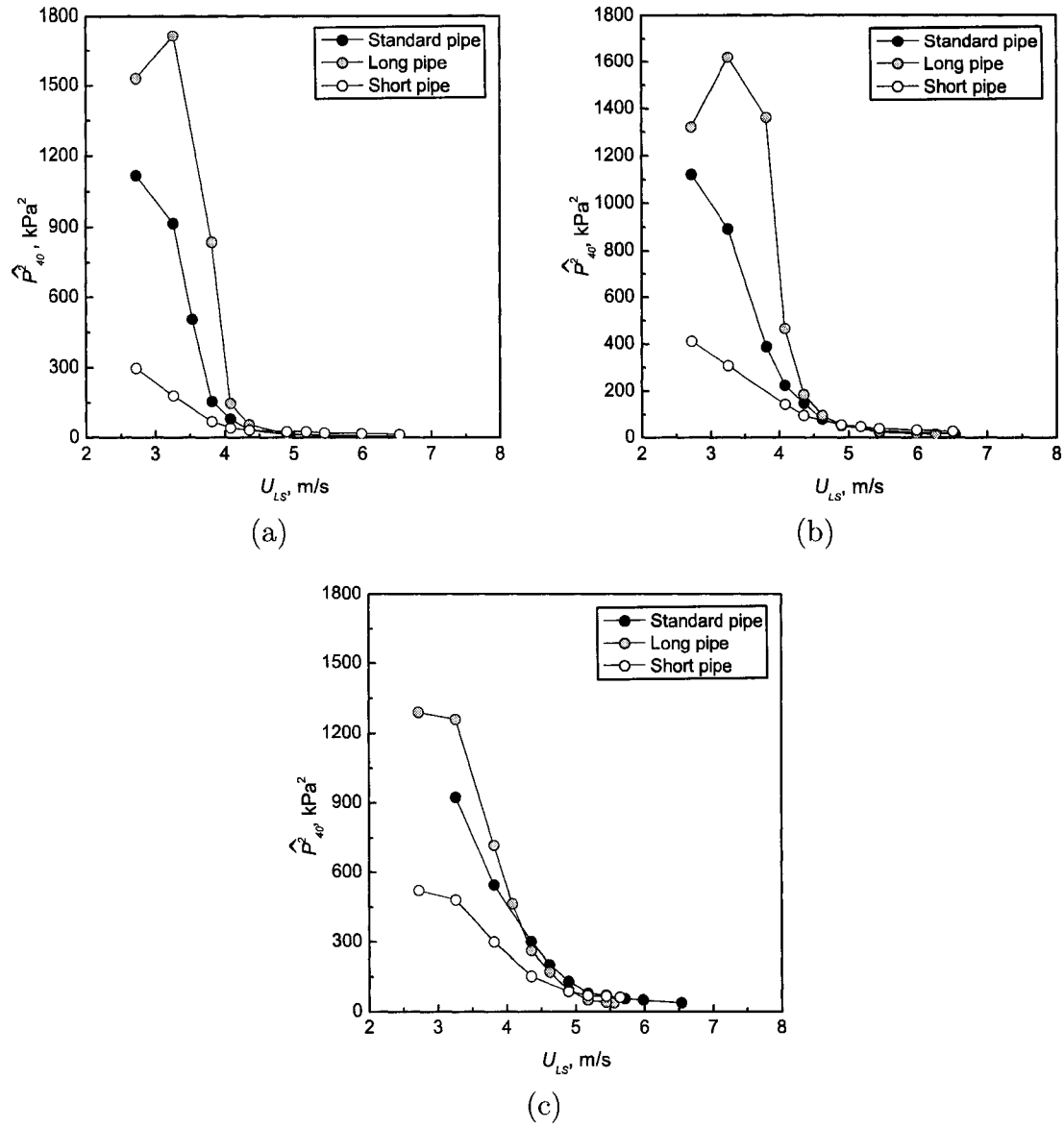

Figure 5.5: Comparison of short and long conduit with respect to the standard, for (a) 1 kg/min, (b) 2 kg/min, and (c) 3 kg/min of air flow.

For unstable conditions, the pulsation strength is greater for increasing pipe lengths. This was noticed during the experiments, and was later reconfirmed with regular-speed videos. Additionally, high-speed videos were taken within a section of the conduit before the nozzle and it was found that the zones with more gas are larger and segregated at the top of the pipe for the long conduit, indicating hydrostatic segregation of the flow over distance (See Figure 5.6). The higher pulsation strength

found for longer pipes can be explained considering that the spray instabilities are caused by the formation of larger bubbles in the conduit, and for a longer conduit the flow along an additional length allows further bubble coalescence. This indicates that these flows are in fact not fully developed, which accentuates the importance of the mixing device on the performance of the system.

(a) (b)

Figure 5.6: Pictures of the flow before the nozzle within a section of the (a) standard, and (b) long conduit, for an unstable condition (2 kg/min of air and 75.7 kg/min of water).

For stable conditions, shorter pipe lengths caused slight instabilities in the spray. This is also due to the flow development, as conditions corresponding to dispersed bubble flow are improved when the flow is allowed to develop further. This behavior was recognized by direct observation of the spray during the experiments, and was reinforced by the area beneath the PSD when enlarging the y-scale of the plots presented in Figure 5.5.

Figure 5.7 illustrates the PSD of the pressure fluctuations signal for a stable and an unstable condition, with the short and long conduit. For unstable conditions, the PSD for the short pipe shows that the signal has frequency components in the range of 10–25 Hz, with a probable dominant frequency at around 13 Hz, whereas for the long pipe a main peak is found at around 5 Hz. The shape of the PSD can also be associated to the flow development along the pipe, for the long conduit the bubbles coalesce and form bigger bubbles with a regular frequency at the nozzle inlet, while for the short pipe the bubbles are distributed in a more irregular way originating a broader range of frequency components. For stable conditions, in both cases, the

PSD presents the power distributed over a broad frequency range with its magnitude much smaller than for the unstable case.

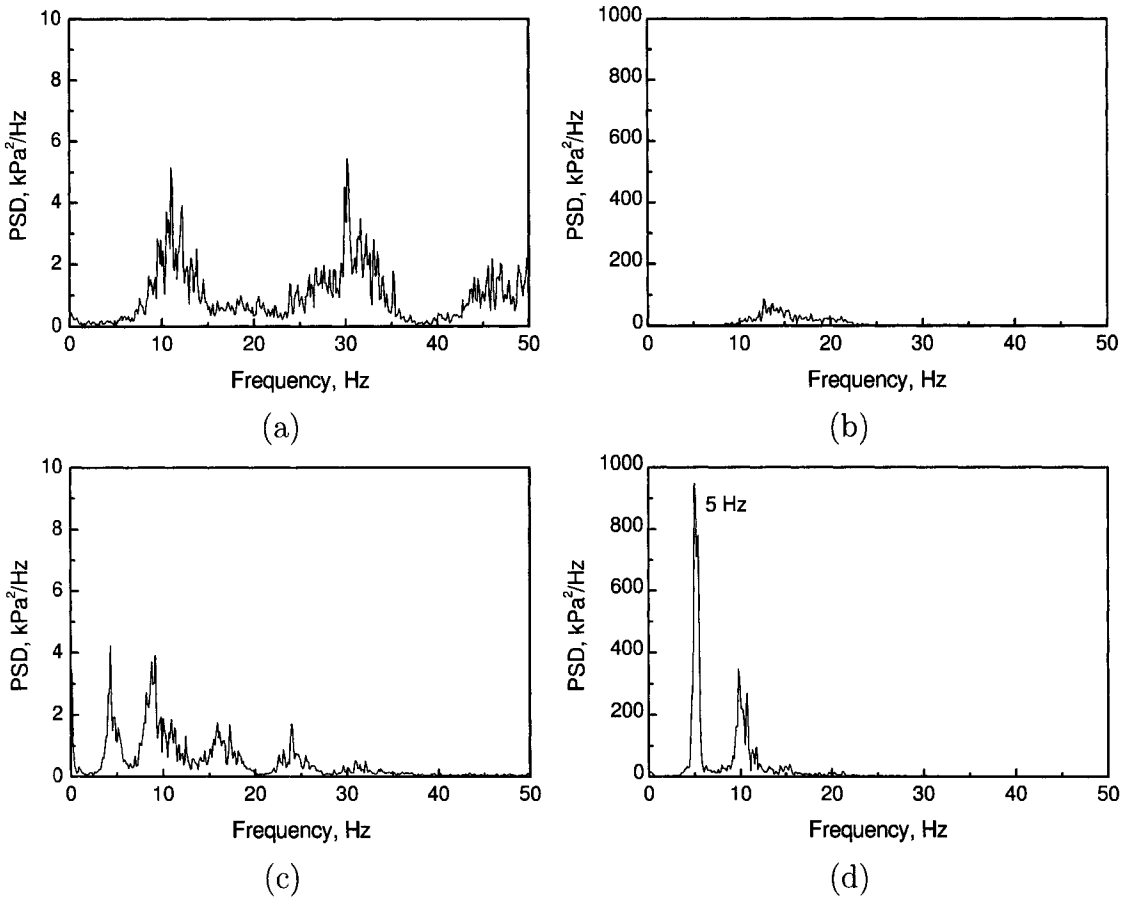

Figure 5.7: PSD of the pressure fluctuation signal for stable (left) and unstable (right) conditions with the short (top) and long (bottom) conduit. Flow rates at 2 kg/min of air and 151.4 and 75.7 kg/min of water, for the stable and unstable condition, respectively.

Figure 5.8 presents the frequency that corresponds to the maximum value in the PSD for an unstable condition with different length to diameter ratios. This is the dominant frequency of the pressure fluctuations, and is associated to the frequency of the pulsation for the unstable conditions. The highest frequency is found for the short pipe, and the smallest for the long pipe, with the standard in between. This can also be explained with the idea of flow development along the conduit; for longer pipes the bubbles continue to coalescence in the additional pipe section and form bigger and less frequent bubbles. The behavior of the frequency pulsation was found to be opposite to the strength of the pulsation: the longer the conduit, the lower the frequency and the higher the strength of pulsation.

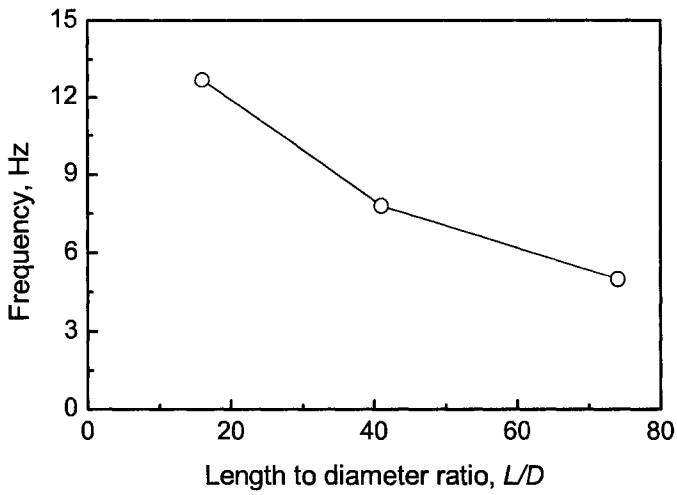

Figure 5.8: Frequency of pulsation as function of the length to diameter ratio (L/D) for an unstable condition (2 kg/min of air and 75.7 kg/min of water).

In summary, the findings for the different length to diameter ratios of the conduit are distinctly related to the flow development in two-phase flow; for longer pipes the coalescence of bubbles is favored for intermittent conditions, while for stable conditions the dispersion of the bubbles is superior.

5.2.2 Sudden expansion-contractions along the pipe

Sudden expansion-contractions of the pipe cross-section are expected to favorably alter the structure of the two-phase flow mixture entering the nozzle. The alternatives evaluated consist of two sudden expansion-contractions of the pipe cross-section along the length of the pipe. Three different increments in the flow area were considered: 78, 150, and 310 %. Based on the nominal diameter of the pipes used in the construction of these arrangements, the three alternatives will be referred as: 1x1.25, 1x1.5, and 1x2, respectively. The flow conditions considered in the three cases covered ranges of air flow from 1 to 3 kg/min and water flow from 75.7 to 181.7 kg/min, which corresponds to superficial velocities in the range of 2.82–11.52 m/s for air and 2.72–6.53 m/s for water. See Appendix A.3 for experimental conditions.

Figure 5.9 presents the trends of the parameter $\widehat{P^2}_{40}$ as a function of liquid superficial velocity for the arrangements with two sudden expansion-contractions of the pipe cross-section. As in the standard, long and short pipe, breakpoints are found in the trends for constant air flow, and the stability transition has been estimated using the criterion previously defined. The conditions corresponding to the breakpoints correlate well with the transition found by direct observation of the spray.

Configuration 1x1.25 presents the transition at approximately 7.5 kg/min and 15 kg/min higher liquid flow rates than the 1x1.5 and 1x2 configurations, respectively. The stability transition at higher liquid flows for the arrangement 1x1.25 is because the change in the flow area is smaller, and, as consequence, the effect on the flow is also smaller.

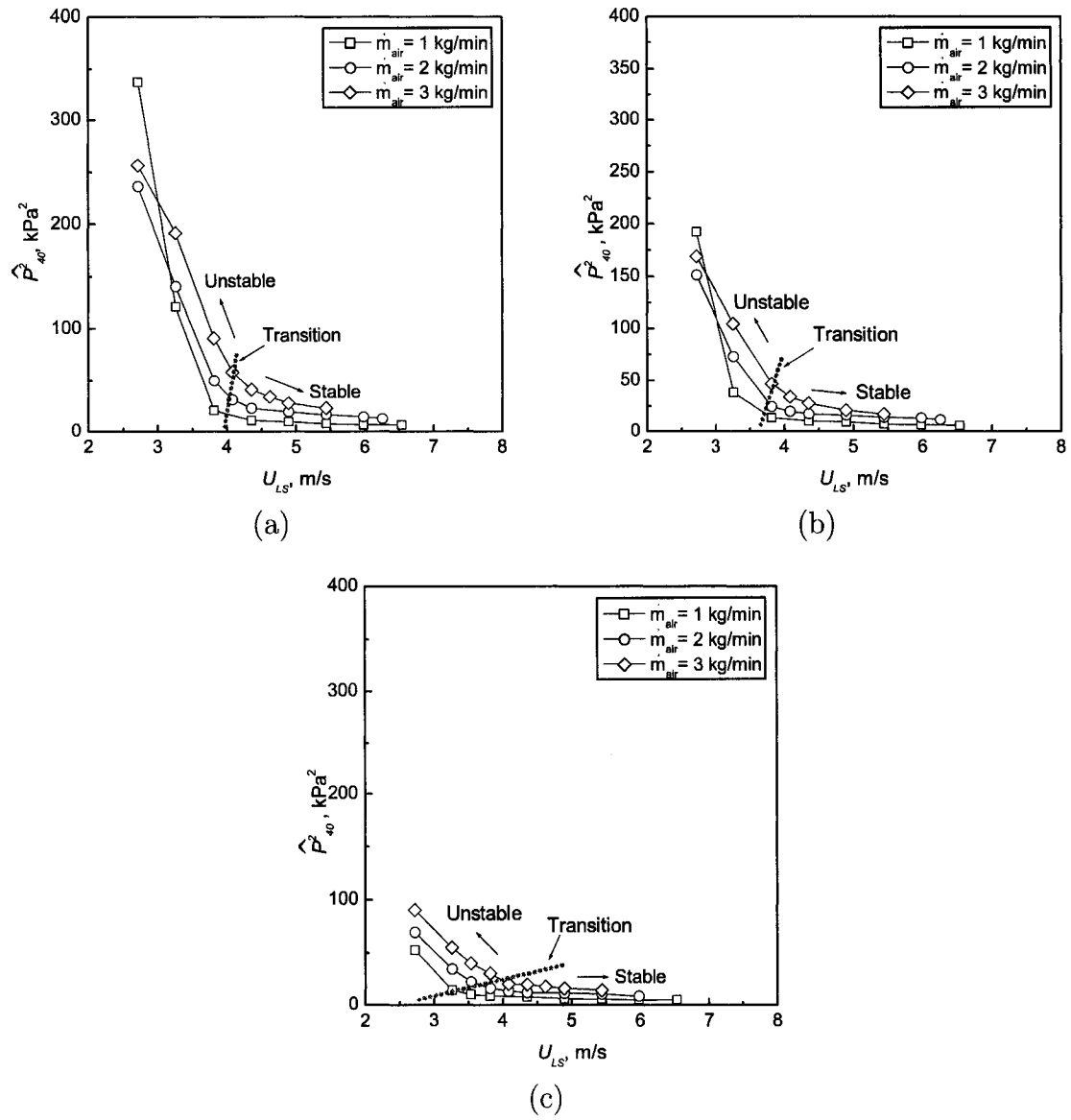

Figure 5.9: Area beneath the PSD for frequencies below 40 Hz ($\widehat{P^2}_{40}$), of the pressure fluctuation signal, for the configurations with sudden expansion-contractions: (a) 1x1.25, (b) 1x1.5, and (c) 1x2.

Figure 5.10 presents a comparison between the results of the standard configuration and those obtained with the different sudden expansion-contractions along the feeding pipe. The strength of the pulsations at unstable conditions is observed to be significantly lower for the arrangements with expansion-contractions. This is probably due to a more homogeneous gas-liquid mixture entering the nozzle. When comparing

the three different sudden expansion-contraction configurations, it is observed that for greater changes in the flow area the pulsation strength for unstable conditions is reduced; highest strength is obtained for 1x1.25, followed by 1x1.5 and then 1x2 configuration.

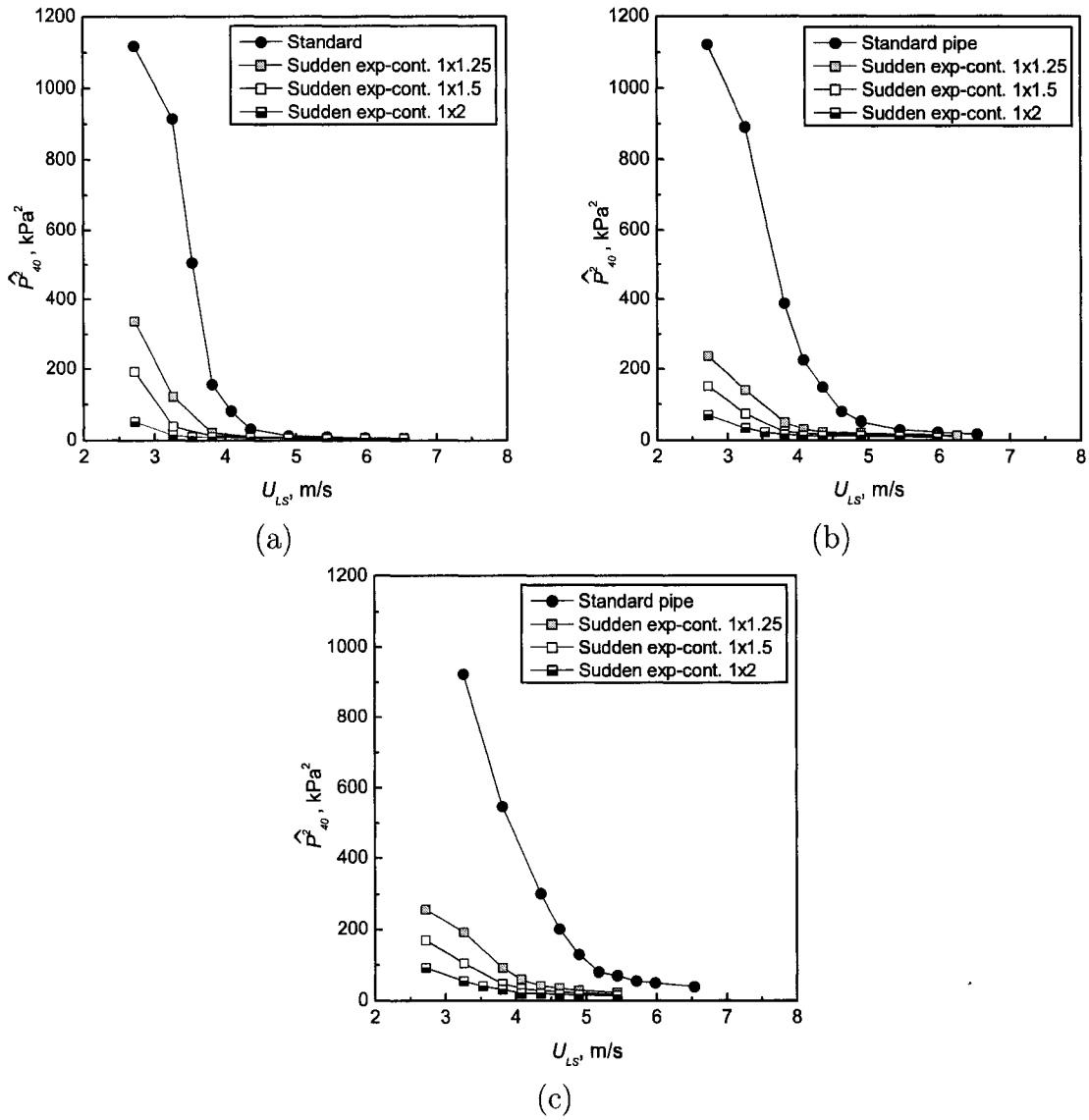

Figure 5.10: Comparison of the different sudden expansion-contractions with the standard pipe for (a) 1 kg/min, (b) 2 kg/min, and (c) 3 kg/min of air flow.

The stability transition takes place at lower liquid flow rates when compared to the standard case, allowing the operation of the system at lower liquid flows without

reaching unstable conditions. As reference, Figure 5.11 depicts a flow map for the alternative 1x1.5 with the operating points evaluated and their corresponding stability condition. Based on the stability transition observed for the 1x1.5 configuration in Figure 5.11 and for the standard case in Figure 5.1, an acceptable decrease of water flow, while maintaining stable conditions, was determined to be 40, 40 and 45 kg/min for constant air flows of 1, 2 and 3 kg/min, respectively. The stability improvement obtained with the sudden expansion-contraction configurations was also clearly observed when conducting the experiments, and later confirmed through videos recorded during the tests.

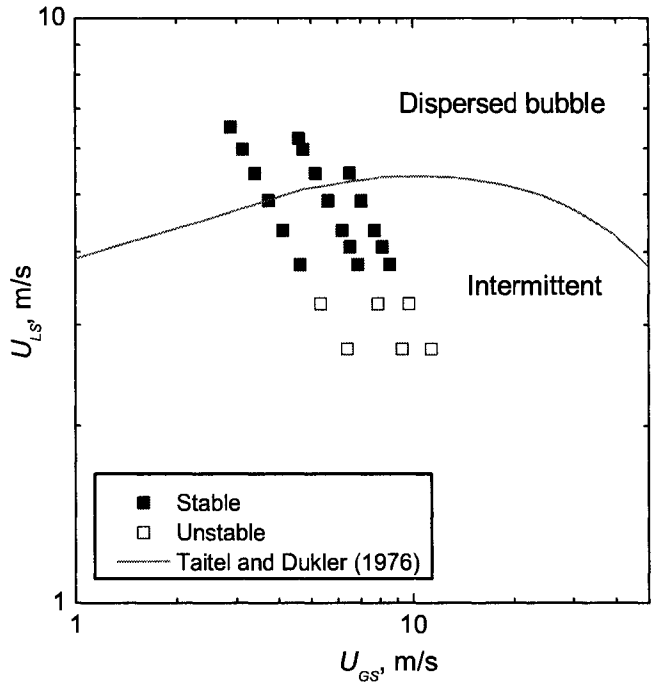

Figure 5.11: Flow map of the operating points with their corresponding stability condition for the 1x1.5 configuration. The transition dispersed bubble–intermittent flow by Taitel and Dukler (1976), is superimposed as reference.

Now, the question arising would be: *What is the cost, in terms of pressure drop, associated to the improvement in the stability range?*. Figure 5.12 presents the pressure drop for the conditions at 2 kg/min of air for the standard and the different expansion-contraction configurations. The pressure drop is not high when compared to the operating pressure for these conditions. For instance, at 2 kg/min of air and

151.4 kg/min of water the operating pressure is 1070.6 kPa, and the pressure drop is 24 and 46.1 kPa, for the standard and the 1x1.5 sudden expansion-contractions configuration, which correspond to 2.2 and 4.3% of the operating pressure. Comparing the pressure drop for the different expansion-contraction configurations, it is found that the greater the expansion in the flow area the higher the pressure drop.

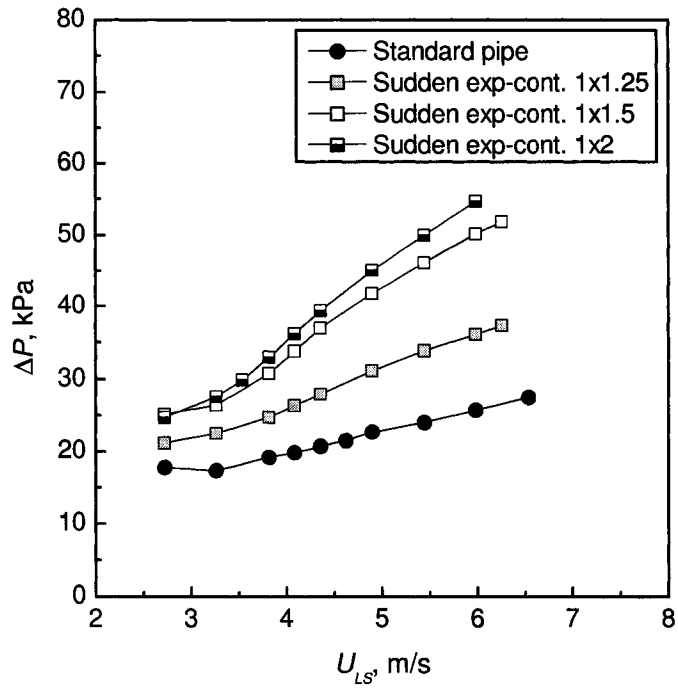

Figure 5.12: Pressure drop along the feeding pipe for the standard and sudden expansion-contractions arrangement.

Figure 5.13 illustrates the PSD of the pressure fluctuations signal for a stable and an unstable condition, with the the different expansion-contraction configurations. For unstable conditions, a main peak is found between 6 and 7 Hz. For stable conditions, in all cases, the power is distributed over a broad range of frequencies with its magnitude smaller than for the unstable case.

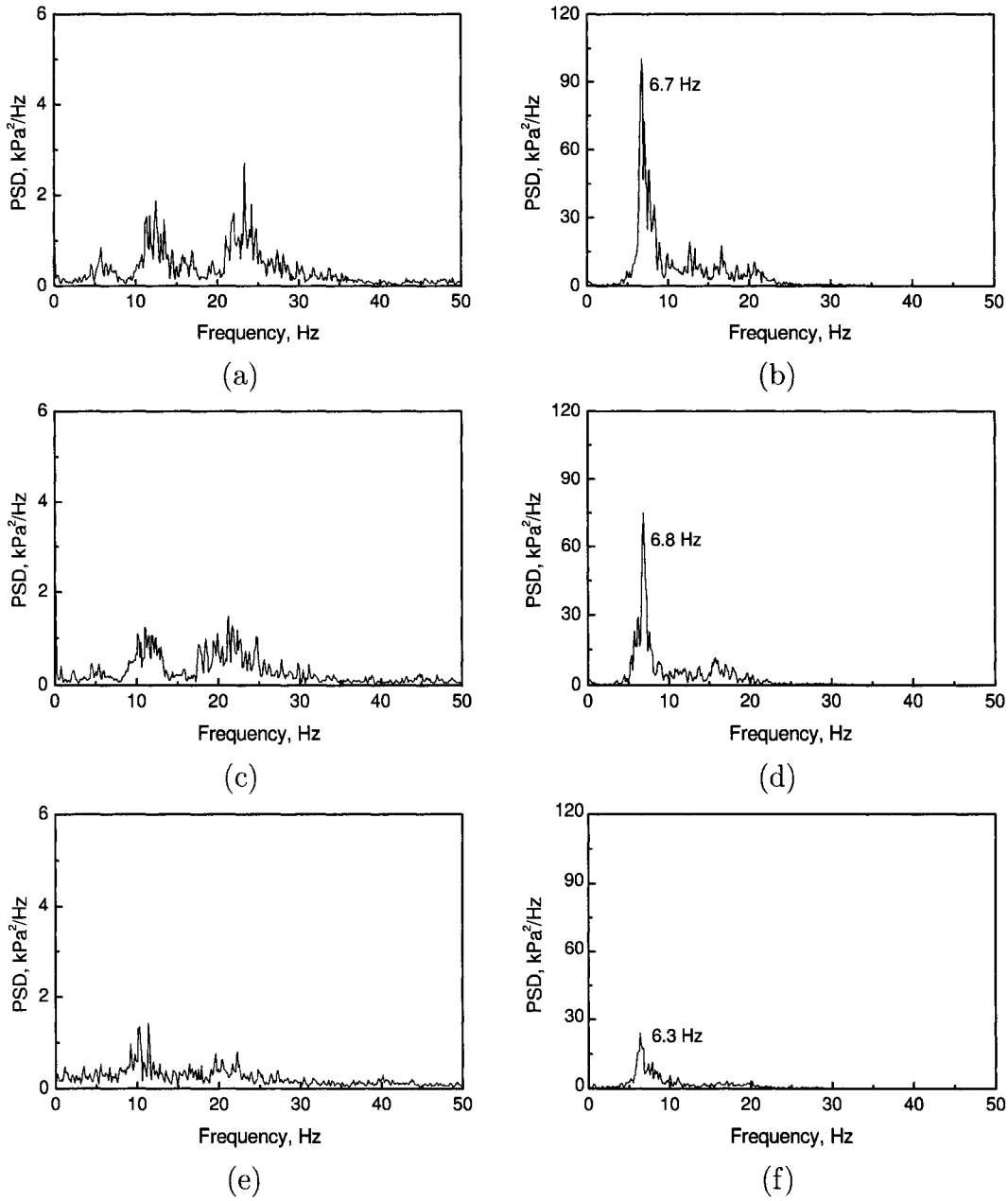

Figure 5.13: PSD of the pressure fluctuation signal for stable (left) and unstable (right) conditions, with the 1x1.25 (top), 1x1.5 (middle) and 1x2 (bottom) configurations. Flow rates at 2 kg/min of air and 151.4 and 75.7 kg/min of water, for the stable and unstable condition, respectively

In summary, the alternative based on sudden expansion-contractions along the pipe allows the operation of the system at lower liquid flows without reaching unstable conditions. This facilitates the usage of greater amounts of gas, with respect to the

liquid phase, to improve the atomization process without compromising the stability of the spray. A balance between pressure drop and stability improvement can help determine the best increment in the flow area. Additionally, industrial restrictions related to the maximum outer diameter of the pipe can limit the largest change in diameter to consider. Finally, it is necessary to perform further evaluation of this alternative to define the optimum length and frequency of the expansion-contractions.

5.2.3 Peripheral obstructions

Obstructions can induce mixing in the two-phase flow along the pipe, changing the distribution of the liquid and gas phase. This effect could be beneficial to improve the stability of the gas-liquid spray. In order to fulfill industrial constraints, the obstructions installed along the pipe are of the peripheral type with an area blockage of 55 %. Two different arrangements were evaluated: (a) 2 obstructions with 33 cm ($L/D = 13.6$) between them, and (b) 4 obstructions with 20 cm ($L/D = 8$) of separation. The flow conditions considered in the case with 2 obstructions covered a range of air flow rates from 1 to 3 kg/min and water flow rates from 75.7 to 181.7 kg/min, with superficial velocities ranging between 2.92–11.42 m/s for air and 2.72–6.53 m/s for water. For the arrangement with 4 obstructions only 2 kg/min of air flow was considered with the water flow ranging between 75.7 and 181.7 kg/min, which corresponds to superficial velocities of 4.44–9.38 m/s for air and 2.72–6.53 m/s for water. See Appendix A.4 for experimental conditions corresponding to the arrangements with peripheral obstructions.

Figure 5.14 presents the trends of the parameter $\widehat{P^2}_{40}$ for the configurations with 2 and 4 peripheral obstructions along the pipe, as a function of the liquid superficial velocity. During the experiments, the spray was never observed completely stable; even for the highest liquid flows there were always fluctuations on the edges of the spray. Consequently, no stability transition is defined in this case.

Figure 5.15 depicts a comparison between the results of the standard pipe and con-

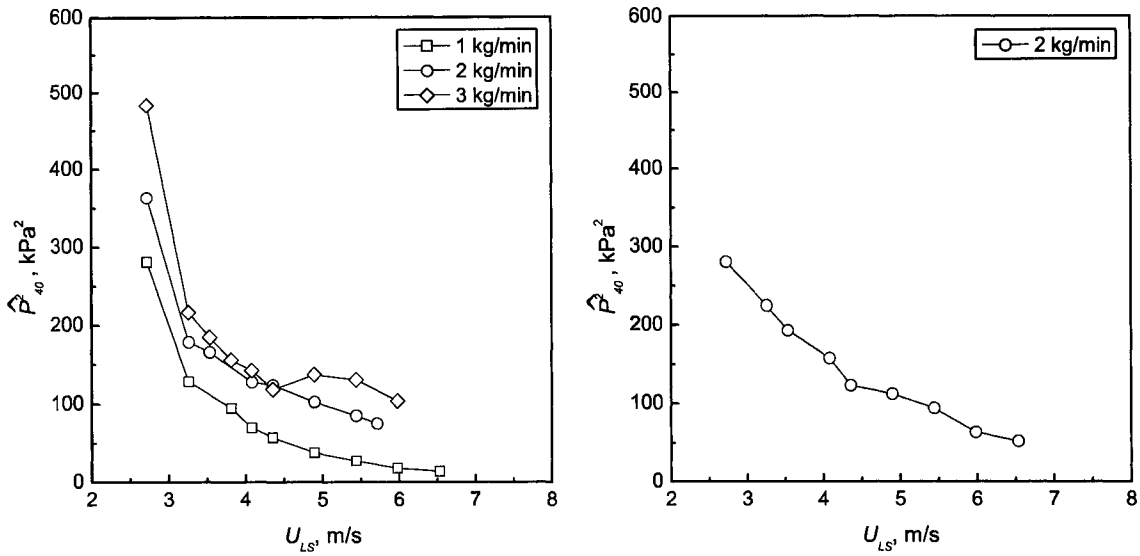

Figure 5.14: Area beneath the PSD for frequencies below 40 Hz ($\widehat{P^2}_{40}$), of the pressure fluctuation signal, for configurations with (a) 2, and (b) 4 peripheral obstructions along the feeding pipe.

figurations with 2 and 4 peripheral obstructions at 2 kg/min of air. The strength of the pulsations is smaller with peripheral obstructions, which was observed during the experiments. This is an indication of the effect of the obstructions in the redistribution of the phases for the unstable conditions. Additionally, it is not observed any positive effect with the installation of additional obstructions, as the results for 2 and 4 peripheral obstructions are very similar.

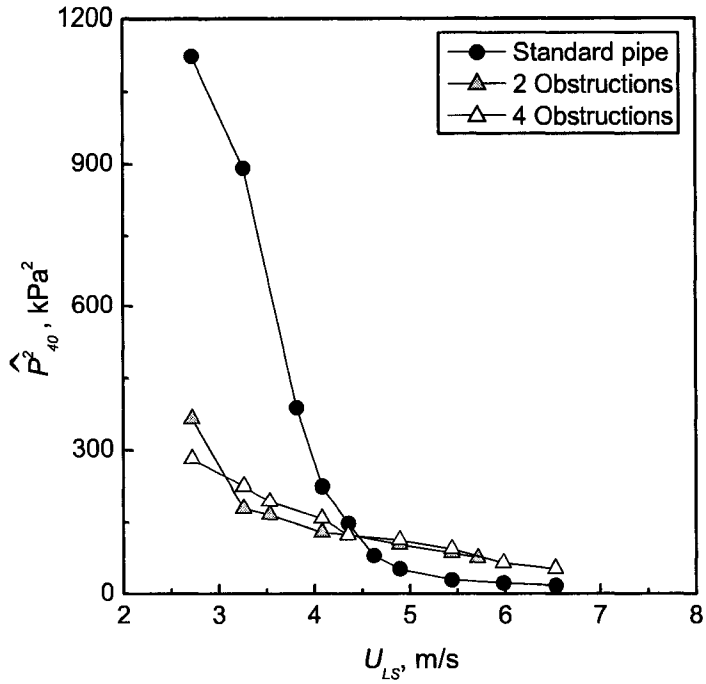

Figure 5.15: Comparison of 2 and 4 peripheral obstructions with the standard pipe for 2 kg/min of air flow.

Figure 5.16 presents the pressure drop for the conditions at 2 kg/min of air for the standard pipe and the arrangements with peripheral obstructions. The pressure drop is very high when compared to the pressure drop obtained with the standard case. For instance, at 2 kg/min of air and 151.4 kg/min of water the operating pressure is 1070.6 kPa and the pressure drop is 240 kPa with 2 obstructions and 439.3 kPa with 4 obstructions, corresponding to 22.4 and 41.0 % of the operating pressure. These values represent very high increments in the pressure drop with respect the standard case, where it is 2.2 % of the operating pressure at the given flow conditions. As expected, the pressure drop is higher for the configurations with more peripheral obstructions along the pipe.

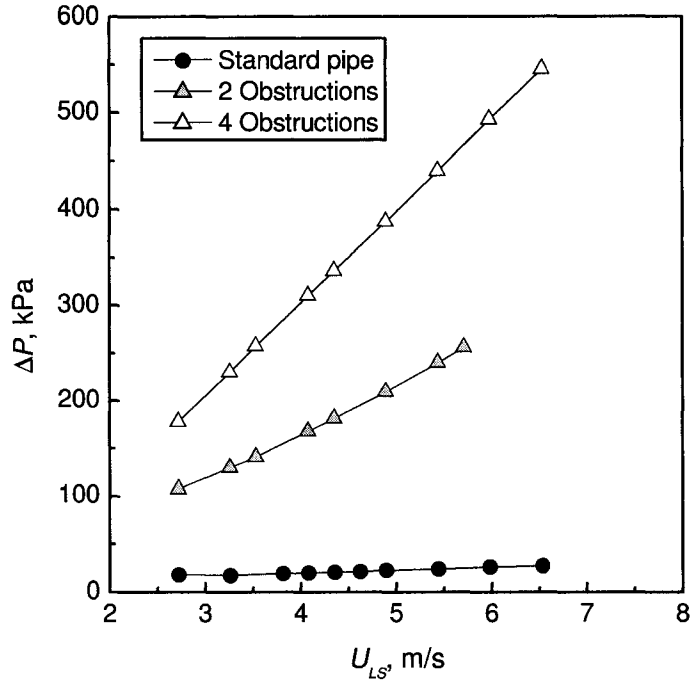

Figure 5.16: Pressure drop along the feeding pipe for the standard conduit and configurations with peripheral obstructions along the pipe.

Figure 5.17 illustrates the PSD of the pressure fluctuation signal for a stable and an unstable condition, for the arrangements with 2 and 4 peripheral obstructions. For unstable conditions, the PSD shows that the signal has frequency components in the range 5–20 Hz. For stable conditions, the PSD presents the power distributed over the frequency range 5–15 Hz. It is thought that the processes occurring through the obstructions can also affect the pressure fluctuations, and add some additional components to the type of signals analyzed in previous cases. As already discussed, this is one of the weaknesses found with analyses based on pressure fluctuations, due to the integral character of this type of signals.

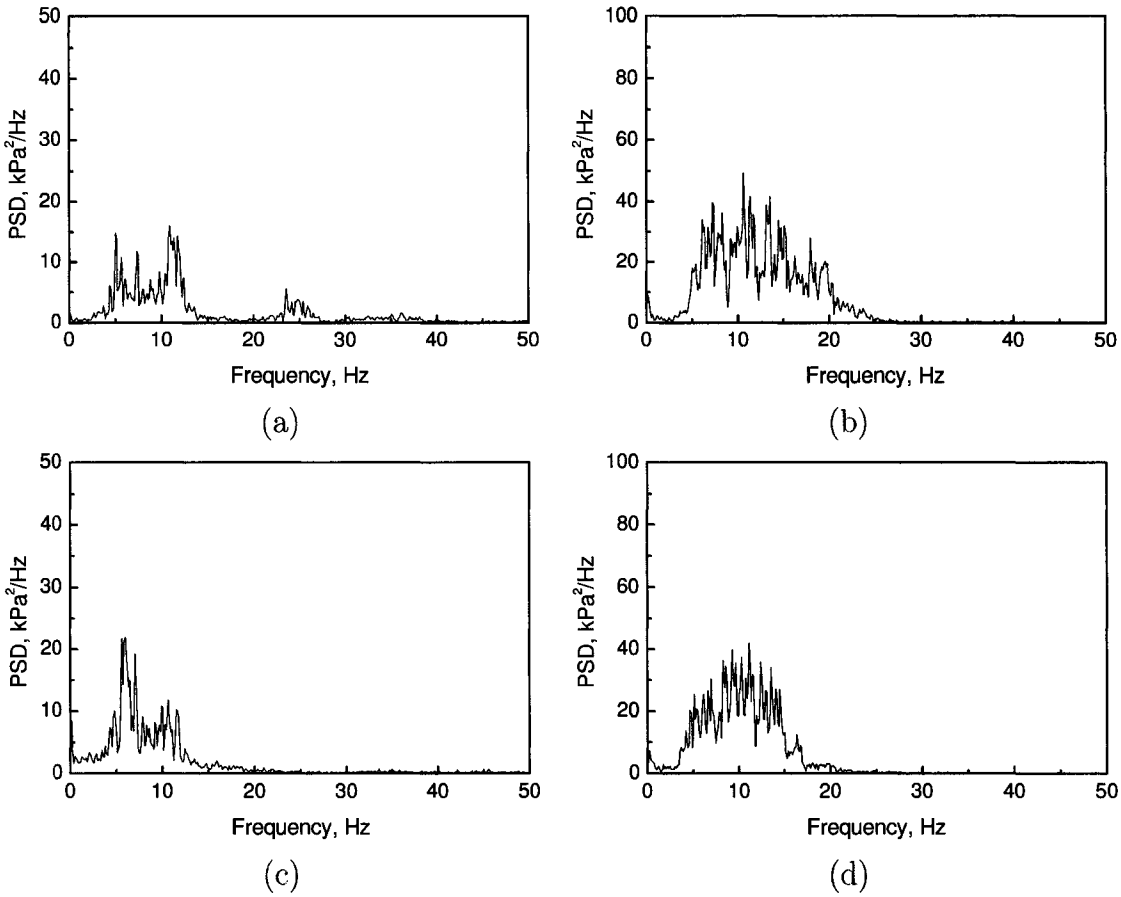

Figure 5.17: PSD of the pressure fluctuation signal for stable (left) and unstable (right) conditions with 2 obstructions (top) and 4 obstructions (bottom) configurations. Flow rates at 2 kg/min of air and 151.4 and 75.7 kg/min of water, for the stable and unstable condition, respectively.

The arrangements with peripheral obstructions along the conduit did not display a good performance, compared to the other designs, which was evidenced since the moment of the experiments. Although the severity of the pulsations was reduced for unstable conditions, the pressure drop along the pipe is very high and the spray for the conditions with higher liquid flow always presented slight fluctuations. Probably, fewer obstructions with greater inner diameter would present an acceptable effect on stability without causing such a high pressure drop. However, considering the performance observed during the experiments, and later with the pressure fluctuation signals analysis, no further evaluation was attempted to optimize this type of arrangement.

5.2.4 Nonintegral roughness

Enhancement of the gas and liquid mixing by increments in the inner surface roughness of the conduit, represents an attractive modification to improve the stability range of the gas-liquid spray. The approach followed to increase the inner surface roughness was the implementation of nonintegral roughness through the insertion of commercially available springs along the whole length of the feeding pipe. This configuration differs from the others because of the presence of elements between the entrance of the nozzle and the transducer installed 10 cm upstream of the nozzle. The flow conditions considered corresponded to 2 kg/min of air flow with the water flow ranging between 75.7 and 151.4 kg/min. In terms of superficial velocities these flow rates correspond to 5.06–9.17 m/s for air and 2.72–5.44 m/s for water. See Appendix A.5 for experimental conditions.

Figure 5.18 presents the trends of the the parameter $\widehat{P^2}_{40}$ at 2 kg/min of air, for the configuration with nonintegral roughness and the standard pipe. The transition has been defined using the criterion previously described. Experimentally, it was recognized that the strength of the pulsation for the unstable conditions was smaller than in the standard configuration.

Figure 5.19 presents the pressure drop for the conditions at 2 kg/min of air for the standard and the nonintegral roughness configurations. The pressure drop is high when compared to the pressure drop found for the standard case. For instance, at 2 kg/min of air and 151.4 kg/min of water the pressure drop along the pipe with nonintegral roughness is 251.7 kPa, which corresponds to 23.5% of the operating pressure.

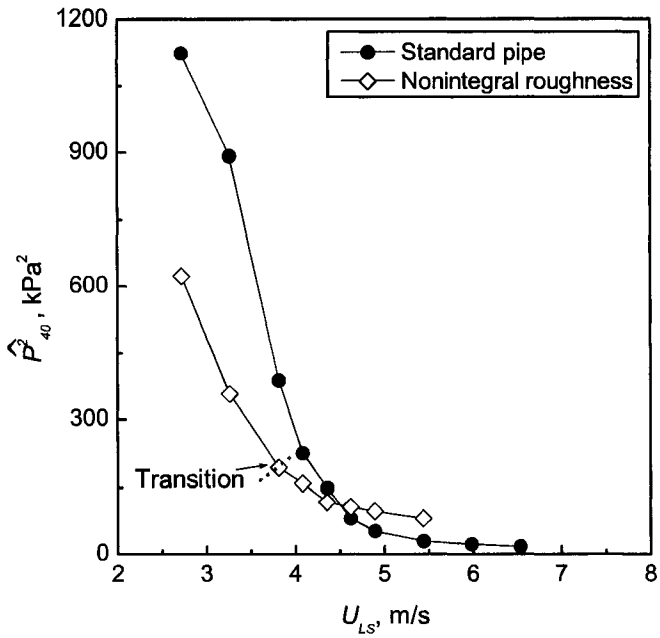

Figure 5.18: Comparison of nonintegral roughness with the standard pipe for 2 kg/min of air flow.

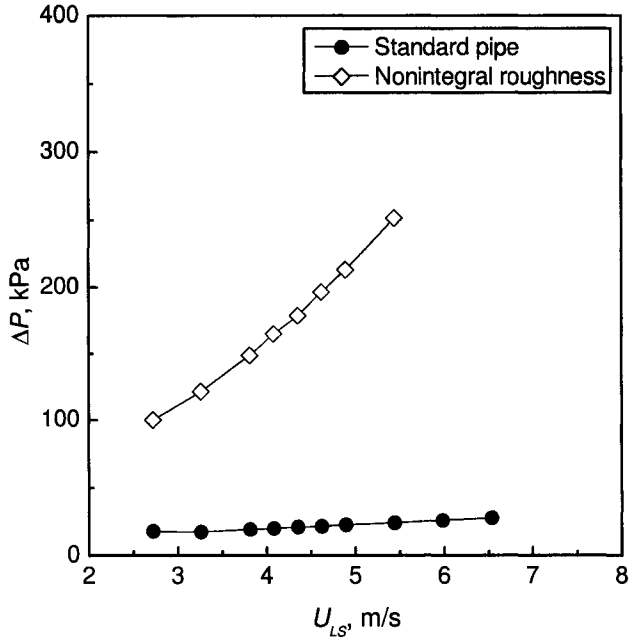

Figure 5.19: Pressure drop along the feeding pipe for the standard and nonintegral roughness configurations.

Figure 5.20 illustrates the PSD of the pressure fluctuations signal for a stable and an unstable condition, for the arrangement with nonintegral roughness. In both cases the power is observed to be distributed over certain frequency range although the maximums values are higher for unstable conditions.

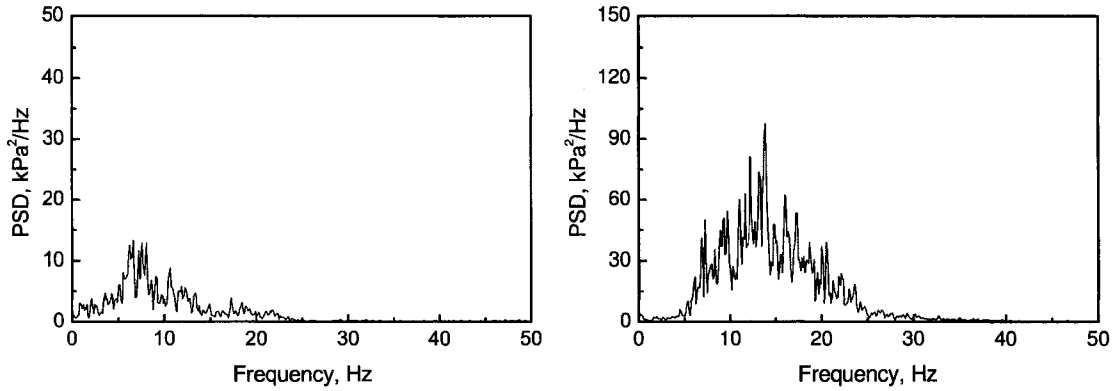

Figure 5.20: PSD of the pressure fluctuation signal for (a) a stable, and (b) an unstable condition, for the configuration with nonintegral roughness. Flow rates at 2 kg/min of air and 151.4 and 75.7 kg/min of water, for the stable and unstable condition, respectively.

As previously mentioned, the signal considered for the analysis and comparison of the different configurations is the one sampled just before the nozzle. This was done with the aim of having the same arrangement after the transducer D1 (installed just before the nozzle) for the different alternatives. However, this is not the case for the integral roughness. It is thought that the presence of disturbing elements along the conduit also contributes to the pressure fluctuations, making the nature of these signals different to those analyzed for other configurations. Additionally, although considerations were taken to prevent the movement of springs within the pipe, it could have happened, affecting the pressure fluctuations. In this regard, no direct comparisons in terms of the magnitude or frequency of pulsation are suggested in this case, with respect to the other configurations. This would lead to conclusions different to the results observed during experiments and later with regular videos. This reinforces the main difficulty in the analysis of pressure fluctuation signals, due to their integral nature.

Although this alternative offered improvements in the range of stability and decreased the pulsation strength, the increment in the pressure drop is very high with respect to that obtained with the standard configuration. This makes the nonintegral roughness unattractive for commercial implementation.

5.3 Overall comparison

Figure 5.21 presents an overall comparison between most of the configurations evaluated. The long pipe was not included because, before hand, it is known that it presents the worst performance in terms of the pulsation strength, and its inclusion in the plot would require a reduction of the resolution for the y-axis. The configuration with the spring is not included due to the reasons presented in the previous section.

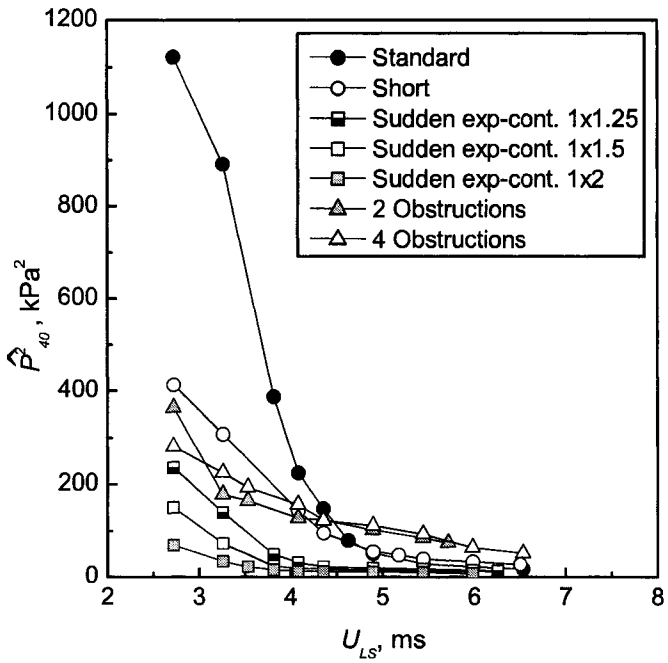

Figure 5.21: Area beneath the PSD for frequencies below 40 Hz ($\widehat{P^2}_{40}$), of the pressure fluctuations, for most of the feeding pipe configurations evaluated at 2 kg/min of air.

The standard conduit depicts the worst performance under unstable conditions, while the configurations with sudden expansion-contractions show the best one. The arrangements with 4 and 2 peripheral obstructions have performances in between.

Figure 5.22 presents the pressure drop along the feeding pipe for the configurations proposed with the aim of improving the mixing of the gas and liquid phases along the pipe. As expected, the configurations with restrictions to the flow (peripheral obstructions and nonintegral roughness) present the highest pressure drop. Although these alternatives offer some benefits in decreasing the pulsation severity, their corresponding pressure drop is very high to be pursued.

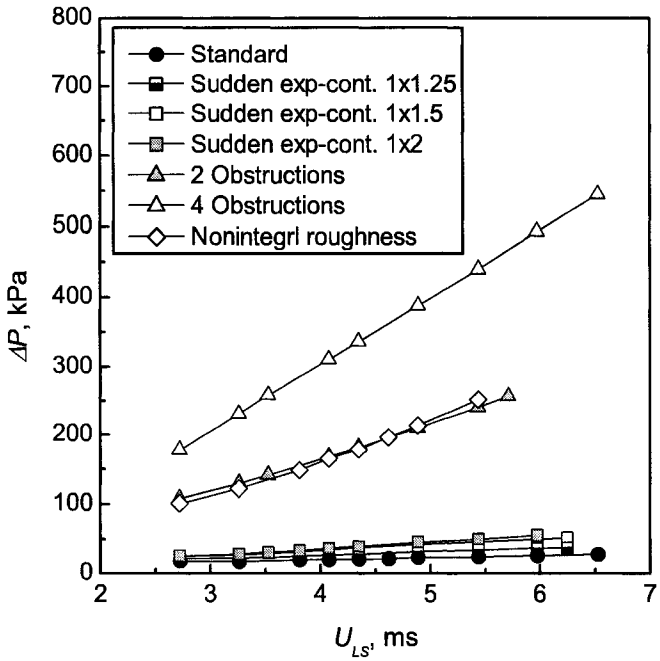

Figure 5.22: Pressure drop along the feeding pipe for configurations improving the gas and liquid mixing along the conduit.

The alternative with sudden expansion-contractions along the pipe displays the best overall performance: low strength of pulsation, wider range of stability and low increment in pressure drop.

Chapter 6

Conclusions and Recommendations

6.1 Conclusions

This study has proposed and experimentally evaluated different alternatives to improve the stability of gas-liquid sprays by altering the two-phase flow pattern at the nozzle inlet. The alternatives are focused on improving the mixing process of the two-phases through modifications of the conduit leading up to the nozzle. Additionally, a technique based on the analysis of the wall pressure fluctuations has been proposed and used to evaluate the spray stability for the different pipe configurations.

The following conclusions are drawn from this investigation:

1. A parameter based on the area beneath the PSD for frequencies below 40 Hz (mean square value of the main frequency components of the pressure fluctuations), permits to determine the stability condition of the spray.

2. The cross-correlation between pressure fluctuations signals sampled along the conduit is a very effective technique to identify the direction of propagation of signals, which indicates the origin of the pressure fluctuations. For unstable conditions, the pressure fluctuations originate in the nozzle and propagate in the upstream direction. For stable conditions, the pressure fluctuations propagate

in the downstream direction and are dominated by disturbances from the mixing device.

3. The gas-liquid spray stability is confirmed to be affected by the flow pattern entering the nozzle. Intermittent flow results in unstable sprays. Stable sprays are obtained from dispersed bubble flow.

4. Longer feeding pipes present higher strength and lower frequency of pulsation for intermittent conditions, whereas shorter pipes display slight instabilities in the spray for the dispersed bubble region. This is suggested to be directly related to the flow development along the feeding pipe. For intermittent flow, the gas bubbles continue to coalesce in longer pipes, forming bigger and less frequent bubbles, whereas for conditions corresponding to dispersed bubble flow the dispersion is improved when the flow is allowed to develop further.

5. All alternatives proposed to improve the mixing process along the pipe, display benefits in damping the strength of the pulsation for the unstable conditions. Their effect on the stability transition differs for the different configurations.

6. A series of sudden expansion-contractions of the pipe cross-section offers an important improvement to the range of stability of the gas-liquid spray, as well as reduces the severity of the pulsation for unstable conditions, without causing important increases to the pressure drop. The positive effect on the stability range and severity of pulsation is greater for the largest change in flow area evaluated.

7. The configurations employing peripheral obstructions and nonintegral roughness reduce the strength of the pulsation for unstable conditions, but have a high pressure drop associated which makes them unattractive for commercial implementation.

8. The pressure fluctuations in two-phase flow are the result of a variety of phenomena occurring in the system; some corresponding to the local flow and others

happening at the entrance, outlet and along the whole system. Therefore, when studying this type of signal it is necessary to do a preliminary analysis to understand what generates the pressure fluctuations and their relations to the characteristics of the system.

6.2 Recommendations

The following suggestions are proposed to be considered in future work:

1. Evaluate the effect on atomization performance of the alternative with sudden expansion-contractions of the pipe cross-section. This would guarantee that no adverse effects are caused on the spray characteristics by implementing this type of configuration.

2. Further tests should be performed to determine the optimum length and number of sudden expansion-contractions along the conduit.

3. Given that the pressure fluctuations for unstable conditions are generated at the nozzle, it is suggested to install the pressure transducer at the nozzle section. This would result in a signal more independent of processes occurring in the feeding system, and would allow a more reliable comparison between different configurations.

4. Evaluate the effect of different mixing device arrangements on the stability of the gas-liquid spray.

5. A rigorous evaluation of the effect of the spray stability on atomization performance should be conducted. This would permit one to have a quantitative indication of how the droplet size, velocity and distribution would be affected by instabilities on the spray.

6. Determine the stability range for the steam-bitumen system at the commercial operations.

Bibliography

Andreussi, P., Paglianti, A., and Sanchez, F. (1999). Dispersed bubble flow in horizontal pipes. *Chemical Engineering Science*, 54:1101–1107.

Ariyapadi, S., Berruti, F., Briens, C., Knapper, B., Skwarok, R., and Chan, E. (2005). Stability of horizontal gas-liquid sprays in open-air and in a gas-solid fluidized bed. *Powder Technology*, 155(3):161–174.

Baker, C. L., Cody, G. D., Joseph, C. A., and Sela, U. (1991). Acoustic monitoring of two-phase feed nozzles. US Patent 5 004 152.

Baker, O. (1954). Simultaneous flow of oil and gas. *Oil and Gas Journal*, 53(12):185–190.

Barnea, D., Shoham, O., and Taitel, Y. (1980a). Flow pattern characterization in two phase flow by electrical conductance probe. *International Journal of Multiphase Flow*, 6(5):387–397.

Barnea, D., Shoham, O., and Taitel, Y. (1982). Flow pattern transition for downward inclined two phase flow; horizontal to vertical. *Chemical Engineering Science.*

Barnea, D., Shoham, O., Taitel, Y., and Dukler, A. E. (1980b). Flow pattern transition for gas-liquid flow in horizontal and inclined pipes. *International Journal of Multiphase Flow*, 6(3):217–226.

Base, T. E., Chan, E. W., Kennett, R. D., and Emberley, D. A. (1999). Nozzle for atomizing liquid in two phase flow. US Patent 6 003 789.

Bendat, J. S. and Piersol, A. G. (1986). *Random Data Analysis and Measurement Procedures.* John Wiley & Sons.

Cai, Y., Wambsganss, M. W., and Jendrzejzyk, J. A. (1996). Application of chaos theory in identification of two-phase flow patterns and transitions in a small, horizontal, rectangular channel. *Transactions of the ASME - Journal of Fluid Engineering*, 118:383–390.

Chan, E. W., Base, T. E., and McCracken, T. (2001). Design and development of syncrude coker feed nozzles - a coker 2000 initiative. Syncrude Research Report 01-02.

Chen, X. T., Cai, X. D., and Brill, J. P. (1997). General model for transition to dispersed bubble flow. *Chemical Engineering Science*, 52(23):4373–4380.

Daniels, L. (1995). Dealing with two-phase flows. *Chemical Engineering (New York)*, 102(6):70–78.

Drahoš, J. and Ĉermák, J. (1989). Diagnostics of gas-liquid flow patterns in chemical engineering systems. *Chemical Engineering and Processing*, 26(2):147–164.

Edwards, C. F. and Marx, K. D. (1995). Multipoint statistical tructure of the ideal spray, part ii: evaluating steadiness using the interparticle time distribution. *Atomization and Sprays*, 5:457–505.

Gomez, L. E., Shoham, O., Schmidt, Z., Chokshi, R. N., Brown, A., and Northug, T. (1999). Unified mechanistic model for steady-state two-phase flow in wellbores and pipelines. In *Proceedings - SPE Annual Technical Conference and Exhibition*, pages 307–320.

Hoogendoorn, C. J. (1959). Gas-liquid flow in horizontal pipes. *Chemical Engineering Science*, 9(4):205–217.

Hosler, E. R. (1968). Flow patterns in high pressure two-phase (steam-water) flow with heat addition. In *Chemical Engineering Progress Symposium Series*, volume 64, pages 54–66.

Huang, F., Takahashi, M., and Guo, L. (2005). Pressure wave propagation in air-water bubbly and slug flow. *Progress in Nuclear Energy*, 47(1-1):648–655.

Hubbard, M. G. and Dukler, A. E. (1966). Characterization of flow regimes for horizontal two-phase flow – 1. In *Heat Transfer and Fluid Mechanics Institute – Proceedings*, pages 100–121.

Hulet, C., Briens, C., Berruti, F., Chan, E., and Ariypadi, S. (2003). Entrainment and stability of a horizontal gas-liquid jet in a fluidized bed. *International Journal of Chemical Reactor Engineering*, 1:A60.

Kirpalani, D. (1999). Novel signal processing approaches for characterization of transient two-phase gas-liquid flow. Master's thesis, University of Ottawa.

Knapper, B. and House, P. (2005). The use of dynamic pressure signals to determine stability of an air-assisted atomizing feed nozzle. *Syncrude Research Dept. Progress Report*, 34(01):191–245.

Kondo, K., Yoshida, K., Matsumoto, T., Okawa, T., and Kataoka, I. (2002). Flow patterns of gas-liquid two-phase flow in round tube with sudden expansion. In *10th International Conference on Nuclear Engineering.*

Lefebvre, A. H. (1989). *Atomization and Sprays.* Hemisphere.

Lefebvre, A. H., Wang, X. F., and Martin, C. A. (1988). Spray characteristics os aerated-liquid pressure atomizers. *AIAA Journal of Propulsion and Power*, 4(4):293–298.

Lin, P. Y. and Hanratty, T. J. (1987). Detection of slug flow from pressure measurements. *International Journal of Multiphase Flow*, 13(1):13–21.

Lockhart, R. W. and Martinelli, R. C. (1949). Proposed correlation of data for isothermal two-phase, two-component flow in pipes. *Chemical Engineering Progress*, 45(1):39–45.

Luong, J. T. K. and Sojka, P. E. (1999). Unsteadiness in effervescent sprays. *Atomization and Sprays*, 9:87–109.

Mandhane, J. M., Gregory, G. A., and Aziz, K. (1974). A flow pattern map for gas-liquid flow in horizontal pipes. *International Journal of Multiphase Flow*, 1:537–553.

Matsen, J. M. (1996). Scale-up of fluidized bed processes: principle and practice. *Powder Technology*, 88:237–244.

Matsui, G. (1985). Identification of flow patterns in horizontal gas-liquid two-phase flow using differential pressure fluctuations. In *Fluid Control and Measurement (Preprints).*, pages 819–824.

Nguyen, D. L., Winter, E. R. F., and Greiner, M. (1981). Sonic velocity in two-phase systems. *International Journal of Multiphase Flow*, 7:311–320.

Otnes, R. K. and Enochson, L. (1978). *Applied time series analysis.* John Wiley & Sons.

Press, W., Flannery, B., Teukolsky, S., and Vetterling, W. (1986). *Numerical Recipes: The Art of Scientific Computing.* Cambridge University Press.

Roesler, T. C. and Lefebrve, A. H. (1989). Studies on aerated-liquid atomization. *International Journal of Turbo Jet Engines*, 6:221–230.

Salcudean, M., Chun, J. H., and Groeneveld, D. C. (1983). Effect of flow obstruction on void distribution in horizontal air-water flow. *International Journal of Multiphase Flow*, 9(1):91–96.

Samways, A. L., Bradbury, L. J. S., and Bruun, H. H. (1997). Pressure measurements and convection velocity evaluations in two-phase flow. *International Journal of Multiphase Flow*, 23(6):1007–1029.

Scott, D. S. (1963). *Advances in Chemical Egineering, Vol. 4.* Academic Press.

Sovani, S. D., Sojka, P. E., and Lefebvre, A. H. (2001). Effervescent atomization. *Progress in Energy and Combustion Science*, 27:483–521.

Tafreshi, Z. M., Kirpalani, D., Bennett, A., and McCracken, T. W. (2002). Improving the efficiency of fluid cokers by altering two-phase feed characteristics. *Powder Technology*, 125(2-3):234–241.

Taitel, Y. (1977). Flow pattern transition in rough pipes. *International Journal of Multiphase Flow*, 3(6):597–601.

Taitel, Y. and Dukler, A. E. (1976). A model for predicting flow regime transitions in horizontal and near horizontal gas-liquid flow. *AICHE Journal*, 22(1):47–55.

Tutu, N. K. (1982). Pressure fuctuations and flow pattern recognition in vertical two-phase gas-liquid flows. *International Journal of Multiphase Flow*, 8(4):443–447.

Vial, C., Poncin, S., Wild, G., and Midoux, N. (2001). Simple method for regime identification and flow characterization in bubble columns and airlift reactors. *Chemical Engineering and Processing*, 40(2):135–151.

Wambsganss, M. W., Jendrzejczyk, J. A., and France, D. M. (1991). Two-phase flow patterns and transitions in a small, horizontal, rectangular channel. *International Journal of Multiphase Flow*, 17(3):327–342.

Wambsganss, M. W., Jendrzejczyk, J. A., and France, D. M. (1994). Determination and characteristics of the transition to two-phase slug flow in small horizontal channels. *ASME Journal of Fluids Engineering*, 116:140–146.

Webb, R. L. (1994). *Principles of enhanced heat transfer.* John Wiley

Weisman, J., Duncan, D., Gibson, J., and Crawford, T. (1979). Effects of fluid properties and pipe diameter on two-phase flow patterns in horizontal lines. *International Journal of Multiphase Flow*, 5(6):437–462.

Whitlow, J. D. and Lefebvre, A. H. (1993). Effervescent atomizer operation and spray characteristics. *Atomization and Sprays*, 3:137–155.

Appendix A

Experimental conditions for different configurations

A.1 Standard

Table A.1: Experimental conditions for the standard feeding pipe

Water flow (kg/min)	Air flow (kg/min)	Pressure (kPa)	Pressure drop (kPa)	U_{LS} (m/s)	U_{GS} (m/s)	Area PSD ($f < 40$ Hz) (kPa^2)	Qualitative stability
181.7	1	937.2	24.3	6.53	2.91	5.6	Stable
166.6	1	856.9	22.9	5.98	3.15	7.3	Stable
151.4	1	778.6	22.6	5.44	3.43	10.1	Stable
136.3	1	701.1	19.2	4.89	3.76	13.9	Transition
121.1	1	621.1	17.6	4.35	4.18	32.0	Unstable
113.6	1	578.0	16.8	4.08	4.45	81.5	Unstable
106.0	1	533.4	16.3	3.81	4.76	155.5	Unstable
98.4	1	478.5	15.5	3.53	5.21	506.0	Unstable
90.8	1	432.3	15.5	3.26	5.66	915.3	Unstable
75.7	1	343.6	16.9	2.72	6.79	1118.6	Unstable
181.7	2	1265.3	27.5	6.53	4.42	17.2	Stable
166.6	2	1163.2	25.7	5.98	4.78	22.4	Stable
151.4	2	1070.6	24.0	5.44	5.15	29.5	Stable
136.3	2	968.7	22.7	4.89	5.64	51.9	Transition
128.7	2	916.8	21.5	4.62	5.93	80.3	Unstable
121.1	2	868.7	20.7	4.35	6.23	147.8	Unstable
113.6	2	813.3	19.8	4.08	6.60	225.6	Unstable
106.0	2	756.4	19.2	3.81	7.04	388.3	Unstable
90.8	2	638.9	17.3	3.26	8.16	891.4	Unstable
75.7	2	528.0	17.8	2.72	9.60	1122.6	Unstable
181.7	3	1507.8	41.5	6.53	5.63	38.5	Stable
166.6	3	1401.8	38.1	5.98	6.03	49.5	Stable
159.0	3	1349.4	37.6	5.71	6.25	55.3	Stable
151.4	3	1294.9	35.8	5.44	6.49	69.2	Stable
143.8	3	1236.1	33.3	5.17	6.77	80.5	Transition
136.3	3	1174.0	32.0	4.89	7.10	129.4	Transition
128.7	3	1118.5	31.0	4.62	7.43	201.6	Unstable
121.1	3	1049.0	29.5	4.35	7.88	301.7	Unstable
106.0	3	934.1	27.4	3.81	8.75	546.8	Unstable
90.8	3	805.5	25.6	3.26	9.99	923.4	Unstable

Water flow (kg/min)	Air flow (kg/min)	Pressure (kPa)	Pressure drop (kPa)	U_{LS} (m/s)	U_{GS} (m/s)	Area PSD ($f < 40$ Hz) (kPa^2)	Qualitative stability
162.8	4	1573.5	38.4	5.85	7.21	81.9	Stable
151.4	4	1487.3	37.3	5.44	7.60	127.3	Stable
143.8	4	1421.2	34.6	5.17	7.93	160.7	Transition
136.3	4	1361.6	33.8	4.89	8.26	235.0	Transition
128.7	4	1291.5	32.4	4.62	8.67	338.1	Unstable
121.1	4	1226.2	31.1	4.35	9.10	464.0	Unstable
106.0	4	1092.8	28.3	3.81	10.12	768.8	Unstable
90.8	4	943.0	26.3	3.26	11.57	992.4	Unstable

A.2 Length to diameter ratio (L/D)

Table A.2: Experimental conditions for the short feeding pipe ($L/D = 16$)

Water flow rate (kg/min)	Air flow rate (kg/min)	Pressure ent. nozzle (kPa)	U_{LS} (m/s)	U_{GS} (m/s)	Area PSD ($f < 40$ Hz) (kPa^2)
181.7	1	947.0	6.53	2.88	14.7
166.6	1	864.8	5.98	3.13	18.6
151.4	1	787.7	5.44	3.40	19.6
143.8	1	747.8	5.17	3.56	25.5
136.3	1	708.0	4.89	3.73	25.8
121.1	1	627.4	4.35	4.14	32.6
113.6	1	585.5	4.08	4.40	42.9
106.0	1	543.2	3.81	4.69	70.1
90.8	1	452.2	3.26	5.46	180.2
75.7	1	365.8	2.72	6.46	297.3
180.9	2	1255.9	6.50	4.45	28.6
166.6	2	1163.6	5.98	4.78	33.7
151.4	2	1065.4	5.44	5.18	39.5
143.8	2	1019.2	5.17	5.39	47.4
136.3	2	971.6	4.89	5.63	56.4
121.1	2	868.1	4.35	6.23	96.2
113.6	2	814.7	4.08	6.59	144.5
90.8	2	653.6	3.26	8.00	308.4
75.7	2	538.2	2.72	9.44	412.7
157.1	3	1334.1	5.64	6.31	62.5
151.4	3	1294.7	5.44	6.49	65.1
143.8	3	1236.0	5.17	6.77	69.1
136.3	3	1179.8	4.89	7.07	85.8
121.1	3	1065	4.35	7.77	151.6
106.0	3	942.5	3.81	8.68	300.5
90.8	3	813.5	3.26	9.90	483.0
75.7	3	685.1	2.72	11.52	521.1

Table A.3: Experimental conditions for the long feeding pipe ($L/D = 74$)

Water flow rate (kg/min)	Air flow rate (kg/min)	Pressure ent. nozzle (kPa)	U_{LS} (m/s)	U_{GS} (m/s)	Area PSD ($f < 40$ Hz) (kPa^2)
181.7	1	932.3	6.53	2.92	4.6
166.6	1	855.3	5.98	3.16	8.8
151.4	1	777.0	5.44	3.44	9.8
136.3	1	700.3	4.89	3.77	16.7
121.1	1	619.3	4.35	4.19	57.0
113.6	1	573.1	4.08	4.48	147.6
106.0	1	518.8	3.81	4.87	838.3
90.8	1	427.5	3.26	5.71	1715.6
75.7	1	342.7	2.72	6.80	1529.4
174.1	2	1200.1	6.25	4.64	16.8
166.6	2	1158.1	5.98	4.80	17.7
151.4	2	1060.4	5.44	5.20	23.5
136.3	2	967.3	4.89	5.65	55.4
128.7	2	915.2	4.62	5.94	96.0
121.1	2	863.5	4.35	6.26	185.0
113.6	2	809.7	4.08	6.63	465.2
106.0	2	743.3	3.81	7.15	1362.9
90.8	2	628.7	3.26	8.27	1619.3
75.7	2	517.6	2.72	9.76	1322.2
154.4	3	1305.4	5.55	6.44	37.3
151.4	3	1286.6	5.44	6.53	39.2
143.8	3	1231.2	5.17	6.80	50.1
136.3	3	1178.5	4.89	7.08	92.7
128.7	3	1118.2	4.62	7.43	170.3
121.1	3	1056.4	4.35	7.83	262.7
113.6	3	992.6	4.08	8.28	464.5
106.0	3	930.1	3.81	8.78	718.8
90.8	3	792.9	3.26	10.13	1260.2
75.7	3	674.3	2.72	11.68	1290.6

A.3 Sudden expansion-contractions along the pipe

Table A.4: Experimental conditions for configuration with 1x1.25 sudden expansion-contractions along the pipe.

Water flow (kg/min)	Air flow (kg/min)	Pressure (kPa)	Pressure drop (kPa)	U_{LS} (m/s)	U_{GS} (m/s)	Area PSD ($f < 40$ Hz) (kPa^2)	Qualitative stability
181.7	1	944.8	30.7	6.53	2.89	6.6	-
166.6	1	866.4	28.7	5.98	3.12	6.8	-
151.4	1	790.2	26.9	5.44	3.39	7.9	-
136.3	1	708.6	25.1	4.89	3.73	9.9	-
121.1	1	630.9	23.2	4.35	4.12	11.2	-
106.0	1	550.9	20.7	3.81	4.63	21.0	-
90.8	1	458.3	18.3	3.26	5.40	120.7	-
75.7	1	364.2	18.4	2.72	6.49	336.8	-
174.1	2	1212.2	37.3	6.25	4.60	13.0	Stable
166.6	2	1166.2	36.1	5.98	4.77	14.5	Stable
151.4	2	1071.3	33.9	5.44	5.15	17.0	Stable
136.3	2	974.2	31.1	4.89	5.62	19.4	Transition
121.1	2	872.7	27.9	4.35	6.20	22.9	Transition
113.6	2	821.0	26.3	4.08	6.55	31.7	Transition
106.0	2	770.9	24.7	3.81	6.93	49.9	Unstable
90.8	2	657.5	22.5	3.26	7.96	140.2	Unstable
75.7	2	540.7	21.2	2.72	9.41	236.2	Unstable
151.4	3	1291.5	37.8	5.44	6.50	23.0	Stable
136.3	3	1183.6	34.3	4.89	7.05	28.0	Stable
128.7	3	1125.9	32.7	4.62	7.38	34.4	Transition
121.1	3	1069.0	30.6	4.35	7.74	41.5	Transition
113.6	3	1012.7	28.8	4.08	8.13	58.1	Unstable
106.0	3	951.8	27.0	3.81	8.60	90.8	Unstable
90.8	3	821.1	24.4	3.26	9.82	191.4	Unstable
75.7	3	684.5	22.6	2.72	11.53	256.4	Unstable

Table A.5: Experimental conditions for configuration with 1x1.5 sudden expansion-contractions along the pipe.

Water flow (kg/min)	Air flow (kg/min)	Pressure (kPa)	Pressure drop (kPa)	U_{LS} (m/s)	U_{GS} (m/s)	Area PSD ($f < 40$ Hz) (kPa^2)	Qualitative stability
181.7	1	944.5	42.0	6.53	2.89	5.7	Stable
166.6	1	862.8	39.2	5.98	3.13	6.6	Stable
151.4	1	784.4	36.5	5.44	3.41	7.3	Transition
136.3	1	706.0	33.8	4.89	3.74	9.3	Transition
121.1	1	629.3	30.8	4.35	4.13	10.4	Transition
106.0	1	549.7	26.3	3.81	4.64	13.5	Transition
90.8	1	465.8	22.2	3.26	5.32	38.4	Unstable
75.7	1	369.5	21.5	2.72	6.41	192.5	Unstable
174.1	2	1214.1	51.8	6.25	4.59	11.4	Stable
166.6	2	1169.3	50.1	5.98	4.75	13.5	Stable
151.4	2	1070.7	46.1	5.44	5.15	14.0	Stable
136.3	2	975.2	41.8	4.89	5.61	15.8	Stable
121.1	2	876.9	37.0	4.35	6.17	17.1	Transition
113.6	2	825.1	33.8	4.08	6.52	19.6	Transition
106.0	2	775.7	30.8	3.81	6.89	24.3	Transition
90.8	2	665.3	26.4	3.26	7.88	72.9	Unstable
75.7	2	547.3	25.2	2.72	9.31	151.2	Unstable
151.4	3	1299.8	50.1	5.44	6.47	16.7	Stable
136.3	3	1187.5	45.3	4.89	7.03	20.8	Stable
121.1	3	1075.7	39.4	4.35	7.70	27.6	Transition
113.6	3	1016.3	36.4	4.08	8.11	33.8	Transition
106.0	3	956.0	34.1	3.81	8.57	46.6	Unstable
90.8	3	827.5	29.0	3.26	9.75	104.6	Unstable
75.7	3	695.4	27.2	2.72	11.37	168.9	Unstable

Table A.6: Experimental conditions for configuration with 1x2 sudden expansion-contractions along the pipe.

Water flow (kg/min)	Air flow (kg/min)	Pressure (kPa)	Pressure drop (kPa)	U_{LS} (m/s)	U_{GS} (m/s)	Area PSD ($f < 40$ Hz) (kPa^2)	Qualitative stability
181.7	1	952.4	53.3	6.53	2.87	5.2	Stable
166.6	1	871.0	48.6	5.98	3.11	5.1	Stable
151.4	1	788.0	44.0	5.44	3.40	5.8	Stable
136.3	1	705.9	39.6	4.89	3.74	6.2	Transition
121.1	1	628.0	35.8	4.35	4.14	8.0	Transition
106.0	1	545.1	31.0	3.81	4.67	9.0	Unstable
98.4	1	507.0	28.8	3.53	4.96	10.3	Unstable
90.8	1	467.2	26.4	3.26	5.31	14.3	Unstable
75.7	1	376.1	23.4	2.72	6.33	52.4	Unstable
166.6	2	1160.6	54.7	5.98	4.79	8.6	Stable
151.4	2	1065.7	50.0	5.44	5.18	10.9	Stable
136.3	2	974.5	45.1	4.89	5.61	11.6	Stable
121.1	2	875.6	39.4	4.35	6.18	12.0	Transition
113.6	2	824.2	36.2	4.08	6.53	13.4	Transition
106.0	2	775.3	33.0	3.81	6.89	16.1	Transition
98.4	2	723.7	29.9	3.53	7.32	22.1	Unstable
90.8	2	668.0	27.6	3.26	7.85	34.1	Unstable
75.7	2	552.9	24.7	2.72	9.23	69.2	Unstable
151.4	3	1286.2	59.3	5.44	6.53	14.2	Stable
136.3	3	1176.2	53.7	4.89	7.09	16.2	Stable
128.7	3	1121.9	49.8	4.62	7.41	17.2	Transition
121.1	3	1068.3	46.3	4.35	7.75	19.4	Transition
113.6	3	1006.6	42.6	4.08	8.18	20.1	Transition
106.0	3	950.2	39.3	3.81	8.62	30.1	Transition
98.4	3	884.3	36.3	3.53	9.19	39.6	Unstable
90.8	3	832.8	34.0	3.26	9.70	54.7	Unstable
75.7	3	694.1	30.8	2.72	11.39	90.2	Unstable

A.4 Peripheral obstructions

Table A.7: Experimental conditions for configuration with 4 peripheral obstructions along the feeding pipe.

Water flow (kg/min)	Air flow (kg/min)	Pressure (kPa)	Pressure drop (kPa)	U_{LS} (m/s)	U_{GS} (m/s)	Area PSD ($f < 40$ Hz) (kPa^2)
181.7	2	1258.3	545.1	6.53	4.44	51.9
166.6	2	1166.8	492.7	5.98	4.76	63.5
151.4	2	1065.8	439.3	5.44	5.18	93.9
136.3	2	968.1	387.5	4.89	5.65	112.3
121.1	2	867.7	335.9	4.35	6.23	122.4
113.6	2	818.5	310.1	4.08	6.57	157.4
98.4	2	715.0	257.6	3.53	7.40	193.0
90.8	2	662.0	230.2	3.26	7.91	224.9
75.7	2	542.4	177.7	2.72	9.38	280.8

Table A.8: Experimental conditions for configuration with 2 peripheral obstructions along the feeding pipe.

Water flow (kg/min)	Air flow (kg/min)	Pressure (kPa)	Pressure drop (kPa)	U_{LS} (m/s)	U_{GS} (m/s)	Area PSD ($f < 40$ Hz) (kPa^2)
181.7	1	931.8	261.3	6.53	2.92	13.8
166.6	1	853.7	232.6	5.98	3.16	18.0
151.4	1	775.5	204.8	5.44	3.44	27.5
136.3	1	698.7	178.6	4.89	3.77	37.8
121.1	1	620.7	153.5	4.35	4.18	57.1
113.6	1	582.3	141.3	4.08	4.42	69.8
106.0	1	540.7	128.8	3.81	4.70	95.0
90.8	1	457.8	107.8	3.26	5.40	128.6
75.7	1	362.3	90.7	2.72	6.51	280.9
159.0	2	1113.6	255.7	5.71	4.97	75.2
151.4	2	1065.9	240.3	5.44	5.17	85.6
136.3	2	968.4	209.6	4.89	5.65	102.9
121.1	2	872.9	181.2	4.35	6.20	124.2
113.6	2	819.0	167.7	4.08	6.56	127.7
98.4	2	712.2	140.9	3.53	7.42	166.0
90.8	2	658.4	129.3	3.26	7.95	178.9
75.7	2	540.5	107.4	2.72	9.41	363.4
166.6	3	1399.2	296.1	5.98	6.04	104.0
151.4	3	1294.0	264.3	5.44	6.49	131.0
136.3	3	1185.2	233.5	4.89	7.04	137.5
121.1	3	1072.4	201.8	4.35	7.72	118.7
113.6	3	1014.6	187.2	4.08	8.12	142.8
106.0	3	953.5	172.2	3.81	8.59	155.7
98.4	3	891.9	157.1	3.53	9.12	184.8
90.8	3	839.7	145.9	3.26	9.63	216.7
75.7	3	692.2	120.0	2.72	11.42	483.2

A.5 Nonintegral roughness

Table A.9: Experimental conditions for configuration with nonintegral roughness along the feeding pipe.

Water flow (kg/min)	Air flow (kg/min)	Pressure (kPa)	Pressure drop (kPa)	U_{LS} (m/s)	U_{GS} (m/s)	Area PSD ($f < 40$ Hz) (kPa^2)	Qualitative stability
151.4	2	1091.6	251.7	5.44	5.06	80.2	Stable
136.3	2	990.2	213.4	4.89	5.53	96.0	Transition
128.7	2	942.0	196.3	4.62	5.79	104.8	Transition
121.1	2	889.3	178.5	4.35	6.10	116.3	Transition
113.6	2	843.9	164.9	4.08	6.39	159.2	Transition
106.0	2	785.4	148.3	3.81	6.81	192.8	Unstable
90.8	2	674.9	121.4	3.26	7.78	357.0	Unstable
75.7	2	557.7	100.2	2.72	9.17	622.2	Unstable

Appendix B

Videos

The CD included contains the following:

- Videos of the spray recorded at 15 fps for approximately 40 s. Three different operating conditions were considered: 75.7, 113.6, and 151.4 kg/min of water and 2 kg/min of air. The configurations for which the videos were recorded are: standard pipe, long pipe, short pipe, sudden expansion-contractions (1x1.25, 1x1.5 and 1x2), and nonintegral roughness.
- High-speed videos for a stable and unstable condition of:
  - Flow entering the nozzle for the configuration with long conduit. These videos were originally recorded at 4000 fps, and the videos included in the CD correspond to approximately 0.4 s of the original process.
  - Spray generated with the standard configuration. These videos were originally recorded at 2000 fps, and the videos included in the CD correspond to approximately 0.4 s of the original process.

The files were named as: **X_Y_Z.avi**

where
X: liquid flow rate (kg/min)
Y: gas flow rate (kg/min)
Z: feeding pipe configuration